# Imaging Genetics through Brain Age Estimation and Image Derived Phenotypes

PhD student

Ahmed Mahdee Abdo Salih

Supervised by

Prof. Gloria Menegaz, University of Verona, Italy

Co-supervised by

Prof. Petia Radeva, University of Barcelona, Spain

Dr. Ilaria Boscolo, University of Verona, Italy

June 7, 2022

# UNIVERSITA' DEGLI STUDI DI VERONA

*DEPARTMENT OF*

*Computer Science*

*GRADUATE SCHOOL OF*

*Natural Sciences and Engineering*

*DOCTORAL PROGRAM IN*

*Computer Science*

*WITH THE FINANCIAL CONTRIBUTION OF*
*(NAME IF THE FUNDING INSTITUTION)*

*The project leading to this application has received funding from the European Union's Horizon 2020 research and innovation programme under the Marie Skłodowska-Curie grant agreement No 754345, under Region of Veneto Decree nr. 193 of 13/09/2016 and under Università degli Studi di Verona*

Cycle / year (1° year of attendance) XXXIV/ 2019

TITLE OF THE DOCTORAL THESIS

Imaging Genetics through Brain Age Estimation and Image Derived Phenotypes

S.S.D. INF
(Please complete this space with the S.S.D. of your thesis – mandatory information)*

Coordinator: Prof./ssa Massimo Merro

Signature _____

Tutor: Prof./ssa Gloria Menegaz

Signature _____

Doctoral Student: Dott./ssa Ahmed Mahdee Abdo Salih

Signature

* For the list of S.S.D. please refer to the Ministerial Decree of 4th October 2000, Attachment A "*Elenco dei Settori Scientifico – Disciplinari*" available at: http://www.miur.it/atti/2000/alladm001004_01.htm

REGIONE DEL VENETO

**ACKNOWLEDGEMENT**

First and foremost, praises and thanks to the God. I would like to express my deep and sincere gratitude to my research supervisor, Prof. Gloria Menegaz, and co-supervisor Assistant Prof. Ilaria Boscolo, Dept. of Computer Science, University of Verona, Italy and co-supervisor Prof. Petia Radiva, Dept. of Informatic, University of Barcelona, Spain for giving me the opportunity to do research and providing invaluable guidance throughout this research. Gloria's dynamism, vision, sincerity and motivation have deeply inspired me. She has taught me the methodology to carry out the research and to present the research works as clearly as possible. It was a great privilege and honor to work and study under her guidance. I am extremely grateful for what she has offered me.

Ilaria Boscolo helped and guided me in all steps of my study specially scientific guidance. She also guided me well in the writing manuscripts for per-reviewed journals. Her opinions and suggestions increased the quality of my work. I am really thankful to her and her positive role.

I would also like to express my gratitude and thankful to Prof. Petia Radiva by inviting at university of Barcelona to perform and complete my research which otherwise I would not be able to complete my whole study.

A special thank to Zahra Raisi-Estabragh at Queen Mary university of London for her unlimited help and support for providing me access to United Kingdom Biobank, clinical feedback and supportive to suggest solutions when needed.

In addition, also thanks to Prof. Steffen E. Petersen at Queen Mary university of London, Prof Karim Lekadir, at University of Barcelona for their generosity to providing the United Kingdom Biobank data-set which helped me to achieve my study.

I would also express my thanks and gratitude to my parents, sisters and brothers for their positive roles in supporting and pushing me to continue my study.

**DEDICATION**

*To my wife*

*Dilgash*

*and my kids*

*Helan and Halan.*

## Contents

**List of Figures**

**List of Tables**

**List of Abbreviations**

AD Alzheimer's disease

AxD Axial diffusivity

brain-PAD Predicted brain age delta

BRR Bayesian Ridge Regression

CMR Cardiac Magnetic Resonance

CNN Convolutional Neural Network

CRFs Cardiovascular Risk Factors

CSF Cerebrospinal fluid

DL Deep learning

DLe Deep learning explainability

dMRI Diffusion MRI

DTI Diffusion tensor imaging

FA Fractional anisotropy

fMRI Functional MRI

GM Gray matter

GWAS Genome wide association studies

ICVF Intracellular volume fraction

IDPs Image derived phenotypes

ISOVF Isotropic volume fraction

LASSO Least Absolute Shrinkage and Selection Operator

LIM Local Interpretable Model-agnostic Explanation

LT Leukocyte telomere

LVEDV Left ventricle: end-diastolic volume

LVEF Left ventricle: ejection fraction

LVESV Left ventricle: end-systolic volume

LVM Left ventricle: mass

LVSV Left ventricle: stroke volume

MAE Mean absolute error

MD Mean diffusivity

MO Mode of anisotropy

MR Mendelian randomization

MRI Magnetic resonance imaging

MSE Mean square error

NODDI Neurite orientation dispersion and density imaging

ODI Orientation dispersion index

PhWAS Phenome wide association studies

$R^2$ Coefficient of determination

RD Radial diffusivity

ROI Regions of interests

RVEDV Right ventricular: end-diastolic volume

RVESV Right ventricular: end-systolic volume

RVSV Right ventricular: stroke volume

SHAP Shapley additive explanation

SLR Simple Linear Regression

sMRI Structural MRI

SNPs Single nucleotide polymorphisms

SRC Spearman's rank correlation

SVR Support Vector Regression

SWI Susceptibility weighted imaging

TL Telomeres length

UKBB United Kingdom Biobank

WM White matter

# Chapter One

# 1 Introduction

## 1.1 Motivation

Aging is a complex procedure that affects body organs system through changes in the structures and functions. Brain is one of the most vital body organs that contributes and interacts with other organs in daily life activities and duties. The central nervous system consists of two main categories that is White matter (WM) and Gray matter (GM). GM contains the cell bodies and is responsible for many body functions, while WM is constituted of tracts that connect different GM regions together [1]. In addition to GM and WM, the brain also involve Cerebrospinal fluid (CSF) which surrounds the brain and spinal cord [2]. The three parts can be visualized using Magnetic Resonance Imaging (MRI) as it is shown in figure 1.1.

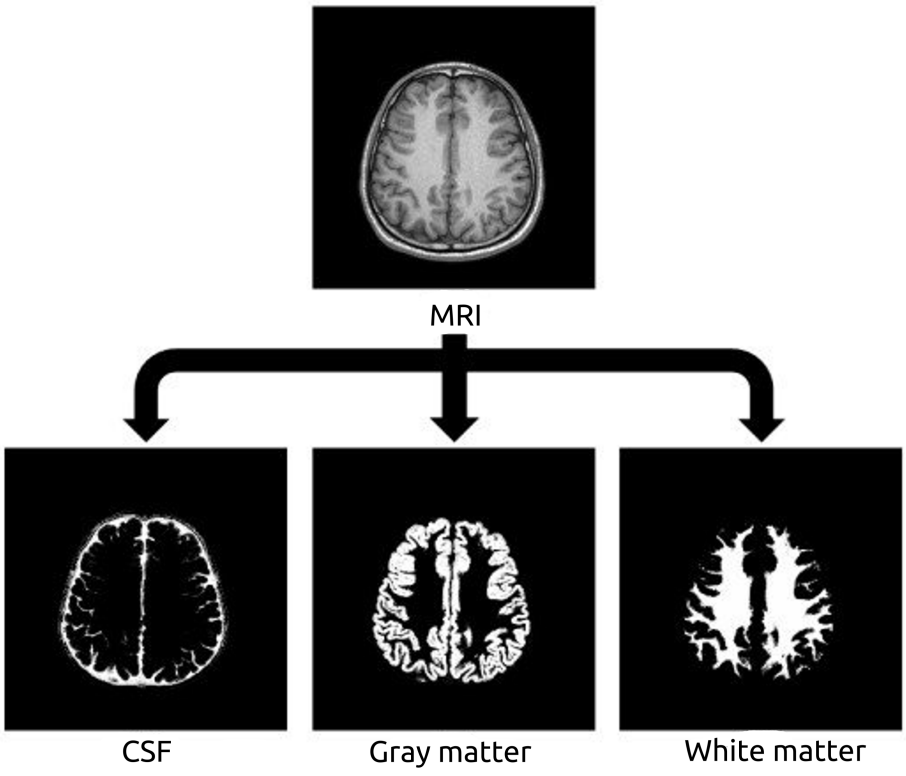


Figure 1.1: Representative MRI image segmented into the three main parts of the brain (cerebrospinal fluid and gray/white matter). Taken from [3].

Brain experiences aging, as other body organs, which results in profound alterations within brain structure, functions and biochemical interactions including gradual volumetric atrophy, moderate neuroinflammation, increased WM hyperintensity, loss of tissues and increase in the level of amyloid beta ($A\beta$) and tau proteins [4]. Brain aging in the absence of neurodegenerative disorders is called normal cognitive aging or non-pathological brain aging [5]. Such aging causes the degradation of cognitive functions and memory. The most common cognitive deficits in older people include difficulties with word recall, processing speed, complex tasks and episodic memory [4]. Figure 1.2 shows MRI images of the brain at different decades and the alterations caused by aging in healthy subjects. It can be noted how the degree of atrophy and WM hyperintensity increase during aging. On the other hand, brain aging might be a backdrop and lead to neurodegenerative disorders such as Alzheimer disease (AD). Brain diseases such as AD cause severe memory loss and cognitive decline [6]. Advanced machine and deep learning models and image processing make it possible to study and estimate the brain age in healthy or pathological individuals. Such studies help to understand how brain is aging and to what extent the apparent age of the brain is inline with the chronological age. In the healthy population, brain age can be exploited to understand the progression of brain in older people and the factors driving the speed of brain aging. Moreover, estimating brain age will also help to identify the informative features within brain regions that drive brain aging and consequently the corresponding cognitive functions related to these regions. This will shed light on the mechanisms ruling the onset of cognitive decline in normally aging's brain. Furthermore, the role of daily life style including healthy diet, regular exercise, alcohol intake, smoking and education as well as genetics factors can be investigated to reveal their role in brain aging. This will help to identify the factors that contribute positively or negatively to brain aging, which would help in better and healthy brain aging.

In addition to the healthy population, brain age estimation could be used to predict a risk of an aging-related disease or monitor the progression of a neurodegenerative disease such as AD. Estimating brain age enables to detect the rate of brain aging at individual level and allows to identify those factors that speed up the aging rate.

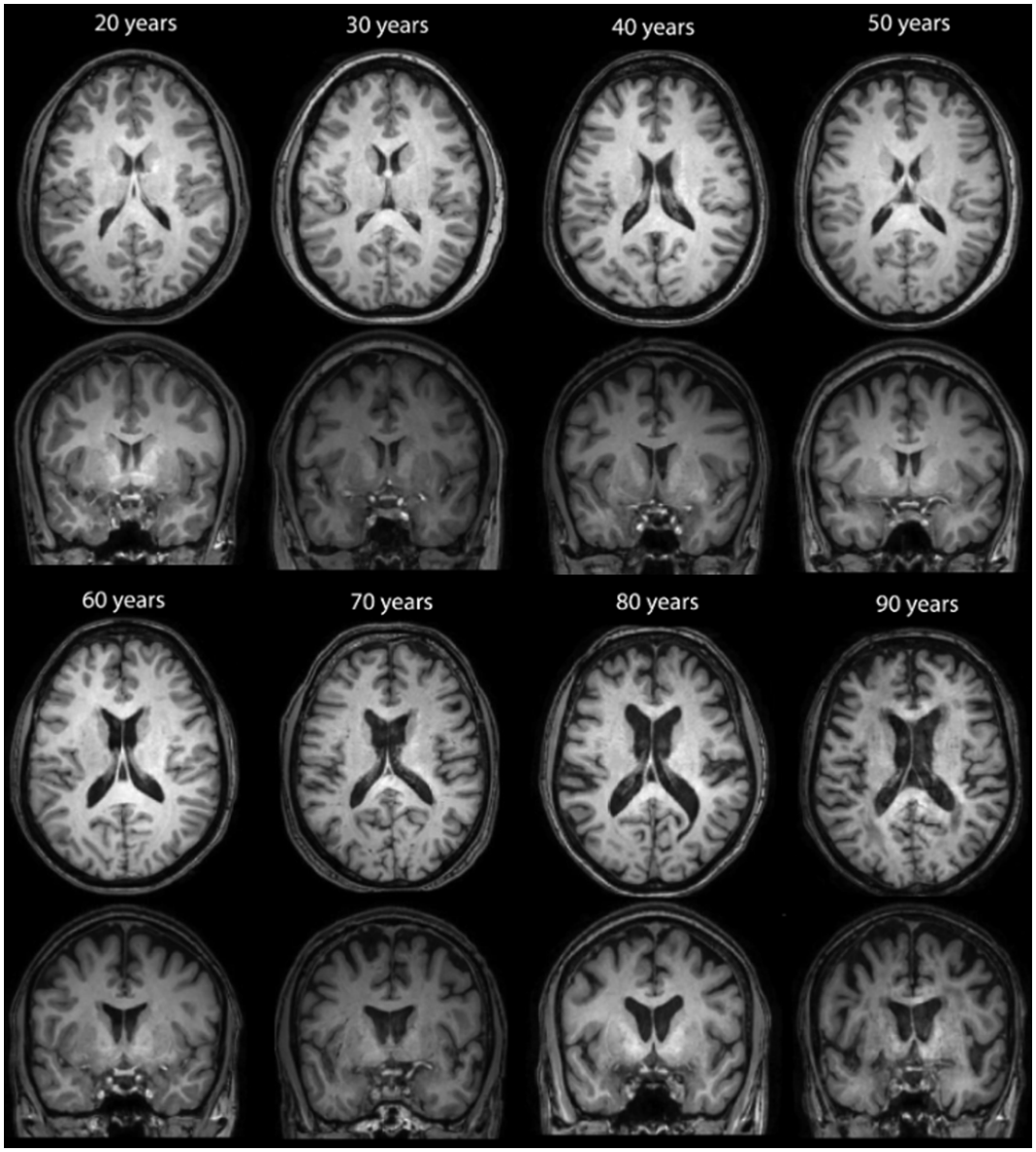


Figure 1.2: MRI images showing the degree of brain alterations, including atrophy, across the lifespan. Taken from [7].

This would help to better understand the sharp cognitive decline and dementia under specific brain conditions in older people. Moreover, brain age estimation could help to understand the effects of non-brain disorders such as cardiovascular diseases on brain aging and give better view of the communication networks between the brain and heart or other organs.

Accordingly, studying brain aging through brain age estimation goes beyond only understanding brain aging, it helps also to understand the effect of different factors that accelerate or slow down this process. The overall aim of such studies is to help

clinicians to be able to predict, diagnose, treat life-threatening diseases including brain disorders and recommend factors that could make individuals healthier.

## 1.2 Brain age estimation

Brain age estimation make use of machine learning and more advanced models such as deep learning to predict an individual's brain age. Regression models are generally used to estimate brain age, having chronological age as the dependent variable, as the actual brain age is unknown, while the independent variables (or predictors) could be any feature extracted from brain images and representing a specific characteristic of the brain tissue itself. In the following subsections, we will explain the regression model used in our study, along with the predictor types and model evaluation criteria.

### 1.2.1 Regression models

Regression models are statistical analyses to estimate a relationship between a predictor or groups of predictors and a continues outcome. The predictors are called the independent variables while the outcome is called the dependent variable [8]. The equation of a simple linear regression which is the most common one is:

$$y = a + x\beta + \varepsilon \tag{1.1}$$

where $y$ is the dependent variable or the outcome or the response variable, $a$ is the intercept, $x$ is the independent or the predictor variable, $\beta$ is the slop and $\varepsilon$ is the residual error.

The regression model is either a univariate regression, when only one predictor is used as independent variable, or a multiple regression where more independent variables are used to estimate an outcome.

Regression analysis could be linear and non-linear. The linear regression analysis can be drawn as a straight line between the predictors and the dependent variables while the non-linear produce a curved line between the independent and dependent variables [9].

**Bayesian Ridge Regression**

Bayesian Ridge Regression (BRR) is a regression model that estimates an outcome using a probabilistic model. It uses the coefficients of ridge regression to find out a posterior estimation under the normal distribution. It estimates the coefficients of the model as distributions instead of one single value as it is the case with the other regression models. The model shows its ability to deal with the hierarchical data structure [10]. In addition, the data in real life are collinear in most cases, the model shows better performance to handle such issue comparing with other linear models [11] [12]. It also includes regularization parameters to reduce the error and stabilize the model [13].

The data we used are collinear and for that we used different models to improve the performance. Among the used model, BRR showed good results compared to other regression models. Therefore, we thought it is worth to devote a section to describe the model and its usefulness to estimate an outcome. We have used the model in most cases in our study due to its performance to produce less error.

### 1.2.2 Overview of the predictors.

The alterations within brain structure and function in both healthy and diseased population is investigated here using MRI. MRI is a non-invasive medical imaging technique that uses magnetic fields and radio waves to construct detailed images rich in quantitative information related to tissue characteristics [14]. Different MRI imaging methods such as structural MRI (sMRI), functional MRI (fMRI) and diffusion MRI (dMRI) were developed to assess different tissue properties [15]. sMRI is exploited to examine the macrostructure of the brain such as cortical thickness, surface area and volume. sMRI can be employed to quantify the alterations within specific brain regions of interest or for the whole brain across different clinical groups. It is used to explore the morphological differences in the regions of the brain that are associated with a specific brain pathology to compare and contrast with healthy cohorts [16]. sMRI was used extensively to examine the progression and detect many brain disorders studies including AD [17], Huntington's diseas [18] and Parkinson disease (PD) [19]. dMRI is another MRI technique that constructs medical im-

ages based on the differences of motion of molecular water within the brain white matter tracts, named Brownian motion. Diffusion weighted imaging presents quantitative and qualitative information related to diffusion properties [20]. The motion of water in brain white matter tracts is anisotropic, however axon membranes limit this motion perpendicular to the fibers. Correspondingly, Diffusion tensor imaging (DTI) uses this properties to provide quantitative micro-architectural measures related to WM structure and integrity [21]. Among them, fractional anisotropy (FA) is a DTI parameter which measures the preferred direction of the water in each voxel of MRI images. It can be used to assess axonal integrity and ranges from 0 to 1. Mean diffusivity (MD) quantifies the overall diffusion in the each voxel within the brain. Axial diffusivity (AxD) measures the water motion along longitudinal direction while the radial diffusivity (RD) quantifies the diffusivity perpendicular to axonal fibers [22]. Neurite orientation dispersion and density imaging (NODDI) is a sophisticated dMRI model that allows to quantify three different tissue compartments: extraneurite, intraneurite and CSF [23]. Orientation dispersion index (ODI), isotropic volume fraction (ISOVF) and intracellular volume fraction (ICVF) are NODDI based matrices [24]. ODI and ICVF measure the coherence and cohesion of fibers orientation and spatial organization of the axons in white matter tracts [25]. In addition, ISOVF quantifies the isotropic component of the free-water compartment [26]. fMRI is another MRI technique that uses blood flow changes to measure brain activity and connectivity. It uses blood oxygenation level-dependent (BOLD) contrast to map brain activities. BOLD signal magnitude is used as a hint of neuronal activity that can be detected through regional cerebral blood flow, oxygenation and volume [27]. Figure 1.3 shows the most common three MRI modalities. sMRI, dMRI and fMRI are used widely in many applications to detect and monitor the progression of specific pathologies and in healthy ageing population. The application domains include early detection of AD [28], dementia [29], PD [30], ischemic attack [31] and prediction of brain age for healthy cohorts [32]. The three MRI modalities provide valuable quantitative measures which could be used to predict brain age for any cohort.

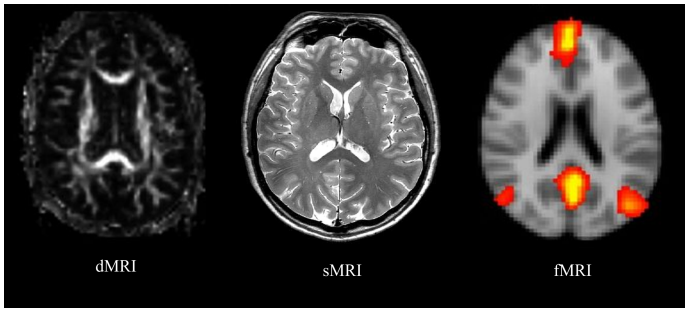


Figure 1.3: The diffusion, structural and functional MRI. The dMRI is the map of FA. The red spots are for default mode network resting-state network.

### 1.2.3 Model evaluation

Each model needs to be assessed to examine its performance. The measure to evaluate a model depends on the type of the model, regression or classification. The performance of the regression model is assessed using mean absolute error (MAE), coefficient of determination ($R^2$) and mean square error (MSE) [33]. The equation of the three mentioned matrices to assess model performance are:

$$MAE = \frac{\sum |y_i - \hat{y_i}|}{n} \tag{1.2}$$

$$MSE = \frac{1}{n}(\sum_{i=1}^{n} y_i - \hat{y_i})^2 \tag{1.3}$$

where $y_i$ is the actual value, $\hat{y_i}$ is the predicted value and $n$ is the number of observations.

$$R^2 = 1 - \frac{SS_{res}}{SS_{tot}} \tag{1.4}$$

where $R^2$ is the coefficient of determination, $SS_{res}$ is the sum of squares of residuals and $SS_{tot}$ is the total sum of squares.

Moreover, Spearman or Pearson correlation coefficient are often used to correlate predicted the brain age and the actual age.

Despite the measures (e.g., MAE) above are used to assess the model performance and comparing different stat-of-the-art studies, they are strongly influenced by distributions of the outcome (actual age) which make it insufficient to use it alone when comparing different models. The distribution of the outcome should be considered when comparing the performance of different models.

## 1.3 Brain age estimation blueprint

Brain age prediction is one of the topics that got much attention from researchers in recent years. It is considered as a biomarker to follow the progression of brain aging in both healthy and patients populations. Moreover, it helps to reveal the effects of different factors in brain aging including the environment and genetics bases. Brain age can be estimated using any regression model as the outcome is a continuous variable. Different classical machine and deep learning models were used to estimate brain age using image derived phenotypes (IDPs). In the model, IDPs are used as the predictors or the independent variables where the actual age is the dependent variable, the actual brain age is being unknown. The predictors could be IDPs extracted from any MRI modality or could be the combination of IDPs from different MRI modalities. In addition, different variables were used as confounds to adjust for when brain age is predicted. The confounds could be related to some characteristics of the subjects such as sex, height and education level or could be related to image acquisition such as volumetric scaling from T1-weighted head image to standard space. The performance of the model is assessed using MAE, $R^2$, MSE, correlation methods or other regression evaluation metrics. After brain age is predicted, "predicted brain age delta" (brain-PAD) is calculated which is the difference between the predicted brain age and the actual age. Positive brain-PAD indicates that the brain age is older than the actual age while negative brain-PAD means the estimated brain age is younger than the actual age. Several studies showed that brain age estimation involve frequent bias related to regression dilution. Such bias would lead to under estimation when brain age is estimated for older subjects, over estimation for younger subjects and more accurately brain age is estimated for subjects whose age is close to the mean age of the subjects. Different statistical methods were proposed to correct estimated brain age [34]. For instance, Beheshti et al [35] proposed a statistical method to correct estimated brain age as follow: first, calculate the regression line between brain-PAD and chronological age in the training set:

$$D = \alpha * \Omega + \beta \tag{1.5}$$

where $D$ is the brain-PAD from training data, $\alpha$ and $\beta$ represent the slope and the intercept of the linear regression model, and $\Omega$ is the corresponding chronological age. Then, these intercept and slope values were used to correct the predicted brain age in the validation set set as follows:

$$CPBA = Predicted\,Brain\,Age - (\alpha * \Omega + \beta) \tag{1.6}$$

Thereafter, different factors will be investigated to examine their effects in brain-PAD and whether they would contribute positively or negatively. Figure 1.4 shows the main steps of brain age estimation and the association with different factors including daily life style, cardiac risk factors and genetics variations which will be explained in the coming sections. The figure shows that the journey of brain age estimation starts with MRI acquisition followed by image processing and features extraction. Different features can be extracted from the MRI images depending on the MRI modalities. Thereafter, brain age can be estimated using a regression model. The final part of the figure shows the association of brain-PAD with different factors. This step helps to understand not only how old is the brain, but rather the factors driving brain aging. The association includes investigating lifestyle and environment through phenome wide association study (PhWAS), genetics using Genome wide association studies (GWAS), brain-aging related diseases and factors that might cause epigenetic defects such as telomeres.

## 1.4 The effect of daily life style on brain aging

After brain age is estimated, brain-PAD is calculated. Then, it is vital to investigate the contribution of daily life style in brain-PAD. Different daily life exposures were examined to reveal their effects in acceleration or slowing down brain-PAD. The investigated lifestyle and environment could be divided into groups such as smoking, alcohol, sleeping, diet and physical activities. In addition, physical measures such as blood pressure, hand grip strength, bone-densitometry of heel, hip circumference and arm fat mass were also used to reveal their effects in brain aging. Furthermore, cardiac risk factors such as diabetes, high cholesterol and hypertension were also examined.

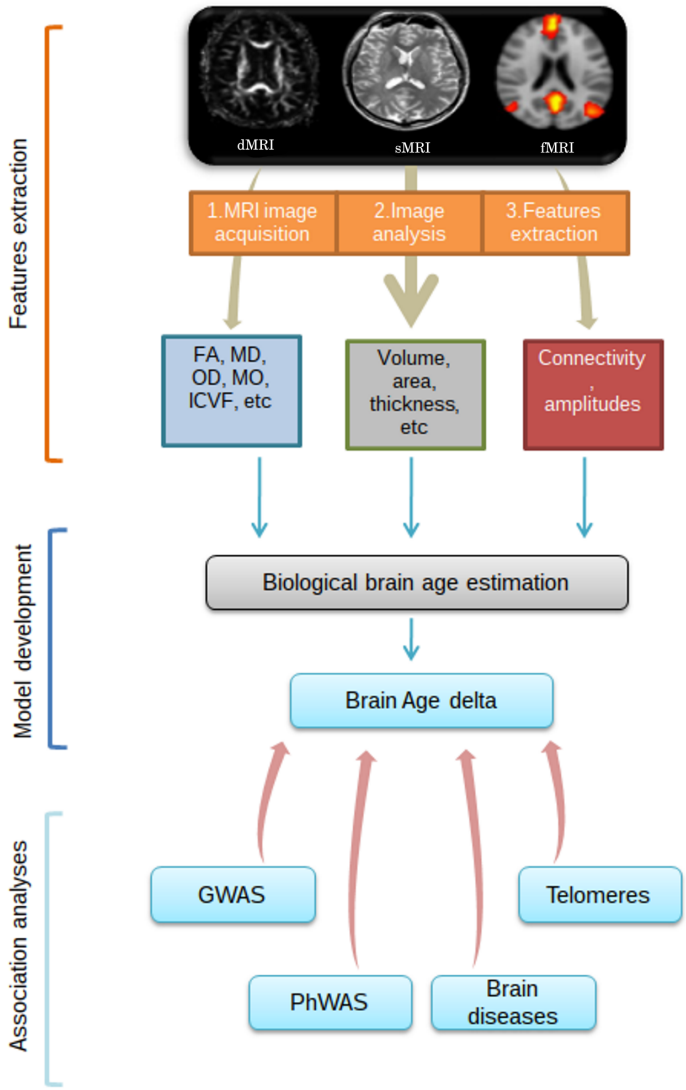


Figure 1.4: The general steps of brain age prediction and the association of brain-PAD with daily life style and genetics factors.

Smith et al,[32] performed brain-PAD association with wide range of lifestyle, environment and physical measures to explore their contribution in brain aging. Their results show that heel bone mineral density, weight, body mass index, hip circumference and arm fat mass were negatively associated with brain-PAD which indicate increasing in brain-PAD causing decreasing in these measures. On the contrary, systolic and diastolic blood pressure, smoking, cardiac index during pulse wave analysis, heart rate, cardiac output and pulse rate associated positively with brain-PAD. Such association means increasing in these measures cause increasing in brain-PAD. In addition, cardiac risk factors and cognitive function demonstrate a

significant association with brain-PAD [36]. Diabetes, stroke, smoking and alcohol are shown increasing brain aging. In addition, older brain aging linked to early sign of cognitive decline and older facial appearance [37]. Figure 1.5 shows the most daily life style factors and genetics variations (will be discussed in the next section) considered to examine their effects on brain-PAD.


Figure 1.5: Daily life style and genetics factors affecting brain-PAD.

## 1.5 The effect of genetics on brain aging

Genetics variations, mostly single nucleotide polymorphisms (SNPs) were examined through genome wide association studies GWAS to detect SNPs and consequently genes that have significant impacts on brain-PAD. The *GNA12* gene which is linked to migration of neurons is significantly associated with brain aging. In addition, *CREB3L4* gene that regulates adipogenesis was also associated with brain aging [38]. Moreover, two SNPs that are linked to reduced sulcal width and reduced white matter surface area were associated with brain-PAD [39]. In addition, several SNPs were shown significant association with brain-PAD including a SNP located in the *MAPT* gene. The mutations in the *MAPT* gene associated with Parkinson's disease and dementia [40].

## 1.6 Explainability models applied to brain age estimation

Deep learning (DL) models have shown successful achievements in divers area including biomedical [41]. They help to discover patterns and structures in massive amount of data in an automatic way. However, such success is accompanied with serious challenges. How the model made the decision, the internal mechanisms of the model, which feature or group of features influenced the model outcome and

to what extent we can trust the outcome, are some of the issues affecting the interpretability of the results [42]. Consequently, complex models are considered black boxes because the rationale behind the model outputs is not always understandable. Deep Learning explainability was emerged to uncover the mysterious around the models mechanisms and increase the trustful uses of the models outcome. DLe is a field that aims at building and developing new methods which help to understand and interpret machine learning models which took tremendous attention in recent years. For that matter, various approaches and methods were developed to explain the model globally or locally [43].

DLe could be used and exploited in brain age estimation when complex models are used to understand the model outcome. It would also helps to identify the most informative predictors to model brain age. In addition, it might also reveal the relationship among the predictors and with the outcome.

Lack of raw brain MRI did not allow us to use explainability methods applied to imaging data such as Grad-CAM [44], Grad-CAM++ [45], Saliency maps [46] and Layer wise Relevance Propagation [47]. Accordingly, we used the explainability methods applied to tabular data.

## 1.7 The causes behind brain alterations

As brain aging, there will be inevitable changes within brain tissues. Brain age estimation exploit these changes to estimate individual's brain age. However, what is the factor or group of factors that drive these changes?, is it a normal aging causing these changes?, could be an indication of a brain disorder?. Answering these questions would help to a large extent to understand brain aging and its related consequences such as the decline of cognitive functions and aging related diseases. For that matter, different statistical and causal methods were used and different factors were considered as the main causes of the alterations such telomeres length (TL) and AD. The casual method were considered because simple correlation between two variables does not imply causation [48]. In addition, there are many hidden and observable factors (confounds), such as sex, that could affect both the exposure and the outcome which makes the association between them is not a cause-and-effect

relationship. The causal methods included Mendelian randomization (MR) which is based on using instrument variables to examine the causation between and an exposure and an outcome.

### 1.7.1 Mendelian randomization

Brain age estimation depends heavily on the brain IDPs and their alterations in both healthy control and patients cohorts. Even in healthy brain aging, brain structure and functions experience notable changes. The alterations within brain IDPs could be related to increasing the risk of an aging related diseases such as AD [49], or the effects of shortening TL [50] or other driving factors. The association between brain-PAD or the alterations of brain function and structure and driving factors was examined using classical statistical and machine learning models including linear regression [50]. In addition, casual methods such as Mendelian randomization was also used to examine the casual association between brain IDPs and new aging driving factors such as TL. MR is a causal method using instrument variables to investigate the casual association between an exposure and an outcome. The valid instrument variables should be independent from the confounds, associated significantly with the exposure and associated with the outcome only through the exposure. These are the three assumptions of MR to chose the valid instrument variables. SNPs are the most commonly used instrument variables because they are independent from the confounds and the association with the exposure and outcome can be investigated through GWAS summary statistics. Figure 1.6 shows the general diagram of MR and the three assumptions.

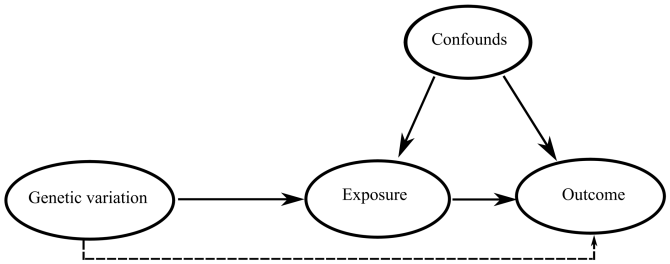


Figure 1.6: Mendelian randomization diagram. The dashed line indicate indirect association while the solid line indicates direct effect.

One of the main advantages of using genetics variation such as SNPs as instrument

variable is that they are not modifiable during lifecourse which leads to reverse causation [51]. The allele of a given SNP was randomly allocated to sperm/egg cells during human gamete formation [52]. Accordingly, they are independent from any confound. The term MR was coined because of its relation to Mendel's Laws [53]. Inverse-variance weighted (IVW) is a typical standard approach to perform MR analysis for two independent samples that relies on the validity of the three assumptions related to instrument variables mentioned above. Weighted median [54], weighted mode and MR-Egger regression [55] methods are used as complementary analysis.

### 1.7.2 Leukocyte Telomere

Leukocyte telomere (LT) are cap structures of chromosomes comprised of tandem repeats of DNA nucleotide sequences [56]. The function of telomeres is to maintain integrity of the chromosomes from degradation. TL are shortening over time with each cell division [57]. Figure 1.7 shows the telomeres and the process of shortening over each cell division. It is believed that TL shortening rate could be a

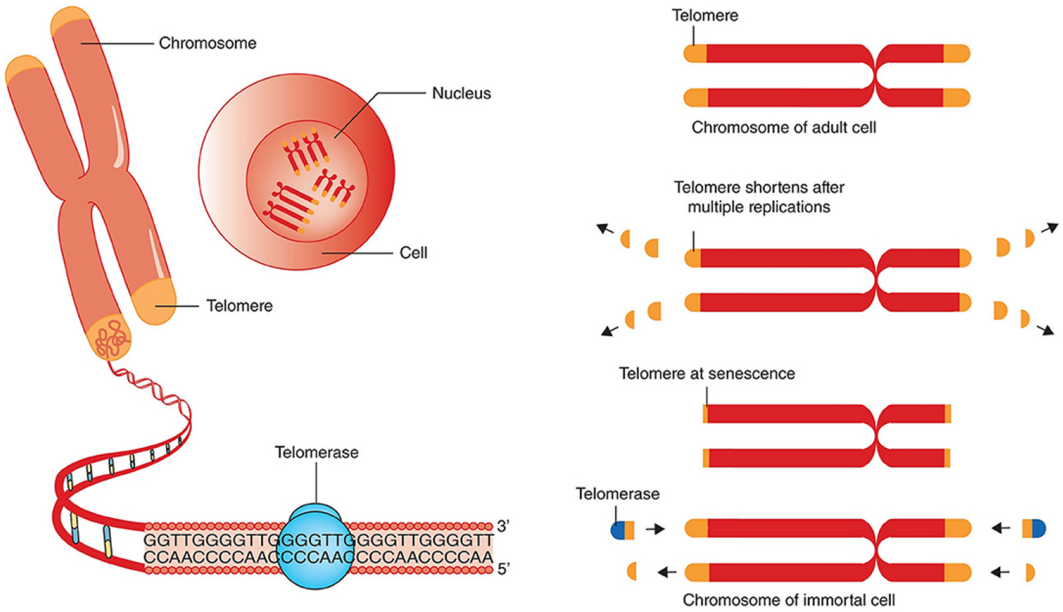


Figure 1.7: Telomeres, their DNA sequence and the shortening over each cell division. Taken from [58].

promising biomarker for the onset of many disease, including those related to aging. There have been many studies to examine the association of TL and wide range of

diseases. The association of TL and AD reveals that shortening TL over time increases the risk of AD [59]. Moreover, a casual association between TL and PD did not reveal any association between TL and increasing the risk of PD [60]. Other diseases and phenotypes were also investigates to test the causal association with TL including blood cell trains [61], cancer and non-Neoplastic [62], systolic blood pressure, pulse pressure, diastolic blood pressure, forced expiratory volume, hypertension and forced vital capacity [63]. Interestingly, shorter TL was associated with appeared older brain age and with brain IDPs extracted from functional MRI [64]. In our study we could not use TL association with brain age as we did not have raw TL measures. In addition, we could not apply MR to assess the causal link between TL and brain age delta for the following reasons. We did not have access to imputed genetic data, instead we had raw genetic data. The raw genetic data might include around 500,000 SNPs after applying quality control steps. Then we could use this number of SNPs to perform GWAS analysis. However, the number is very small comparing to around 15 million SNPs if we used imputed genetic data. We did performed GWAS analysis using the small number of SNPs. When we moved to the next step to perform MR, most of the TL-SNPs were not available in brain delta GWAS and even not appropriate SNPs proxies could be used. For that reason, we preferred to use brain IDPs in our analysis instead of brain age delta.
Using MR to examine the causality between TL and brain IDPs would help to consider TL as a vital factor in brain aging. Moreover, including IDPs from wide range of MRI modalities would provide better possibility of detecting casual associations between TL shortening and brain structure and function.

### 1.7.3 Case study: Alzheimer's disease

Aging related diseases such as AD could cause notable changes in brain structure and function or could increase the rate of atrophy compared to healthy controls. Casual association between 1,578 heritable brain IDPs and AD were investigated using 2-samples MR and other casual methods [65]. Their results indicate 35 IDPs that are causally associated with AD. In addition, the same set of 1,578 brain IDPs were used to examine the casual association using multivariate imaging wide association

study (MV-IWAS), 2-samples MR and other casual methods [49]. Their results detected many casual associations using different casual methods. Consequently, AD among other brain disorders is worth to investigate whether the alterations in the brain might be related to a potential neurodegenerative disease.

## 1.8 United Kingdom Biobank

United Kingdom Biobank (UKBB) is a large biomedical data research and resource involving varieties of data for a half millions of UK volunteers. It has collected and continue to collect deep phenotypic and genetics data related to participants aged from 40 and 69 at the time of recruitment [66]. The aim of UKBB is to provide the medical, blood and biological samples and genetics data globally for researchers across the world to investigate, diagnose, treat and predict different life-threatening disease. All participants provided a formal consent at the recruitment time. The participants have answered wide range of questions related to their lifestyle, health-related factors, socio-demographic with completing physical measures. The collected samples included urine, saliva and blood which can be tested later with different factors such as proteomic and genetics. Further measures were collected related to eye, arterial stiffness, electrocardiograph test and a hearing test. The participants also provided a formal consent to follow up their health-related records [67]. Moreover, UKBB conducted cognitive tests through touchscreens for five minutes at baseline. The assessment testes included visual memory, processing speed and the time of reaction. In addition, some participants performed other tests such as prospective memory, fluid intelligence and working memory [68]. Figure 1.8 shows the wide range of biomedical data collected for each participants taken from [69].
The availability of different kinds of data including tabular and images motivated and encouraged researchers from different research areas including computer science to implement and test different algorithms and statistical models. Machine learning is one of the computer science research fields that shows successful achievements in different domains including biomedical. Machine learning needs reasonable amount of data to train, test and validate a model. The abundance of UKBB data provides the required amount of data to train different machine learning mod-

els which is the key to improve the model performance.

Brain scan using MRI was performed using the modalities, T1, T2 FLAIR, task functional MRI, rest functional MRI, swMRI and diffusion MRI. Structural (T1, T2) brain MRI was acquired using sagittal orientation at 1x1x1mm and 1.05x1x1mm resolution using Siemens 32-channer head coil. The pipeline applied to T1-imaging included brain extraction, defacing and segment brain MRI into cortical and subcortical regions as well as calculating several global volumes such as grey and white matter volume. Diffusion MRI acquired using a spin echo echo-planar sequence T2 weighted baseline volume, 50b = 2000s mm and 50b = 1000s diffusion weighted volumes with 1000 distinct diffusion encoding directions. The steps applied to diffusion MRI included eddy correction and head motion. More details on image acquestions and processing can be found at [70].

During my PhD study, I used UKBB in different ways either directly as measures or their publicly available results such GWAS. The data I used included brain IDPs extracted from different MRI modalities through UKBB application number 2964. These IDPs were used to estimate brain age in different projects. The UKBB application that we had access did not include raw brain MRI as the application was intended for cardiac MRI analysis. For that reason we used the available brain IDPs in my study. For the same reason, we also compared our work with those used brain IDPs and did not include those used raw brain MRI as the comparison is not feasible. In addition, I used genetics data from UKBB to perform GWAS analysis between brain-PAD and genetics variations to explore the influence of genetics bases in brain aging. Finally, different variables representing daily life style, body measures, environment and diet were used from UKBB to perform associations. Consequently, it is worth to mention UKBB in my thesis to give the reader an overview about the used data.

## 1.9 Research contributions and thesis organization

This thesis investigates brain age estimation using brain IDPs from different MRI modalities, mostly for healthy cohorts. In pervasive sense, we mainly focused on brain age estimation using different machine learning models, applying explainable

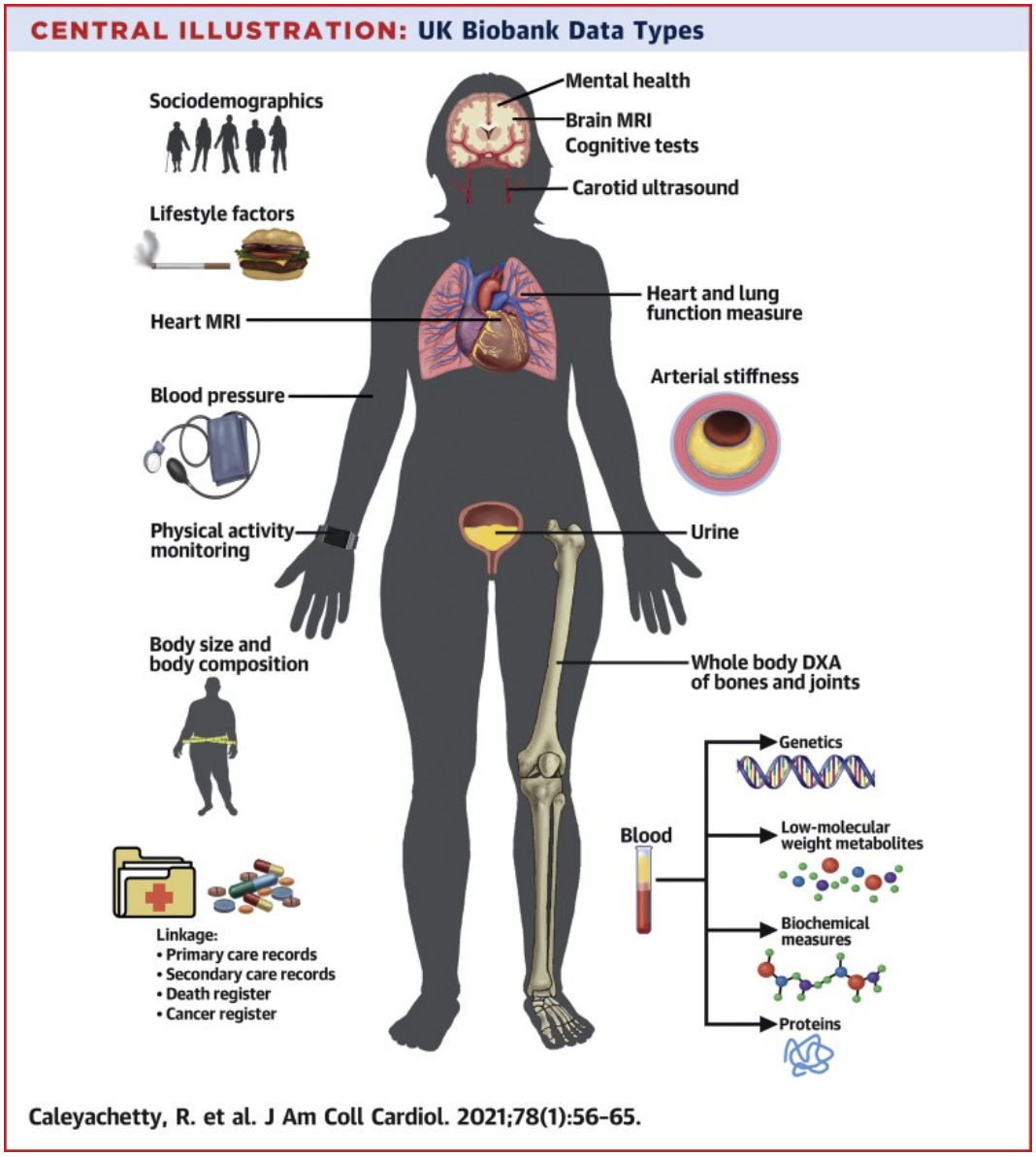


Figure 1.8: UKBB data covering wide range of measures from different part of the body.

machine learning methods, using different approaches to cluster the brain IDPs before feeding the model, and reveal the effect of daily life style and genetics factors in brain aging for different regions of interests within brain. In addition, we examined the factors behind the alterations within brain structure and function in both healthy and patients populations using causal methods. The main contributions of this thesis are summarized in the following points:

- We performed a comparative study using different machine learning models. Many papers published their model performance using a different number

of predictors from different MRI modalities and machine learning models, which made it hard to compare their performance. In Chapter 2, we used 4 machine learning models and 714 brain IDPs extracted from 3 MRI modalities, sMRI, dMRI and susceptibility weighted imaging (SWI). Moreover, we identified the most significant features to model brain age. In addition, we performed an analysis to reveal the association of 8 cardiovascular risk factors and 5 IDPs cardiac magnetic resonance with brain-PAD. The main results of chapter 2 is published in MICCAI workshop on computational diffusion MRI in 2020 [71].

- In Chapter 3, we used 2 well-know machine learning explainability methods that is SHAP [72] and LIME [73] to explain the model globally and locally to identify the most informative predictors. In addition, we presented a new scheme for the assessment of the robustness of explainable methods applied to brain age estimation. We used different number of folds, cross validation and Spearman's rank correlation to assess the validity of the explainable methods. In the chapter we show that the explainable methods were more robust to present a trusted list of significant features when there were more subjects in the training sets. The main contribution of this chapter was published in the IEEE 34$^{th}$ International Symposium on Computer-Based Medical Systems (CBMS) 2021 [74].

- In Chapter 4, we estimated brain age using brain IDPs extracted from only dMRI. In particular, 5 fiber groups were identified based on previous findings using a white matter tracts atlas and IDPs were extracted from each bundle. For each group of dMRI IDPs, which represent a different tract group, we estimated brain age, performed GWAS and conducted an association with daily life style, cardiac risk factors and IDPs extracted from cardiac magnetic resonance. We showed that fiber groups would experience different rate of aging. The main results of the chapter were published on the Nature Scientific Reports journal 2021 [75].

- In Chapter 5, we used MR as a causal method to assess the casual association

of TL and 3,935 brain IDPs extracted from 6 MRI modalities in healthy populations. We conducted this analysis to investigate if TL is the main factor that drives the alterations within brain tissue in healthy brain aging. Our results revealed casual association of telomere length and 193 brain IDPs extracted from dMRI. The main results were submitted to PLOS One journal and are currently under review.

- In Chapter 6, we investigated the casual association of a brain neurodegenerative disease and brain IDPs. This is because there are many studies claiming that the alterations of brain IDPs might be consequences of a brain disorders. For that matter, we used MR for the second time to assess the casual association of AD and the same set of brain IDPs (3,935). Our results showed that indeed there is a causal association of AD and 30 brain IDPs extracted from sMRI, dMRI and fMRI. The main contribution of the chapter is drafted to be submitted to the Brain Communications journal.

**List of publications**

1. **Salih, A.**, Galazzo, I.B., Jaggi, A., Estabragh, Z.R., Petersen, S.E., Lekadir, K., Radeva, P. and Menegaz, G., 2021. Multi-modal Brain Age Estimation: A Comparative Study Confirms the Importance of Microstructure. In Computational Diffusion MRI (pp. 239-250). Springer, Cham. https: doi.org//10.1007/978-3-030-73018-5_19

2. Brusini, L., Boscolo Galazzo, I., Akinci, M., Cruciani, F., Pitteri, M., Ziccardi, S., Bajrami, A., Castellaro, M., **Salih, A.**, Pizzini, F.B. and Jovicich, J., 2020, October. Microstructural modulations in the hippocampus allow to characterizing relapsing-remitting versus primary progressive multiple sclerosis. In International MICCAI Brainlesion Workshop (pp. 70-79). Springer, Cham. https:doi.org//10.1007/978-3-030-72084-1_7

3. **Salih, A.**, Galazzo, I.B., Raisi-Estabragh, Z., Petersen, S.E., Gkontra, P., Lekadir, K., Menegaz, G. and Radeva, P., 2021, June. A new scheme for the assessment of the robustness of explainable methods applied to brain age estimation. In 2021 IEEE 34th International Symposium on Computer-Based Medical Systems (CBMS) (pp. 492-497). IEEE. https:doi.org/ /10.1109/CBMS52027.2021.00098

4. Boscolo Galazzo, I., Brusini, L., Akinci, M., Cruciani, F., Pitteri, M., Ziccardi, S., Bajrami, A., Castellaro, M., **Salih, A.M.**, Pizzini, F.B. and Jovicich, J., 2021. Unraveling the MRI-Based Microstructural Signatures Behind Primary Progressive and Relapsing–Remitting Multiple Sclerosis Phenotypes. Journal of Magnetic Resonance Imaging. https:doi.org//10. 1002/jmri.27806

5. **Salih, A.**, Boscolo Galazzo, I., Raisi-Estabragh, Z., Rauseo, E., Gkontra, P., Petersen, S., Lekadir, K., Altmann, A., Radeva, P. and Menegaz, G., 2021. Brain age estimation at tract group level and its association with daily life measures, cardiac risk factors and genetic variants. Scientific Reports, 11(1). https://www.nature.com/articles/s41598-021-99153-8

6. Boscolo Galazzo, I., Cruciani, F., Brusini, L., **Salih, A.**, Radeva, P., Storti, S. and Menegaz, G., 2022. Explainable Artificial Intelligence for Magnetic Resonance Imaging Aging Brainprints: Grounds and challenges. IEEE Signal Processing Magazine, 39(2), pp.99-116. `https://ieeexplore.ieee.org/document/9721177`

**List of papers under review**

1. Telomere length is causally connected to brain MRI image derived phenotypes: A Mendelian Randomization study. First author. Submitted to PLOS One journal. First author.

2. Investigating Explainable Artificial Intelligence for MRI-based Classification of Dementia: A New Stability Criterion for Explainable Methods. Submitted to ICIP2022. First author.

3. Heart age estimation. Submitted to Communication biology journal. Sharing first authorship with a researcher from Queen Mary University of London.

4. Brain age estimation for ischemic heart disease cohort. Share first authorship. Submitted to Journal of the American College of Cardiology (JACC) and currently under review.

5. Cardiovascular disease and mortality sequalae of COVID-19 in the UK Biobank. Co-author. Submitted to European Heart Journal.

# Chapter Two

# 2 Comparative study to estimate brain age

## 2.1 Introduction

Neuroimaging data have been extensively used to assess brain changes during aging, under both healthy and disease conditions. Moreover, they can be exploited to predict "brain age" which is the apparent biological age of an individual and depends on several endogenous (subject-specific) as well as exogenous (environmental) factors. Metrics derived from various brain MRI sequences have been adopted to estimate brain age, either using raw data or handcrafted features. Brain-PAD is calculated by subtracting chronological age from the estimated one. While a younger-appearing brain might be the result of a healthy life style [76], having an older-appearing brain has been previously associated with poor future outcomes [36] and with an increased likelihood to develop neurodegenerative illnesses such as AD [39].

Statistical models for brain age estimation have been proven to be highly accurate, with prediction performance featuring high $R^2$ values and low MAE in the range of 4-5 years [36]. Most of the studies have investigated this aspect with features derived from a single brain MRI technique, most commonly, conventional T1-weighted sMRI. Morphometric measures from sMRI, such as volume and thickness of grey matter structures, should not be overlooked as they provide information on the individual degree of brain atrophy that encodes aging-induced degeneration [77]. However, more recently, dMRI, SWI, and resting-state fMRI have been explored for potentially providing a richer set of IDPs bringing complementary information [32] [36]. Thus, consideration of IDPs derived from multiple brain MRI sequences would be the most promising approach allowing deeper phenotyping and more complete capturing of the different factors shaping the aging process.

Regarding modeling approaches, the performance depends on the statistical method utilised, as demonstrated by several authors. In a recent paper, Jonsson and colleagues (2019) applied deep learning as well as eight different regression methods

to sMRI-based features extracted from three well-known databases that is Icelandic, the UK Biobank, and the IXI, showing notable differences in the performance parameters across the different models [39]. Niu et al. [76] report similar variation in model performance in their study of brain age estimation with four regression models using several neuroimaging variables (sMRI, dMRI, and resting-state fMRI) in healthy controls and patients with anxiety disorders. In addition, the authors showed the potential for superior prediction accuracy with a multi-modal vs single-modal approach.

The recent availability of large imaging databases has provided new opportunities to exploit the importance of a multi-modal approach for brain age prediction. In this context, the UKBB represents an important resource thanks to its comprehensive repository with genetic and phenotypic data for 500000 subjects aged between 40 and 69 (at recruitment). The UKBB imaging study includes detailed MRI, providing high quality multi-modal neuroimaging data including sMRI, dMRI, SWI and fMRI [78]. These data are linked to detailed clinical, biological and lifestyle information. The availability of such a rich research resource has motivated many researchers to focus on brain age estimation with promising results [32] [36] [40] [39]. Smith et al. [32] estimated brain age using simulated and real data by applying simple linear regression. With regard to real data, 2641 IDPs covering sMRI, fMRI and dMRI were used for 19000 participants. The results, among others, attained MAE = 3.6 years.

In [36], phenotypes from six different MRI modalities were chosen to estimate brain age for 17461 subjects, running a Least Absolute Shrinkage and Selection Operator (LASSO) regression for each modality (MAE range = 3.897 - 5.928 years, where minimum e maximum were found for dMRI and task fMRI, respectively). When all the IDPs were combined, age was more accurately predicted (MAE = 3.515 years). Thirty-four IDPs were deemed informative for the prediction of the brain age after bootstrapping, and were predominantly from sMRI and dMRI.

Ning et al. [40] aimed at assessing the correlation between brain-PAD and alcohol intake, smoking and genetic variations. To this end, 403 morphometric measurements from sMRI were chosen along with LASSO regression (MAE = 3.8 years).

A significant association between brain-PAD and the consumption of alcohol and smoking could be demonstrated.

Finally in [39], sMRI data for 12395 subjects were used to estimate brain age using transfer learning and 3-D Convolutional Neural Network (CNN). In this study, two sequence variants were identified having a strong relation with the brain-PAD. The MAE of the model was 3.63 years.

In the literature many papers can be found aiming at estimating brain age using data from different resources. In addition, different IDPs were used in the model to estimate brain age. These IDPs could be extracted from only one single modality such as sMRI, dMRI or could be derived from multi MRI modalities. Moreover, the number of the IDPs used in the model as predictors is vary and cannot be compared in most cases due to the big variance among them. One other notable and significant factor observed in these works is different models were used to estimate brain age. Simple linear regression was used in many cases while more advanced machine learning models such as deep learning were used in other cases. In addition, different number and kinds of confounds were used to adjust for when brain age was estimated. These factors are shown to be significantly associated with the IDPs and the outcome, which considering different sets of confounds might affect the outcome of the model. The great variability in the number of subjects, IDPs, MRI modalities and statistical models precludes a straightforward comparison of all the studies. However, existing work suggests that: i) sMRI provides relevant IDPs for estimation of brain age; ii) dMRI-based phenotypes are similarly informative and need to be further investigated; and iii) a multi-modal approach can improve, in general, the estimation accuracy.

In consequence, a systematic comparison among different statistical methods is necessary which has not been addressed in existing literature. Therefore, we compared four regression methods in combination with different IDPs for brain age prediction, aiming at providing a balanced comparison across different single-modal and multi-modal approaches. In particular, we focused on LASSO, Simple Linear Regression (SLR), BRR and Support Vector Regression (SVR), while the IDPs used as predictor were derived from sMRI, dMRI and SWI with a clear numeric prevalence of

dMRI. Model performance was assessed using several parameters including MAE, $R^2$ and adjusted $R^2$. Moreover, the associations between individual IDPs and brain-PAD values were calculated for the best model. Finally, the association between brain-PAD with selected biomedical and behavioral features was extracted to assess potential clinical/biological utility.

## 2.2 Data

Data were obtained from UKBB. All the analyses here performed rely on the IDPs extracted centrally by researchers involved in the project [79]. Data were available from n = 16394 participants (age range = 40-70 years, n = 8652 females, n = 7742 males). This comprised a set of 714 IDPs for each subject, representing the summary metrics for sMRI, SWI and dMRI. From sMRI images, morphometric measures of brain volumes were reported as distinct IDPs, both normalised/not normalised for overall head size, in details: total brain volume (GM + WM); volumes for WM, GM and CSF (separately for each compartment); volume of peripheral cortical GM. Volume measures for subcortical structures were also calculated as further IDPs (e.g., thalamus, putamen, hippocampus), generally separated for left/right hemispheres and not normalised for head size. From SWI data, a T2* image was used and the median T2* value estimated as a separate IDP for each subcortical regions of interests(ROIs) identified from sMRI. Finally, several spatially-specific IDPs were extracted from dMRI data by following two different approaches. Indeed, nine dMRI-based indices derived from i) the DTI, such as FA and MD, and ii) NODDI model, such as ODI and ISOVF, were calculated and averaged over specific areas/tracts. In the first approach, dMRI maps were aligned to a population-based WM tract skeleton and all the DTI/NODDI measures averaged over 48 regions defined using the Johns Hopkins University tract atlas [80]. In the second, probabilistic tractography was run for each subject and all the dMRI-based measures averaged within 27 distinct WM tracts. The final set of neuroimaging phenotypes included 25 IDPs from sMRI, 14 from SWI and 675 from dMRI. Full details on the acquisition protocols and image processing pipelines for the UKBB brain data are available at `https://biobank.ctsu.`

ox.ac.uk/crystal/crystal/docs/brain_mri.pdf. The present analyses were conducted under data application number 2964. All participants provided formal consent, details on the UKB Ethics can be found at https://www.ukbiobank.ac.uk/the-ethics-and-governance-council.

## 2.3 Methods

### 2.3.1 Brain age estimation

Four different regression methods including LASSO [81], SLR [82], SVR [83] and BRR [13] were used to estimate the apparent brain age, all having chronological age as the dependent variable. All these models were implemented using Scikit-learn [84] library version 0.22.2 in Python 3.6.9.

In order to examine the impact of different imaging modalities, each of the four methods was run with single-modal and multi-modal brain IDPs, leading to seven different combinations per method. All the imaging features (independent variables) were normalized to zero mean and unit variance to account for the different measurement scales, while the actual age was demeaned only [32]. Gender and education were considered as confound variables and regressed out of all IDPs as in [85] [86]. Data were randomly split into training (80%, n = 13115) and testing (20%, n = 3279) sets, respectively. The test set was used to predict brain ages on unseen data.

Hyper-parameters for BRR, LASSO and SVR were tuned on the training data (further split on 80% for training and 20% for validation) with GridSearchCV and the optimal model was retained. After the parameters were optimized from training data, the optimal model was applied to estimate brain age in the test set. The performance of each model was assessed using ($R^2$) and the MAE. Adjusted $R^2$ was also calculated to account for the different number of predictors in each model.

Recent literature has demonstrated a proportional bias in brain age calculation, which might be caused by dilution bias of the prediction model [35] [87]. Moreover, this bias is also closely connected to the fact that brain age is overestimated in younger subjects and underestimated in older ones, while is more accurately predicted for participants whose actual ages are closer to the mean age of the training

dataset [36] [32]. All these elements lead to a significant dependence of the brain-PAD on chronological age, which resulted to be negatively correlated. Therefore, common practice is to apply a statistical age-bias correction procedure to overcome these limitations [32] [35]. In this study, we adopted the procedure proposed by Beheshti et al. [35] that relies on a linear model given by the following equation:

$$D = \alpha * \Omega + \beta \tag{2.1}$$

where $D$ is the brain-PAD (estimated from training data), $\Omega$ is the chronological age of the training data, $\alpha$ and $\beta$ represent the slope and the intercept. These two measures are subsequently used to correct the brain age predictions in the test set as described in equation 2.2:

$$CPBA = Predicted\,Brain\,Age - (\alpha * \Omega + \beta) \tag{2.2}$$

where CPBA stands for corrected predicted brain age.
After brain age was estimated and bias corrected in the test set, brain-PAD was calculated for each subject. Pearson correlations for predicted brain age *vs* actual age (CPA) and brain-PAD *vs* actual age (CBDA) were calculated twice for each model, before and after bias correction.

### 2.3.2 Associations with IDPs and non-IDP variables

For the best model results, Pearson correlations between brain-PAD values and individual IDPs were calculated in order to identify the strongest associations, highlighting the features which contribute most to the modelling of the brain-PAD as suggested in [32]. The resulting p-values were Bonferroni-corrected for multiple comparison. Of note, the fully deconfounded versions of the IDPs were used in this step (including gender, education and age as confounds). As several studies demonstrated a significant association between brain and heart functionality, especially relying on brain volumetric measurements [88] [89], we also investigated whether a correlation between brain-PAD and heart measures was present. In order to perform this analysis, five measures from Cardiac Magnetic Resonance (CMR)

and eight CRFs were considered. The correlation analysis was performed on a subgroup of the test set (n = 2730), as these measures were not available for all the test set subjects. CMR scans were performed on 1.5 T scanners using a standardised acquisition protocol [90]. The following indices derived for the left ventricle were retained: end-diastolic volume (LVEDV), end-systolic volume (LVESV), stroke volume (LVSV), mass (LVM), and ejection fraction (LVEF). Eight CRFs were also tested, covering biomedical and lifestyle measures: smoking status, material deprivation, body mass index, alcohol intake frequency, physical activity, diabetes diagnosis, presence of hypertension and high cholesterol. Smoking status and alcohol intake frequency were based on self-reports. Material deprivation was reported by UKB as the Townsend deprivation index. A continuous value for the amount of physical activity, measured in metabolic equivalent minutes/week, was calculated. Body mass index was derived from height and weight measures recorded at the baseline. Diabetes, hypertension, and hypercholesterolaemia were defined by cross-checking across self-report and blood biochemistry data. All the cardiac variables were initially normalized to zero mean and unit variance, and the main potential confounds (gender and age) regressed out from the data. Pearson correlation was finally computed between each of these measures and brain-PAD values derived from the twenty-eight model combinations, and the results were Bonferroni-corrected to account for multiple comparison problems.

## 2.4 Results

### 2.4.1 Brain age estimation

Results are summarised in Tables 2.1 and 2.2 reporting the overall performance of the four regression methods combined with the different IDPs. Table 2.1 reports the estimation performance for the test subjects in terms of MAE values before bias correction, as this represents the actual model performance. Results demonstrated that using all the 714 IDPs from the three imaging modalities provided the best model performance in terms of MAE for all regression methods. In particular, BRR gave the best results (MAE = 3.482 years), closely followed by LASSO (MAE = 3.483 years), while SVR performed less accurately among the four tested methods. When

considering the different feature types, the performance of the models using SWI only was worst (MAE $\approx$ 6.0 years) compared to the other single-modal approaches that is sMRI (MAE $\approx$ 4.5 years) and especially dMRI (MAE $\approx$ 3.7 years). When considering the multi-modal models, adding dMRI phenotypes improved the accuracy of all methods. These results were further confirmed by the $R^2$ and adjusted

Table 2.1: Prediction performance of the four regression methods combined with different imaging features. Results are reported in terms of MAE values (years), and the optimal one for each IDPs combination is highlighted in bold.

| **Mean Absolute Error** | | | | | |
|---|---|---|---|---|---|
| **IDPs** | **Number of features** | **BRR** | **SVM** | **SLR** | **LASSO** |
| sMRI | 25 | 4.509 | **4.471** | 4.506 | 4.509 |
| SWI | 14 | 6.026 | 6.0411 | **6.024** | 6.025 |
| dMRI | 675 | **3.733** | 3.758 | 3.761 | 3.738 |
| sMRI+SWI | 39 | 4.429 | **4.393** | 4.424 | 4.427 |
| sMRI+dMRI | 700 | **3.498** | 3.559 | 3.525 | 3.5 |
| SWI+dMRI | 689 | **3.717** | 3.74 | 3.741 | 3.719 |
| All | 714 | **3.482** | 3.526 | 3.512 | 3.483 |

Table 2.2: Prediction performance of all the tested models in terms of $R^2$ and Adjusted $R^2$ values.

| | **BRR** | | **LASSO** | | **SLR** | | **SVR** | |
|---|---|---|---|---|---|---|---|---|
| **IDPs** | $R^2$ | Adj_$R^2$ | $R^2$ | Adj_$R^2$ | $R^2$ | Adj_$R^2$ | $R^2$ | Adj_$R^2$ |
| sMRI | 0.445 | 0.441 | 0.446 | 0.441 | 0.446 | 0.441 | 0.445 | 0.440 |
| SWI | 0.085 | 0.081 | 0.085 | 0.081 | 0.085 | 0.081 | 0.075 | 0.071 |
| dMRI | 0.613 | 0.512 | 0.612 | 0.511 | 0.606 | 0.504 | 0.604 | 0.501 |
| sMRI+SWI | 0.464 | 0.458 | 0.464 | 0.458 | 0.465 | 0.458 | 0.468 | 0.462 |
| sMRI+dMRI | 0.654 | 0.560 | 0.653 | 0.559 | 0.648 | 0.553 | 0.642 | 0.545 |
| SWI+dMRI | 0.618 | 0.516 | 0.61 | 0.515 | 0.611 | 0.507 | 0.609 | 0.505 |
| All | 0.658 | 0.562 | 0.657 | 0.562 | 0.652 | 0.555 | 0.650 | 0.553 |

$R^2$ parameters (Table 2.2), for which the lowest value was reached using the SWI IDPs ($R^2$ = 0.075-0.085). When the IDPs from sMRI and dMRI were used jointly in the model, the performance was improved and very close to the one reached by using all the IDPs, and this finding held for all the four regression methods. For the sake of completeness, CPA and CBDA were calculated before and after bias correction, leading to the results summarised in Table 2.3. When using all the 714 IDPs, the correlation between brain-PAD and actual age decreases towards zero after applying the bias correction steps. Conversely, CPA increased after bias correction in all four methods. Figure 2.1 shows the correlation between brain-PAD and the actual age. The figure shows that after the correction steps were implemented, the correlation drop down to around zero. It confirms that the predicted brain age was affected by bias.

Table 2.3: Correlation values between predicted brain age vs actual age (CPA) and between brain-PAD vs actual age (CBDA), before and after bias correction.

| The model | Before correction | | After correction | |
|---|---|---|---|---|
| | CPA | CBDA | CPA | CBDA |
| BRR | 0.811 | -0.592 | 0.903 | -0.014 |
| LASSO | 0.810 | -0.576 | 0.900 | -0.018 |
| SLR | 0.807 | -0.559 | 0.896 | -0.026 |
| SVR | 0.806 | -0.597 | 0.902 | -0.015 |

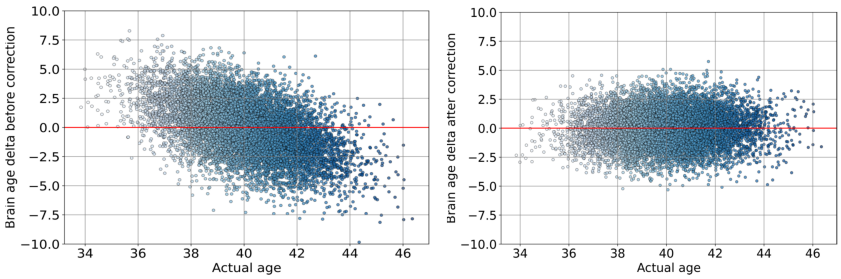


Figure 2.1: The correlation between brain-PAD and actual age before and after the correction steps were implemented.

### 2.4.2 Association with brain IDPs

Considering that the BRR method combined with all the IDPs reached the lowest MAE and highest $R^2$/adjusted $R^2$, here we report associations between individual IDPs and brain-PAD values estimated from this model. In particular, Table 2.4 shows the first ten significant correlations (after correction for multiple comparisons), revealing a strong and significant association between these IDPs and the brain-PAD. As further note, the association between brain-PAD values and individuals IDPs were largely overlapped for the other regression methods, especially concerning the features in the top 10 positions. The order of the most significant features that are associated with the brain-PAD is similar in the four methods, although the correlation values changed across them.

As it can be appreciated, the volumetric measurements from sMRI such as GM volume and volume of peripheral cortical GM (both normalised for head size) were negatively correlated with the brain-PAD. Diffusion measures from DTI (such as MD, L1, L2 and L3) and from NODDI (such as ISOVF) in fornix were positively correlated with the brain-PAD, while FA revealed an opposite pattern.

Table 2.4: Strongest associations between brain-PAD values estimated from the winning model (BRR with all IDPs) and individual IDPs for test set subjects.

| IDPs | Correlation |
|---|---|
| Volume of grey matter (normalised for head size) | -0.511 |
| Volume of peripheral cortical grey matter (normalised for head size) | -0.496 |
| Volume of brain, grey+white matter (normalised for head size) | -0.443 |
| Mean ISOVF in fornix on FA skeleton | 0.409 |
| Mean L1 in fornix on FA skeleton | 0.403 |
| Mean MD in fornix on FA skeleton | 0.402 |
| Mean L3 in fornix on FA skeleton | 0.396 |
| Mean L2 in fornix on FA skeleton | 0.389 |
| Mean FA in fornix on FA skeleton | -0.388 |
| Mean L2 in fornix cres+stria terminalis on FA skeleton (left) | 0.371 |

### 2.4.3 Association with cardiac variables

Table 2.5 reports Pearson correlations between brain-PAD derived from the winning model (BRR with all IDPs) and CMR/CRFs measures (test set). For CMR, no significant associations were found after multiple comparison correction ($p_{FDR} > 0.05$), and only the correlation with the LVM was significant before correction ($p = 0.021$). Regarding CRFs, all parameters except exercise and alcohol were significantly associated with the brain-PAD ($p_{FDR} < 0.05$) .

Table 2.5: Correlation between CMR, CRFs and brain-PAD.

| Cardiovascular Risk Factors | | | | Cardiac Magnetic Resonance | | | |
|---|---|---|---|---|---|---|---|
| Measure | Correlation | p-value | $p_{FDR}$ | Measure | Correlation | p-value | $p_{FDR}$ |
| Smoking | 0.056 | 0.003 | 0.024 | LVEDV | 0.006 | 0.725 | 1 |
| Deprivation | 0.067 | 0 | 0.003 | | | | |
| Body Mass Index | 0.053 | 0.005 | 0.040 | LVESV | -0.004 | 0.795 | 1 |
| Alcohol | 0.038 | 0.046 | 0.369 | | | | |
| Exercises | 0.001 | 0.920 | 1 | LVSV | 0.015 | 0.420 | 1 |
| Diabetes | 0.087 | 0 | 0 | | | | |
| Hypertension | 0.066 | 0 | 0.004 | LVM | 0.044 | 0.021 | 0.107 |
| High Cholesterol | 0.056 | 0.003 | 0.025 | LVEF | 0.024 | 0.209 | 1 |

## 2.5 Discussion

In this study, we investigated whether chronological age could be accurately predicted using brain MRI IDPs as predictor variables in various statistical models using data in the UKB. In particular, we focused on four well-known regression methods (SLR, SVR, LASSO and BRR) and considered measures from sMRI, SWI and dMRI as IDPs, either alone or in combination. Regarding the regression methods, overall, BRR achieved the highest accuracy as measured by MAE, R2 and adjusted R2 values. In particular, when dealing with a relatively small number of

IDPs ($< 50$), for example in models with sMRI/SWI features only, better results were obtained using SVR and SLR. Conversely, in cases where a greater number of features was included, BRR reached the best performance, possibly because of its ability to handle multicollinearity between IDPs [91] [92].

Previous studies addressing modelling brain age using UKB data report MAE values between 3.5 - 3.8 years. Of note, Peng et al. [93] achieved the lowest MAE (2.14 years) although leveraging from deep CNN model, Simple Fully Convolutional Network, using sMRI from UKB for 14503 participants. In our study, the accuracy reached by BRR model in the different conditions was comparable (and even better in some cases) to such benchmarks, despite the generally lower number of subjects and MRI features.

Regarding the imaging predictors, models including all the 714 IDPs from the three brain MRI sequences had the best performance. However, when considering models with single-modal IDPs, dMRI reached the highest accuracy in terms of MAE values (MAE $\approx$ 3.7 years) compared to sMRI (MAE $\approx$ 4.5 years) and especially SWI (MAE $\approx$ 6.02 years), and this was further confirmed by the $R^2$/adjusted $R^2$ values. This might indicate that age-related alteration of brain can be better detected by dMRI, in agreement with literature findings [94].

The variations in the models performance when one MRI modality used to estimate brain age needs a further statistical test to confirm that the difference is significant.

A previous study also found similar results and further confirm that dMRI phenotypes are more informative than SWI IDPs in predicting brain age [36]. Phenotypes from sMRI and dMRI were generally the most informative for age prediction, as further supported by the correlation analysis between brain-PAD values and IDPs. Indeed, the strongest associations were found for features based on these modalities. In particular, our study revealed that brain-PAD was negatively correlated with volumetric measures, while positively correlated with both ISOVF and diffusivities in the fornix.

GM volume was the most informative phenotype, in line with previous studies [36] [32]. This might be related to the fact that brain volume changes considerably over time and decreases during the aging process, causing atrophy [95] and macroscopic vari-

ations. Our analysis highlighted a prominent role of dMRI IDPs. Differences in diffusion properties across the life span have been demonstrated along specific WM tracts [94]. Diffusivity and FA values across the fornix spanned the first 10 ranking position, preceded only by atrophy measures in GM and WM. Noteworthy, the fornix is among those tracts that mature very early [96]. The IDPs that are present in the top 10 association ranking are, besides FA and MD, ISOVF, that is the isotropic volume fraction as estimated by the NODDI model, and the three tensor eigenvalues L1, L2 and L3 that represent the axial (L1) and transversal (L2, L3) diffusivities. A reduction in the FA and an increase in diffusivity, as indicated by a positive correlation of ISOVF, MD, L1, L2 and L3 with brain-PAD, could indicate impaired WM integrity. Moreover, myelin breakdown might be measured by radial diffusivity (L2 and L3) alterations, while increasing in apparent diffusivity value might be a sign of axonal disruptions [97]. Furthermore, AD (L1) and RD (L2 and L3) have been observed to increase in elderly people which may be a signal of deterioration of the WM fibers [98]. Noteworthy, ISOVF has been observed to increase in older people in most of the major tracts, pointing to a disrupted integrity [99]. Our results are in agreement with such findings reporting a negative association of FA and a positive association of L1 , L2, L3 and MD in fornix with brain-PAD. Fornix tracts have a vital role in memory tasks, specially episodic memory. Alteration in diffusion measures during aging process might be good biomarkers for neurological diseases that are related to memory impairments [96]. This could indicate that such IDPs are more prone to alteration over the life span of an individual at least over specific WM tracts, making them potential biomarkers for the aging process in health and disease.

Regarding the associations with CMR measures, our study revealed a significant association with LVM, however there was loss of statistical significance after multiple comparison correction. A previous study reported association of increase in LVM with alterations in WM microstructure in elderly people [100]. In our study, the limited age range in the UKB did not permit consideration of relationship in very old individuals. Among the CRFs, all measures except exercise and alcohol were significantly correlated with brain-PAD ($p_{FDR} < 0.05$), inline with what described by

Cole et al [40][101], despite using a different number of IDPs and subjects for estimating brain-PAD. In conclusion, results suggest that dMRI IDPs play a prominent role in reducing the MAE and rank high in the association study, providing evidence of the potential of dMRI IDPs as biomarkers of aging in health and disease. Future work will investigate the integration of other IDPs such as functional MRI, graph-based measures from brain connectomes as well as the genetic information to pursue the holistic path.

# Chapter Three

# 3 Explainable deep learning

## 3.1 Introduction

DL has shown successful achievements in many applications including within the medical field [102] [41]. However, decisions generated by complex DL models are not transparent and so the rationale for model outputs is not always understandable. Accordingly, complex models such as DL are considered as a "black box". The ability to explain the decision making of DL tools is key to facilitating their acceptance. Thus, breaking down the black box is highly important.
DLe aims at uncovering the mysteries of how models make decisions and how each feature contributes to the overall model output [103]. Shapley additive explanation (SHAP) and Local Interpretable Model-agnostic Explanation (LIME) [73] are two widely used DLe methods [104] [105] [106].
Brain age has been estimated using different models and data-set [32] [36]. This leads to identify different sets of significant features that model brain age.

### 3.1.1 Explainability methods

#### SHAP

SHAP is an DLe method that explains how the model makes a decision and the contribution of each feature both globally and locally. It helps to rank the features in the model and that features ranked list is one of the model explanation goals. It is a model-agnostic method that means it can be applied to any model. It is an additive feature importance measure. It is based on game theory where each feature is considered as a player and the output or the prediction is the payoff [72]. The aim of SHAP is to calculate the contribution of each feature to explain the prediction of an instance $x$. SHAP calculates a value for each feature based on collation game theory. The data instance of the features acts as a players in the game. A player can be a single feature as in the case of tabular data. In addition, a player could

be a group of features as the case to use image data and groups of pixels that are identified as the informative ones, then the prediction distribution among them. The SHAP value tells us how the prediction is fairly distributed among the features. The equation to calculate SHAP value for a feature is as follows:

$$g(z^{'}) = \phi_0 + \sum_{j=1}^{M} \phi_j z_j^{'} \tag{3.1}$$

where $g$ is the explanation model, $z^{'}$, is a binary variable that represents whether $x_j$ is present or not, $M$ is the maximum coalition size and $\phi_j$ is feature attribution for a feature $j$ and $\phi_0$ is the bias. This value shows to what extent the feature is significant in the model's decision. SHAP has three desirable properties that are: local accuracy, missingness and consistency. Local accuracy means the sum attributions of local feature equals the difference between the base rate and the model output. Missingness is that the feature has no impact if it is missing in the original data and attributed to zero. Finally, consistency is the impact of a significant feature that should not be decreased if the model is changed [72].

**LIME**

LIME is a local surrogate model-agnostic interpretability method that explains and helps to illuminate a machine learning model which results in comprehensible predictions. It explains the prediction for a single subject and therefore it is suitable for local consideration. LIME ranks the features based on their contribution to predict an outcome which is one of the aims of explainablity methods [73]. Furthermore, LIME performs sample-based evaluation, not model-based one. Surrogate models are those which are trained to approximate the model prediction. However, it does not train a global surrogate model, instead it trains a local surrogate model to explain the predictions for an individual. LIME generates a new data-set by permuting the original data with their corresponding predictions. Then it calculates the similarity between the original and the new permuted data. Thereafter, it uses the permuted data to predict the outcome. Then, it selects $m$ number of features that best describe the predicted outcome. It uses a simple linear model with $m$ features weighted by

the similarity measures to the original data. Finally, the resulting features weight explains the contribution of the feature locally [73]. The formula of LIME is as follows:

$$\varepsilon(x) = argmin_{g \varepsilon G} \pounds(f, g, \pi_x) + \Omega(g) \tag{3.2}$$

where $\varepsilon(x)$ is the explanation, $\pounds$ - a loss function, $\Omega(g)$ - the complexity term, $g$ - is the explainer, $f$ - is the model that we want to explain, $G$ - is the complete hypothesis space for the given explainability method and $\pi_x$ is a weight assigned according to the $x$ proximity.

### 3.1.2 Validating explainability methods

There have been various approaches to evaluate DLe methods [107]. Three main levels have been proposed to evaluate explainability given by the models that is application-grounded [108], human-grounded [109] and functionality-grounded evaluation [110]. The application-grounded evaluation conducts an experiment in real-world application and then evaluates and tests it by an end-user who is expert in the domain. This method is expensive due to the expert involvement as well as because it is difficult to compare results from different domains. Human-grounded evaluation is cheaper, as it does not require experts in the domain, it assess the method using laypersons. However, it disregards experts in its assessment. Finally, functionality-grounded evaluation does not require human evaluation. In contrary, it evaluates the explanations using some sort or proxies such as measuring the uncertainty in the explanations methods and model sparsity [111].
Functionality-grounded might be the promising one as it evaluates automatically the explainability methods by using some quantitative rather than qualitative methods as it is the case for human and application-grounded evaluation.

Several proxies have been proposed to evaluate the explainability methods based on the functionality-grounded strategy. Silva et al. [112] proposed three functionality-grounded evaluation methods that is Completeness, Correctness and Compactness. Completeness means the explainability should be possible to be implemented in other domains when the audiences can validate and verify it. They consider completeness by using a fraction of the training set covered by the explanation. Correct-

ness means that the explanation should be accurate and measures it by the accuracy. Finally, the compactness is measured by the time needed to understand the explanation is proportional to its length.

Montavon et al. [110] proposed other two proxies that can be implemented to evaluate the explainability methods that are Explanation continuity and Explanation selectivity. Explanation continuity assumes that if two data points are almost equivalent, then the explanations of their predictions should be also equivalent. They quantify the continuity by looking for strongest variation of the explanation $R(x)$ in the input domain. Explanation selectivity assumes that there should be a sharp reduction in model performance when relevance features that are identified by the explainability methods are removed from the model. This approach was proposed for image data named pixel-flipping. They first sort the features from the most relevant one to the least relevant one. Then they record the current function of $f(x)$. Thereafter, they remove the $ith$ relevant feature and record again the function value. They repeat it based on the number of the features in the model. Finally, they plot all the recorded function values and return the area under the curve for the plot.
However, explainability might be affected negatively by the sample size used to train and test the model [113] [114] which is not considered in the previous approaches. Small sample size might reduce the model performance and leads to identifying relevant features incorrectly. In our approach, we propose a validation scheme based on Spearman's rank correlation and cross-validation as proxy to functionally evaluate the explainablity methods. Our method identifies significant features in a DL model for brain age estimate using the UKBB [67]. Precisely, our study aims to: i) estimate brain age using DL, ii) describe a novel application of SHAP values to the prediction of brain age using UKBB data, iii) interpret the model globally and identify significant features by SHAP, iv) interpret the model locally and identify significant features by LIME and v) evaluate SHAP and LIME methods using a new validation scheme based on cross-validation and Spearman's rank correlation as proposed proxy.

## 3.2 Dataset

The data used from the UKBB include three brain MRI modalities, sMRI, SWI and dMRI. 714 features for 16394 subjects (7742 male and 8652 female) were used in our study to estimate the brain age. The features were composed of 25 sMRI IDPs, 14 SWI IDPs and 675 dMRI IDPs. The IDPs were extracted from brain MRI images centrally by researchers at UKBB and made them available within the UKBB data showcase `http://biobank.ctsu.ox.ac.uk/crystal/index.cgi`. These brain MRI IDPs represent different quantitative measures of brain structure and function. The phenotypes extracted from sMRI reflect volumetric measures of the brain regions while the IDPs extracted from dMRI represent the movements of molecular water in the brain tissue that is represented in summary metrics using DTI and NODDI. SWI is another MRI technique that is sensitive to local components which results in distortions of the magnetic field. The phenotypes extracted from SWI represent various local components in the brain tissues such as diamagnetic calcium, blood and iron [115]. Full details of the acquisition parameters can be found in [116]. The majority of UKBB participants was healthy at the time of scanning. Therefore, no subject has been excluded in our study [32].

Several studies have demonstrated the association between brain aging and vascular risk factors and cardiac index [117] [118]. Accordingly, the association was calculated between brain-PAD and conventional CMR features. The CMR included seven metrics: LVEDV, LVESV, LVSV, LVM, right ventricular end-diastolic volume (RVEDV) , right ventricular end-systolic volume (RVESV) and right ventricular stroke volume (RVSV). Indexation to body surface area (calculated according to Du Bois equation) was applied to volume and left ventricular mass measures. The association was conducted for 3049 subjects that had both CMR data and brain-PAD in the test set. P-value was corrected for the number of features using the Bonferroni method [119].

## 3.3 Methods

### 3.3.1 Feature processing

Given the problem of brain age estimation, we consider as features IDPs extracted from three brain MRI modalities that is structural MRI, diffusion MRI and susceptibility weighted imaging MRI. The features were standardized to have the same range and mean value of zero while the actual age was demeaned and used as the dependent variable [32]. Gender and education levels were used as confounds [40] and regressed out the IDPs using a linear regression model.

### 3.3.2 Deep Learning model

DL models are artificial neural networks that consist of multiple layers so-called hidden layers between the input and output layers. Each layer involves many nodes which transform the data into more abstract components. In addition, it also involves activation functions between the layers that define the output of a node by a given input. Moreover, they might involve dropout layers that deactivate some nodes in a layer or layers to regularize the model. DL has the ability to learn and make decisions on its own. Another valuable advantage of DL is that it can handle the non-linear relationships between the input data and the outcome [120]. The general architecture of a DL model is illustrated in figure 3.1. There is no standard

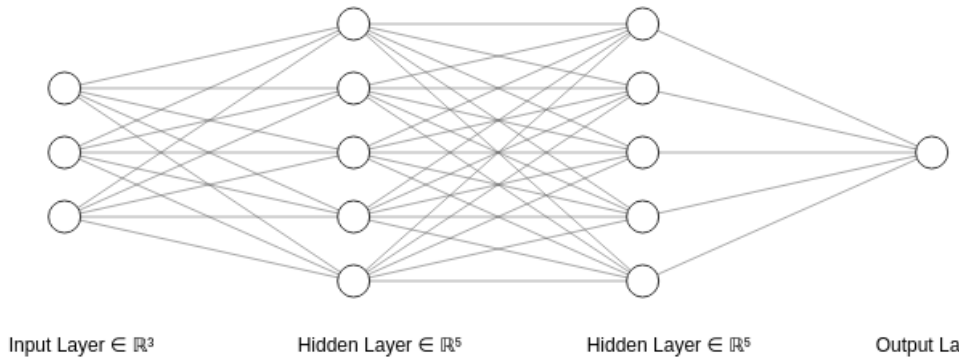


Figure 3.1: General architecture of DL.

method to chose the number of hidden layers, the number of nodes in each layer, which activation function and dropout rate to use. In that matter, hyperparameter-tuning is used to find the optimal architecture of the model by using many parame-

ters and those who produce the lower error in the output are considered the optimal ones [121].

The DL model applied to brain age estimation was designed based on hyper-parameter tuning using training data. The data was divided randomly into training (80%) and testing sets (20%); the latter comprised unseen data and was used to test the model performance. The architecture of our DL model involved 4 fully connected layers. Table 3.1 shows the tuned parameters with the values used to find the optimal values for each parameter. Optimal parameters were chosen based on MAE as the

Table 3.1: The parameters used in our DL model for brain age estimate

| Parameters | Value |
|---|---|
| Number of neurons in layer 1 | 150: 750. jumping by 50 |
| Number of neurons in layer 2, 3 and 4 | 50: 350. jumping by 50 |
| Activation function | relu, softmax and sigmoid |
| Dropout rate | 0 :0.2. jumping by 0.05 |

valuation criterion as follows:

$$MAE = \frac{1}{n}\sum_{i=1}^{n}\left|Y_i - \hat{Y}_i\right| \tag{3.3}$$

where $Y$ is the actual value, $\hat{Y}_i$ is the predicted value and $n$ is the number of observations. Table 3.2 shows the best parameters that achieved lowest MAE in the training data-set and validated on validation data-set using Randomized SearchCV [122]. These values were used as the optimal parameters for the model and were used on the test data. We had to apply the correction to the predicted brain age to account for

Table 3.2: The best parameters based on the MAE

| Parameters | Value |
|---|---|
| Number of neurons in layer 1 | 350 |
| Number of neurons in layer 2, 3 and 4 | 50, 100 and 300 respectively |
| Activation function in Layer 1, 2, 3, 4 | sigmoid, relu, relu and relu respectively |
| Dropout rate in layer 1, 2, 3, 4 | 0.15, 0, 0 and 0 respectively |

more accurate estimates for subjects with age close to the mean age [34]. Different methods have been proposed to correct the estimated brain age. We adopted the method proposed by [35]. First, the brain age was predicted in the training data and the brain-PAD was computed by subtracting chronological age from the predicted brain age. We used the brain-PAD in the training with actual age to calculate the

slope and intercept utilizing a simple linear regression model as in the equation: $BAD = \alpha * \Omega + \beta$, where *BAD* is the brain-PAD (estimated from the training data), $\Omega$ is the chronological age of the training data, $\alpha$ and $\beta$ represent the slope and the intercept, respectively. The two measures, $\alpha$ and $\beta$, were subsequently used to correct the predicted brain age in the test set as described in:

$$CPBA = Predicted\,Brain\,Age - (\alpha * \Omega + \beta),$$

where CPBA stands for the corrected predicted brain age in the test set. After we estimated the brain age and corrected the bias, the brain-PAD was calculated for each subject in the test set. The correlation between the predicted brain age, brain-PAD and actual age was calculated. The correlation was computed twice, before and after the correction steps to check the effectiveness of the correction.

### 3.3.3 Applying SHAP and LIME

We have calculated SHAP value for each feature in the training data. Because we used cross-validation in the training data where the data was divided into 10 folds, nine for training and one for validating, the SHAP value was calculated 10 times for each validation fold. The value is computed by fitting the model with training data to SHAP and then calculation of the SHAP value for the validation folds. *N* lists (in our case, $N = 10$) of significant features are sorted by the most significant representing the *N* data validation folds. These ranked lists of the significant features are based on the samples selected for each fold. Thereafter, SHAP value is obtained for the test data as unseen data. The SHAP value for each feature in the test data was computed by fitting the model with the whole training data, and then calculate it for test data.

LIME was calculated locally for a subject chosen randomly in each fold from the validation data. It was calculated by fitting the model with training data to LIME, then it is estimated for a subject in the validating data. Thereafter, LIME was obtained for a subject in the test data chosen randomly. Accordingly, *N* lists of significant features were considered for *N* subjects in the validation and test data sorted by the most significant one (in our case $N = 11$).

### 3.3.4 A new evaluation scheme based on Spearman's rank correlation

Using different numbers of samples in the model might have significant effects on the model output and can result in identifying different sets of significant features to explain the model decision [114] [123]. Then the question is which one of these lists of significant features should be considered to explain the model. Our hypothesis is that significant features explaining the model should depend as few as possible from the concretely selected training set. That is differently selected subsets of training data should give the same explanation. For this reason, we applied a resampling method such as cross-validation to consider different sets of samples from the population and obtain the corresponding lists of significant features. Then, instead of considering one list of features to explain the model, we get the list of features most correlated to the rest lists using different number of folds. Hence, we compute a ranked correlation between the ranked lists to check if there is a significant correlation among the lists. If the correlation is significant, then we conclude that the explainability method could identify the significant features for each sample correctly. On the contrary, if the correlation is not significant among the ranked lists, then we conclude that the explainability method is not consistent and stable to explain the model.

Spearman's rank correlation is a non-parametric measure to assess the correlation between two ranked lists of variables. It also assesses the monotonic relationships between the variables. Its value ranges from -1 to 1, -1 meaning highly negative correlation between the ranks, 1 highly positive correlation between the ranks while 0 means there is no association between the ranks. The formula to calculate the rank correlation is as follows:

$$p = 1 - \frac{6\sum d_i^2}{n(n^2-1)} \tag{3.4}$$

where p is the Spearman's rank correlation (SRC), $d_i$ - the difference between the ranks of corresponding variables and $n$ - the number of observations [124]. The interpretation of the SRC varies from one domain to another. For example in the medicine field, 0.2 and below is considered as weak, 0.2 to 0.5 as fair, 0.6 to 0.7 as

moderate, 0.8 to 0.9 as strong and 1 as perfect [125].

We used the SRC [124] to evaluate the consistency and variability of SHAP and LIME outcomes. From each LIME and SHAP, we consider $N = 11$ lists of significant features, one for each fold and one for the test data. In our validation scheme, we proposed to use the Spearman's correlation between the lists of the folds and the test for each SHAP and LIME as well as between the SHAP and LIME estimates. Then, we used the SRC value and the corresponding statistical significance [125], for validation.

### 3.4 Results

This section presents the results achieved by means of the proposed method for assessing the robustness of explainability methods. The mean of MAE of the brain age estimate using different numbers of folds was 3.44 with standard deviation 0.105. The SRC coefficient between the ranked lists of significant features of the SHAP method for each fold and the test data is summarized in Table 3.3 in the case of 10 folds. The correlation value ranged from 0.82 to 0.99 with p-value less than 0.001. The value was consistent across the folds and the test data indicating a high level of consistency. Table 3.4 shows the Spearman's rank correlation coefficient

Table 3.3: Spearman's rank correlation between the ranked lists of significant features for each fold and for the *test* data. F1, F2 stands for fold-1, fold-2, etc.

| Fold | Test | F1 | F2 | F3 | F4 | F5 | F6 | F7 | F8 | F9 |
|---|---|---|---|---|---|---|---|---|---|---|
| Test | – | | | | | | | | | |
| F1 | 0.83 | – | | | | | | | | |
| F2 | 0.83 | 0.84 | – | | | | | | | |
| F3 | 0.84 | 0.86 | 0.85 | – | | | | | | |
| F4 | 0.84 | 0.85 | 0.83 | 0.86 | – | | | | | |
| F5 | 0.83 | 0.86 | 0.83 | 0.85 | 0.87 | – | | | | |
| F6 | 0.83 | 0.84 | 0.84 | 0.85 | 0.85 | 0.85 | – | | | |
| F7 | 0.85 | 0.85 | 0.84 | 0.87 | 0.85 | 0.85 | 0.85 | – | | |
| F8 | 0.83 | 0.83 | 0.82 | 0.85 | 0.84 | 0.82 | 0.84 | 0.84 | – | |
| F9 | 0.84 | 0.85 | 0.82 | 0.85 | 0.85 | 0.84 | 0.86 | 0.85 | 0.84 | – |
| F10 | 0.99 | 0.83 | 0.83 | 0.84 | 0.84 | 0.83 | 0.83 | 0.85 | 0.83 | 0.84 |

between the ranked lists of significant features for each fold and the test data locally by LIME when 10 folds were used. The correlation value ranged from 0.89 to 0.76 with p-value less than 0.001. Again, the correlation values were consistent across the folds and the test data. Analysing the p-value, one can conclude that the correlation is significant. We examined the impact of using different numbers of folds

Table 3.4: The rank correlation between the ranked lists of significant features using LIME value for each fold and for the *test* data.

| Fold | Test | F1 | F2 | F3 | F4 | F5 | F6 | F7 | F8 | F9 |
|---|---|---|---|---|---|---|---|---|---|---|
| Test | – | | | | | | | | | |
| F1 | 0.76 | – | | | | | | | | |
| F2 | 0.76 | 0.78 | – | | | | | | | |
| F3 | 0.75 | 0.78 | 0.78 | – | | | | | | |
| F4 | 0.77 | 0.78 | 0.78 | 0.79 | – | | | | | |
| F5 | 0.77 | 0.78 | 0.77 | 0.77 | 0.81 | – | | | | |
| F6 | 0.76 | 0.77 | 0.77 | 0.78 | 0.79 | 0.80 | – | | | |
| F7 | 0.76 | 0.78 | 0.79 | 0.79 | 0.80 | 0.81 | 0.79 | – | | |
| F8 | 0.78 | 0.78 | 0.77 | 0.79 | 0.78 | 0.79 | 0.78 | 0.77 | – | |
| F9 | 0.77 | 0.77 | 0.76 | 0.78 | 0.79 | 0.78 | 0.80 | 0.79 | 0.78 | – |
| F10 | 0.89 | 0.77 | 0.76 | 0.76 | 0.76 | 0.76 | 0.76 | 0.78 | 0.79 | 0.76 |

(3, 5, 10, 20, 40) on the correlation between the ranked lists of significant features. Figure 3.2 shows the mean and standard deviation of the correlation values between the ranked lists of significant features using different number of folds. We observed that the mean value increased with the number of folds until a plateau was reached for 20 folds, where it stabilizes. In addition, the standard deviation value was very small from 10 folds on and much smaller when we increased the number of folds indicating that the values of correlation clustered around the mean value. Moreover, the figure shows that the mean values in the case of 20 and 40 folds are very close, suggesting that there may be no further benefit from using higher number of folds beyond this level. Changing the number of folds amounts to changing the cardinality of the training set. Figure 3.3 shows the mean and standard deviation of the correlation values between the ranked lists of significant features for training sets of changing cardinality. As it can be observed, the mean value of the correlation among the rankings increases with the number of training samples, while the variance decreases, as expected. Table 3.5 shows the Spearman's rank correlation between the ranked lists of significant features for SHAP and LIME. Despite the fact that SHAP was calculated for all samples globally and LIME was calculated for one single sample chosen randomly from the validation set for each fold, the correlation is significant between both methods in all folds and the test data.

## 3.5 Discussion

The proposed criterion to assess feature ranking robustness rests on the assumption that invariance with respect to folds and methods witnesses in favor of robustness. It

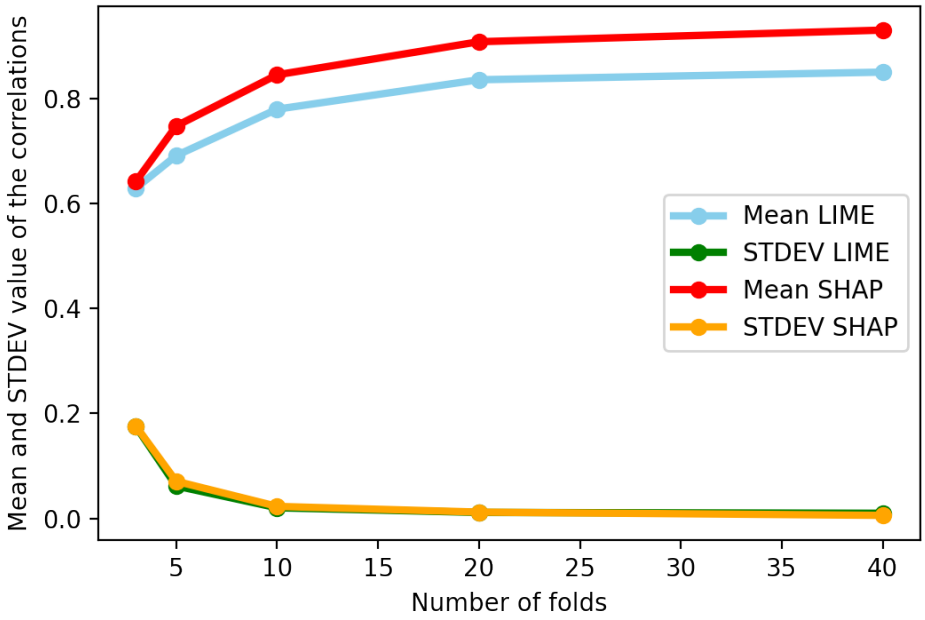


Figure 3.2: Mean and standard deviation of the correlation between the ranked lists of significant features as a function of the number of folds.

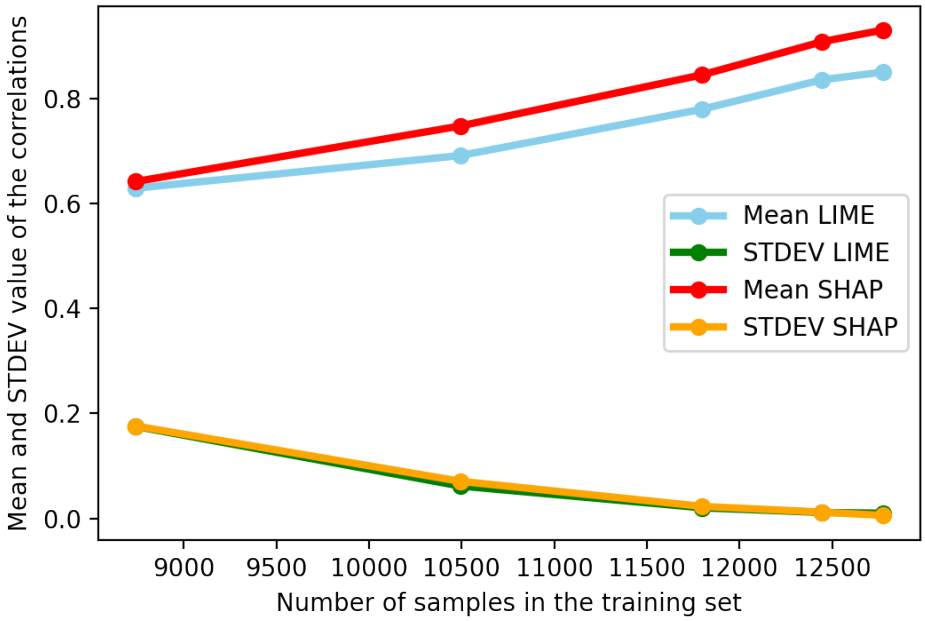


Figure 3.3: Mean and standard deviation of the correlation between the ranked lists of significant features in respect with number of the validation samples.

also reflects some aspects of previously proposed proxies [112] [126]. Our robustness criterion can be considered as a complementary test to what has been proposed

Table 3.5: The rank correlation between the lists of significant features between SHAP and LIME. *F* represents fold number, *SH* stands for SHAP and *LI* stands for LIME.

| Fold | TestSH | F1SH | F2SH | F3SH | F4SH | F5SH | F6SH | F7SH | F8SH | F9SH | F10SH |
|---|---|---|---|---|---|---|---|---|---|---|---|
| TestLI | 0.90 | 0.78 | 0.78 | 0.78 | 0.78 | 0.79 | 0.78 | 0.78 | 0.78 | 0.78 | 0.90 |
| F1LI | 0.79 | 0.88 | 0.79 | 0.80 | 0.81 | 0.81 | 0.78 | 0.79 | 0.78 | 0.79 | 0.79 |
| F2LI | 0.8 | 0.81 | 0.91 | 0.81 | 0.81 | 0.79 | 0.79 | 0.80 | 0.79 | 0.79 | 0.80 |
| F3LI | 0.79 | 0.81 | 0.80 | 0.90 | 0.81 | 0.81 | 0.89 | 0.80 | 0.79 | 0.79 | 0.79 |
| F4LI | 0.79 | 0.80 | 0.79 | 0.81 | 0.91 | 0.83 | 0.80 | 0.79 | 0,78 | 0.80 | 0.79 |
| F5LI | 0.79 | 0.82 | 0.80 | 0.81 | 0.82 | 0.92 | 0.81 | 0.80 | 0.78 | 0.80 | 0.79 |
| F6LI | 0.80 | 0.80 | 0.79 | 0.82 | 0.81 | 0.82 | 0.90 | 0.80 | 0.80 | 0.81 | 0.80 |
| F7LI | 0.80 | 0.81 | 0.80 | 0.82 | 0.82 | 0.83 | 0.81 | 0.89 | 0.79 | 0.81 | 0.80 |
| F8LI | 0.81 | 0.79 | 0.80 | 0.80 | 0.81 | 0.81 | 0.80 | 0.79 | 0.89 | 0.79 | 0.81 |
| F9LI | 0.79 | 0.79 | 0.79 | 0.81 | 0.81 | 0.80 | 0.82 | 0.81 | 0.80 | 0.91 | 0.79 |
| F10LI | 0.89 | 0.78 | 0.78 | 0.79 | 0.79 | 0.80 | 0.77 | 0.79 | 0.79 | 0.78 | 0.87 |

previously [112] [126]. Still, one can see that there is a relation between different criteria. High correlation between the ranked lists of significant features could indicate greater completeness, because more samples are involved in the explainability from the training sets. Moreover, cases of high correlation fulfil the sensitivity criterion because the explainability method has attributed a nonzero value to the significant features in all folds. However, in case of low correlation, the proposed stability criterion indicates lower performance in completeness and sensitivity analysis because fewer samples were used. In addition, arbitrary and unstable features attribution might be reflected in low correlation values.

Our method also fulfills the Compactness criterion as when the correlation is high, this indicates that the explainability method is able to capture the main causes (features on the top ranked lists) of the decision made by the model. Regarding Correctness, we observed that even when we had low correlation value among the lists of significant features, MAE did not increase and was very close to when we had high correlation values. This is probably related to the fact that Correctness was suggested and evaluated for binary classification whereas in this work we used a regression model for the brain age estimation. Finally, we are aware that the proposed proxy might not be applicable when there is a huge number of features, so the generalization of the method is under investigation.

In this work, we presented a new simple validation scheme for explainability methods based on Spearman's rank coefficients and cross-validation. We tested both SHAP and LIME to identify the important features in the DL model (for brain age

estimation) using different number of folds that led to different number of samples in the training and validation sets. Then we used Spearman's rank correlation to calculate the agreement between the ranked lists of significant features for each fold. Overall, SHAP and LIME performed better for the identification of significant features for larger training sets. Depending on one single list of significant feature might be inaccurate; instead, using cross-validation and ranked correlation among the lists might provide more evidence of the robustness of the feature ranking as assessed relying on Sperman's rank correlation.

# Chapter Four

# 4 Brain age for different fiber groups

## 4.1 Introduction

Aging is a complex process with substantial impact across multiple organ systems, yet to be fully characterised. In the specific case of the brain, previous studies have found evidence of considerable structural alterations of WM and GM structures as well as of morphological and functional connectivity changes across different areas [76]. These modifications are associated with distinct aspects of cognitive functions, emotions, and neurodegenerative disorders [127]. Several studies have demonstrated that groups of WM tracts that share the same function experience similar alterations during the life course and in specific brain disorders. In particular, Yang et al. [128] investigated the association of brain aging with WM integrity and functional connectivity in a group of healthy subjects. Their findings demonstrated that Projection, Association and Commissural fibers were substantially affected by aging resulting in a significant reduction of their WM integrity, while Brainstem tracts were relatively preserved. In another study, Bender et al. compared different diffusion-based indices estimated over Association, Commissural and Projection fibers again in a healthy population [129], demonstrating a greater microstructural decline over time in the first fiber group compared to the Commissural and Projection ones, and a differential aging of cerebral WM. Moreover, the tracts that connect frontal and parietal heteromodal cortices have been shown to be more prone to age-related differences than those from projection fibers [130]. In this context, the so-called "lastly maturing, first going out" phenomenon, grounding on previous MRI evidence [129] [131] [132], is of great importance. This refers to a mirroring pattern of development and aging of the human brain, where the last regions to develop are degenerating relatively early [131]. In particular, primitive sensorimotor structures encounter the most rapid development and greatest preservation, while more advanced structures (e.g., prefrontal cortex) seem to have slower de-

velopment and faster decline, leading also to differential developmental trajectories across WM tracts [130] [132] [131]. Therefore, existing work suggests differential aging-related changes depending on the specific WM fiber groups, which might result in diverse patterns of disease and cognitive impairment. However, the determinants of these different alteration patterns have not been adequately investigated so far.

Neuroimaging modalities can be adopted to estimate the so-called brain age which allows monitoring the longitudinal progression of brain during lifecourse. This is defined as the apparent biological age of the brain, when comparing individuals' data against a population dataset spanning a range of ages [39] [32]. The difference between predicted brain age and actual (chronological) age, generally referred to as brain-PAD, is often computed to verify whether a subject's brain appears younger or older than their chronological age [74]. Indeed, since humans do not experience brain aging at the same rate and pronounced differences possibly related to genetic and environmental factors are present, brain-PAD can be exploited as a novel biomarker to assess brain aging progression in both healthy and diseased populations. Greater brain age (positive brain-PAD) has been associated with increased risk of neurodegenerative diseases, whilst younger brain age (negative or small brain-PAD) correlates with healthy environmental exposures and lifestyle habits [36]. Among these factors, daily lifestyle, physical activity, electronic device use, and sleeping habits have all shown significant effects on brain progress during the lifecourse [40] [32], with smoking and greater alcohol intake frequency closely linked to increased brain-PAD for instance. Similarly, genetic factors also have a crucial role in brain aging.

In a recent study, Jonsson and colleagues [39] demonstrated the presence of two SNPs significantly associated with brain-PAD by relying on a GWAS, which were correlated with reduced WM surface area and reduced sulcal width[39]. Other studies identified several SNPs associated with brain-PAD, with the most significant ones located in *MAPT* [40] and *TMEM106B* genes [133]. These two genes have been shown to be closely associated with frontotemporal dementia [134], and *MAPT* has also been considered as a model of interaction in Parkinson's disease

between functional disease outcomes and genetic [135].

Furthermore, there is a growing evidence suggesting complex cross-system interactions between brain and cardiovascular systems [88] [89] [136]. Indeed, CRFs have been already associated with poorer cognitive function. Precisely, higher body mass index (BMI) has been linked to poorer performance across multiple cognitive indications including working memory, attention, delayed recall, and category fluency [137]. In addition, other risk factors such as diabetes and hypertension have been associated with unhealthy brain aging, abnormal neuroanatomical alterations, and increasing risk of developing AD [117]. Finally, DeLange and colleagues [138] demonstrated that CRFs such as stroke risk score and alcohol intake are associated with older appearing brains. All these elements deserve further investigations to better understand whether they might influence the brain aging processes differently.

In this context, neuroimaging data derived from MRI sequences have demonstrated to provide accurate estimates of the apparent age of individuals' brains, generally relying on age regression models [139]. Most brain-age models only use T1-weighted structural MRI, reflecting brain volumes. However, the possibility to use complementary modalities mapping different aspects of brain structure and function has opened the way to the estimation of modality-specific brain aging models. In particular, dMRI, resting-state/task fMRI and SWI are currently exploited in different studies to extract novel IDPs to be used in specific brain-age models, thanks to the new opportunities offered by large-scale multimodal databases such as the UKBB [86]. Statistical methods for modeling brain age using neuroimaging data are generally highly accurate, with MAE of predictions in the range of 4-5 years for most of the studies relying on different regression approaches such as simple linear regression, SVR and LASSO [32] [36] [40] [139].

In addition, most of these previous studies have demonstrated better results when including multimodal neuroimaging data rather than a single modality in the models [138] [140] [141]. In particular, findings from these multimodality studies suggest that dMRI measures have higher accuracy in predicting brain age compared to those derived from fMRI, SWI or even anatomical images in some cases [36] [76].

The diffusion-based features are generally extracted starting from the microstructural maps estimated using different models, such as DTI and NODDI, and then averaging the corresponding values over several WM tracts. FA along with indices of diffusivity (MD/AxD/RD) can be estimated from the DTI model, informing on the degree of anisotropy/diffusivity of diffusion process [142]. Conversely, more complex indices are derived from NODDI, a compartmental model where brain microstructure is described in terms of a set of predefined parameters that is neurite ODI, representing the directional overall coherence of modeled axons, ISOVF, showing the unhindered water volume fraction, and ICVF that represents neuronal density [24] [143] [144]. Previous works have demonstrated the importance of DTI and NODDI IDPs for estimating brain age in both healthy and diseased populations [145] [146]. Moreover, microstructural patterns have been demonstrated to follow different trajectories in brain aging within WM structures. In particular, FA tends to decrease during aging while MD, AD and RD have the opposite pattern [99] [32].

In this study, we aimed at estimating and comparing diffusion-specific brain ages in a large cohort free from clinically diagnosed neurological disease from the UKBB database, relying on dMRI measures of different fiber groups in order to assess the impact of aging on WM at the tract-group level. Indeed, investigating brain aging for tracts with shared functionality may permit a more accurate and disease-specific risk assessment compared to brain aging for the whole brain. In addition, for each fiber group, we evaluated the relationship between brain predicted ages and several factors spanning across different scales, relating in particular to daily lifestyle, health, cardiac measures and genetics to verify whether a differential association might be present in specific WM tracts. This will also allow to identify those factors that can negatively impact brain aging, providing further insights on its complex mechanisms.

## 4.2 Data

### 4.2.1 Participants

Data from n = 16394 participants with complete brain and cardiac MRI assessment were initially downloaded from the UKBB database. Of these, 1059 subjects who reported neurological disorders that could directly affect cognitive function were excluded in order to include only people who met criteria for being neurologically intact at the time of scanning. These were identified using the self-reported medical conditions at baseline extracted from detailed questionnaires that the UKBB participants had to answer, the relevant ICD-10 code, hospital episode statistics, and algorithmically-defined outcomes. This led to a final group of 15335 subjects (mean age 54.79 $\pm$ 7.45, 7277 males, 8058 females). The complete list of conditions and ICD-10 codes used as inclusion/exclusion criteria are available in Appendix, table 1.

All the methods were conducted in accordance with the relevant guidelines and regulations and all participants provided informed consent. UKBB received ethical approval from the NHS National Research Ethics Service on 17th June 2011 (Ref 11/NW/0382) and extended on 10th May 2016 (Ref 16/NW/0274). More details can be found on the UKBB resource page `https://biobank.ndph.ox.ac.uk/showcase/catalogs.cgi`. The present analyses were conducted under data application number 2964.

### 4.2.2 Brain and Cardiac MRI features.

The UKBB brain imaging protocol was implemented on a 3T Siemens scanner (Skyra, VD13A SP4, Siemens Healthcare, Erlangen, Germany) and included six different sequences, covering structural, diffusion and functional imaging for a total of 35 minutes scan time. In particular, a multi-shell protocol has been used for dMRI data, with two b-values (b = 1000, 2000 s/mm$^2$), a 2-mm isotropic resolution and a multiband acceleration factor of 3. 50 diffusion-encoding directions were acquired per shell, covering a total of 100 distinct directions over the two b-values. Cardiac MRI was performed on a 1.5T Siemens scanner (MAGNETOM Aera, Syngo Platform VD13A, Siemens Healthcare) according to a pre-defined protocol [147] [148].

Left and right ventricular (LV, RV) function was assessed using standard long and short axis acquisitions.

### 4.2.3 Genotype data.

UKBB genotyped genetic data for 488377 participants were obtained using two genotyping arrays. A small subsets of the participants (49950) involved in UKBB Lung Exome Variant Evaluation (UK BiLEVE) study were genotyped using the Applied Biosystems UK BiLEVE Axiom Array by Affymetrix. Conversely, the majority of the participants (438427) was genotyped using the closely related Applied Biosystems UKBB Axiom Array. More details about genotyping and genotype calling steps can be found in [66].

## 4.3 Methods

### 4.3.1 Brain microstructure feature extraction.

In the current study, we relied on the IDPs derived centrally by the researchers involved in the UKBB project and made available via the data showcase ( `https://biobank.ctsu.ox.ac.uk/crystal/index.cgi`). Of these, we focused on the 675 dMRI IDPs extracted for each participant using the following pipeline. First, both the diffusion tensor and the NODDI models were fitted to the pre-processed data leading to nine voxelwise microstructural maps, namely FA, MD, axial diffusivity (L1), radial diffusivities (L2, L3) and mode of anisotropy (MO) from DTI, and ICVF, ISOVF, and ODI from NODDI. Two sets of measures were used as microstructural features, both obtained from the UKBB repository and extracted following two different approaches [86] [70]. The first used tract-based spatial statistics (TBSS). Each individual dMRI map was aligned to a standard-space WM tract skeleton and a series of ROIs was then defined as the overlap of this skeleton with 48 standard-space tract masks from the JHU ICBM-DTI-81 atlas [80]. For each skeletonised microstructural index, the mean value was calculated in each region, leading to a total of 432 IDPs (that is 48 ROIs times 9 IDPs). The second relied on probabilistic tractography. A total of 27 major tracts were identified using standard-space start/stop ROI masks defined by AutoPtx toolbox (http://fsl.fmrib.ox.ac.uk/fsl/fslwiki/AutoPtx). The mean value of each DTI/NODDI parameter was calculated across each tract and

weighted by the tractography output as in Alfaro et al. [70] in order to emphasize values in regions most likely to belong to the tract of interest, resulting in a total of 243 IDPs (27 tracts times 9 IDPs). Table 2 in the appendix shows these tracts and their fiber group.

Each ROI and tract was subsequently assigned to one out of five fiber groups (FG) following the fiber tract-based atlas [149]. In particular, the following FG were considered: i) Association; (cortex-cortex connections); ii) Brainstem; iii) Commissural (left-right hemispheric connection); iv) Limbic; and v) Projection (cortex-brainstem, cortex–spinal cord and cortex-thalamus connections) fibers. Each FG consisted of a different number of tracts, that is: 22 for Association, 13 for Brainstem, 13 for Commissural, 9 for Limbic, and 18 for Projection. An illustration of these five fiber families is reported in figure 4.1, where the different tracts are depicted in different colors. *Association* fibers interconnect different cortical areas in

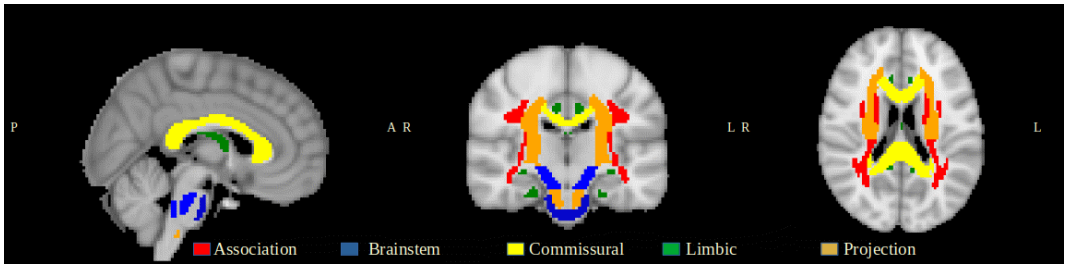


Figure 4.1: White matter tract groups

the same hemisphere [150]. These might be short association fibers that connect adjacent gyri, or long association fibers linking more distant parts of the cerebral cortex. Important examples of this category are the superior/inferior longitudinal fasciculus, inferior fronto-occipital fasciculus, and uncinate fasciculus [151]. *Brainstem* fibers involve the tracts that connect cerebrum to the spinal cord and cerebellum[152]. These includes the corticospinal tract, the posterior column-medial lemniscus pathway and the spinothalamic tract. *Commissural* fibers interconnect corresponding cortical regions of the two hemispheres and are mainly represented by the corpus callosum and anterior commissure [150]. *Limbic* fibers involve structure in both sides of thalamus [153]. Fornix is one of the main vital tract of this system [154], alongside the Cingulum bundle that connects parietal, frontal and temporal lobe [155]. Finally, *Projection* fibers connect cortical areas with deep nu-

clei, cerebellum, brainstem, and spinal cord [156]. Corticospinal and corona radiata tracts are the two main examples for this category [157]. By subsequently assigning each ROI and tract to the respective FG, summary IDP values could be derived by averaging across ROIs and tracts, respectively, in each FG. In this way, the whole set of IDPs were assigned to each FG resulting in a total of 18 IDPs (9 from the ROI-based and 9 from the tract-based analyses).

### 4.3.2 Cardiovascular feature extraction.

CMR data were analysed using an automated pipeline [158]. The extracted cardiovascular indices included measures of LV and RV structure and function. Specifically, the indices derived for the LVEDV, LVESV, LVSV and LVM. The RV indices included RVSV, RVEDV, RVESV were considered. LV and RV volumes are markers of cardiac remodelling, from these stroke volume may be derived as a measure of ventricular function. LVM is an independent risk predictor in clinical cohorts and an indicator of heart aging in population cohorts. To correct for variation in CMR metrics related to body size, these measures were indexed to body surface area (calculated as per Du Bois formula) [159]. As an additional measure of arterial health in a larger sample, we considered arterial stiffness index (ASI) derived from finger plethysmography [160]. ASI was measured at the baseline UKBB visit using the PulseTrace PCA2 (CareFusion, USA) device according to a pre-defined protocol, UKBB Arterial Pulse-Wave Velocity (2011) that is available at `https://biobank.ndph.ox.ac.uk/showcase/showcase/docs/Pulsewave.pdf`. Outliers were removed from the ASI variable using a 1·5× interquartile range (IQR) rule. Finally, CRFs included hypertension, diabetes, deprivation (reported in UKBB as the Townsend index), body surface area (BSA), BMI and exercise level.

### 4.3.3 Lifestyle features.

Regarding daily life measures, 38 variables were available in the UKBB database at baseline. The lifestyle and environment measures included seven categories that are: physical activity (7 measures), sun exposure (2 measures), electronic devise use (2 measures), smoking (2 measures), sleeping habits (5 measures), alcohol (3 measures) and diet (17 measures). All the used variables are available in appendix,

table 3.

### 4.3.4 Brain Age estimation.

All the analyses performed in our study were carried out using Python 3.8.5 and Scikit-learn version 0.23.2. A tract-based healthy aging model was defined for each of the five FGs, using the corresponding 18 dMRI IDPs as neuroimaging predictors and the chronological age as dependent variable. To account for the different measurement scales, the features were normalized to zero mean and unit variance [32]. Sex, education level, height and volumetric scaling from T1-weighted head image to standard space were used as covariates considering that they could be statistically associated with the outcome variable, as previously reported in similar studies [32] [36] [161]. A Bayesian ridge regression model was run in combination with a 10-fold cross-validation, where the data samples were randomly assigned into ten equal-sized groups. For each group of left out data, the other 90% of subjects were used to estimate the model parameters which were then applied to this additional group for validation. The performance of each model was assessed using MAE and Coefficient of Determination ($R^2$).

Several studies have revealed a proportional bias in brain age estimation related to regression model dilution, leading to a significant age-dependency between brain-PAD and chronological age [35] [87] that needs to be statistically corrected. In this study, we adopted the method proposed by Beheshti et al. [35] which entailed calculating the regression line between brain-PAD and chronological age in the training set:

$$D = \alpha * \Omega + \beta \tag{4.1}$$

where $D$ is the brain-PAD from training data, $\alpha$ and $\beta$ represent the slope and the intercept of the linear regression model, and $\Omega$ is the corresponding chronological age. Then, these intercept and slope values were used to correct the predicted brain age in the validation set set as follows:

$$CPBA = Predicted\,Brain\,Age - (\alpha * \Omega + \beta) \tag{4.2}$$

where CPBA represents the corrected predicted brain age (bias-free). After bias correction, the brain-PAD was calculated as the actual age subtracted from the brain-predicted age. Pearson correlation was calculated between actual and predicted brain age as well as actual age and brain-PAD, both before and after the bias correction steps. An ensemble tract-based aging model was finally defined using the overall 90 dMRI IDPs (18 from each FG), and the same analyses detailed above were implemented.

### 4.3.5 Association analysis

In order to highlight the role of the different variables to model brain age, the association between brain-PAD values as resulting from the five FG models and a set of imaging/non-imaging variables was assessed using linear regression model. This included the corresponding 18 dMRI IDPs, 14 CRFs/CMR measures, and 38 daily life measures. In addition, the same analyses were performed for the brain-PAD values derived from the ensemble model, with the only difference being represented by the associations with the whole set of 90 IDPs for the dMRI part (rather than 18 only). In all models, brain-PAD represented the outcome measure, while the feature of interest was the independent variable alongside all the above mentioned covariates plus age [32, 36]. The resulting p-values were Bonferroni-corrected for multiple comparisons at alpha= 0.05 [162], assuming that each model is independent from the others. In details, the p-values were multiplied by the number of tests performed in each analysis, that are 18 for the associations with the IDPs in each of the five FG models and 90 for the Ensemble model. The association was considered significant if the corrected p-value was less then 0.05.

Of note, Cook's distance was used to identify potential influential observations before performing the association analyses. In particular, a subject was removed if the Cook's distance was greater than 3 times the mean distance of all the subjects [40]. The association between genetic variants and brain-PAD values as resulting from each model was also conducted. The quality control steps on SNPs included Minor allele frequency (MAF) thresholding at 0.01, missing rate less than 0.02 and Hardy-Weinberg equilibrium p-value >=1E-6. Quality control on samples ensured

that all participants had genotyping rate > 0.98, heterozygosity rate within ±3 standard deviation, matched genetic/reported gender and were of European ancestry (according to both genetic ethnicity based on principal component analyses and self-reported ethnicity). Related samples were removed based on kinship coefficient > 0.1. The quality control steps resulted in 574492 autosomal SNPs and 12364 subjects for the GWAS analyses. Thereafter, linear regression was performed using PLINK [163] and adjusted for education, gender, age, volumetric scaling from T1-weighted head image to standard space, and 40 genetic principal components of ancestry. For each GWAS analysis, FUMA[164] was used to map the significant SNPs to genes based on positional mapping and eQTL. Using FUMA and GTEx (`https://gtexportal.org/home/`), we also identified Expression quantitative trait loci (eQTL) to take advantage of gene expression. Finally, we looked at UKBB genetic data (`http://big.stats.ox.ac.uk/`) [78] to find association between the significant SNPs and other phenotypes.

## 4.4 Results

### 4.4.1 Brain age estimation.

The impact of aging was separately assessed in terms of MAE and $R^2$ values after fitting the five considered multivariate linear FG-based models plus the ensemble one. The mean and standard deviation of such values across a ten-fold cross-validation were reported in order to probe the reliability of the estimation. Results are summarized in Table 4.1 where the columns 2 to 6 correspond to the five FGs, that is, Association, Brainstem, Commissural, Limbic and Projection fibers, and the last column reports the results for the FG ensemble. In the table, the Pearson correlation coefficient between the actual age and the predicted age before (CAPB) and after (CAPA) correction, the actual age and the brain-PAD before (CADB) and after (CADA) correction are also reported in the last four rows.

As it can be observed, the performance is quite uniform across FG, with the exception of the Brainstem group especially regarding the $R^2$ value that is the lowest. The best MAE was obtained for the tract ensemble model followed by the Limbic FG, which also corresponds to the highest $R^2$. The last four rows prove that the age-bias

was successfully removed.

Table 4.1: Performance of the five FG-based models plus the ensemble one to estimate brain age in terms of MAE and $R^2$. The last four rows provide the CAPB, CAPA, CADB and CADA, respectively. The best performing model is identified by star symbol.

| Matrices | Association | Brainstem | Commissural | Limbic | Projection | Ensemble |
|---|---|---|---|---|---|---|
| Mean $R^2$ | 0.26 | 0.11 | 0.26 | 0.29 | 0.25 | $\star$ 0.42 |
| STDV $R^2$ | 0.02 | 0.01 | 0.01 | 0.02 | 0.03 | 0.015 |
| Mean MAE | 5.24 | 5.86 | 5.23 | 5.08 | 5.28 | $\star$ 4.55 |
| STDV MAE | 0.1 | 0.09 | 0.11 | 0.12 | 0.13 | 0.08 |
| CAPB | 0.51 | 0.33 | 0.51 | 0.54 | 0.5 | 0.65 |
| CAPA | 0.91 | 0.95 | 0.91 | 0.9 | 0.91 | 0.89 |
| CADB | -0.85 | -0.94 | -0.86 | -0.83 | -0.86 | -0.75 |
| CADA | -0.001 | -0.003 | -0.001 | -0.001 | -0.001 | -0.006 |

### 4.4.2 IDPs association with brain-PAD.

Linear regression results describing the relationships between the bias-adjusted brain-PAD values for the five FG-based models and each microstructural IDPs are illustrated in Figure 4.2. In addition, results for the ensemble model are also reported, including in this case the associations with 90 dMRI IDPs rather than 18 as in the case of the previous five FG models. The coefficient values are unitless as we standardized the IDPs and brain-PAD before performing the analysis. The coefficient value refers to how many standard deviations a dependent variable (brain-PAD) will change per standard deviation increase in the independent variable (individual IDPs). A highly similar association pattern is apparent across FG, though higher variability was observed for the Limbic FG. More specifically, all the IDPs were significantly associated with brain-PAD in Association and Commissural groups, while few associations did not reach significance in the other three tract groups, that is: mean L1 and mean ICVF in Brainstem, weighted mean L1 in Limbic and weighted mean MO in Projection fibers. Considering the different imaging variables, anisotropy (FA, ICVF, OD and MO and respective weighted versions) and diffusivity (MD, L1, L2, L3, ISOVF and weighted versions) indices led to associations of opposite direction, as expected, in almost all the cases. More precisely, FA and weighted FA showed a significant negative association with brain-PAD in all five groups, while MD/weighted MD presented the opposite pattern and appeared to more strongly contribute to modelling the outcome in all cases. Similarly, in-

creased L1, L2 and L3 plus their weighted versions were associated with increased the brain-PAD for all groups, except L1 and weighted L1 in Brainstem and Limbic FGs, respectively. Finally, the weaker associations were observed for MO and weighted MO in all models. Consistently with what above, for NODDI-based measures, the diffusivity index ISOVF was positively associated with the brain-PAD in all cases. A slightly different pattern was observed for OD and its weighted version across the FG, that presents a higher variability. OD is positively associated with the brain-PAD, as expected, in Brainstem and Limbic fibers, though not in the weighted version, and has a different pattern in the other three groups, with a prevalence of a negative association of the weighted version. The association between the IDPs and the brain-PAD was also assessed FG-wise relying on the Ensemble model, revealing that the pattern was preserved though with slightly different values. In particular, the association was slightly reduced with respect to the values that were obtained for FG-specific brain-PADs. Check table 4 in the appendix for more details regarding the association.

### 4.4.3 CRFs and vascular measures association with brain-PAD.

Figure 4.3 reports the results of the linear regression analyses between the bias-adjusted brain-PAD values and the CRFs/CMR measures, revealing consistent patterns across the five FG models. In all conditions, several measures were significantly associated with PAD after multiple comparison correction, in particular increased brain-PAD was associated with a diagnosis of diabetes, hypertension and increased LVM, as well as with reduced LVSV/RVSV and RVEDV/RVESV. Greater BMI was also associated with increased brain-PAD in three out of five models (Projection, Brainstem and Limbic), with the last two fiber groups also showing a positive relationship between brain-PAD and BSA. Of note, the model based on Limbic fibers presented the highest number of significant associations and the direction of the relationships was consistent in all the five FC-based models. The same trend was observed for the Ensemble model. These associations followed the same pattern compared to the other five FG models. More precisely, the association results were closer to those found for the the Brainstem and Limbic FG, especially in eight out of 14 measures. Check table 5 in the appendix for more details regarding the

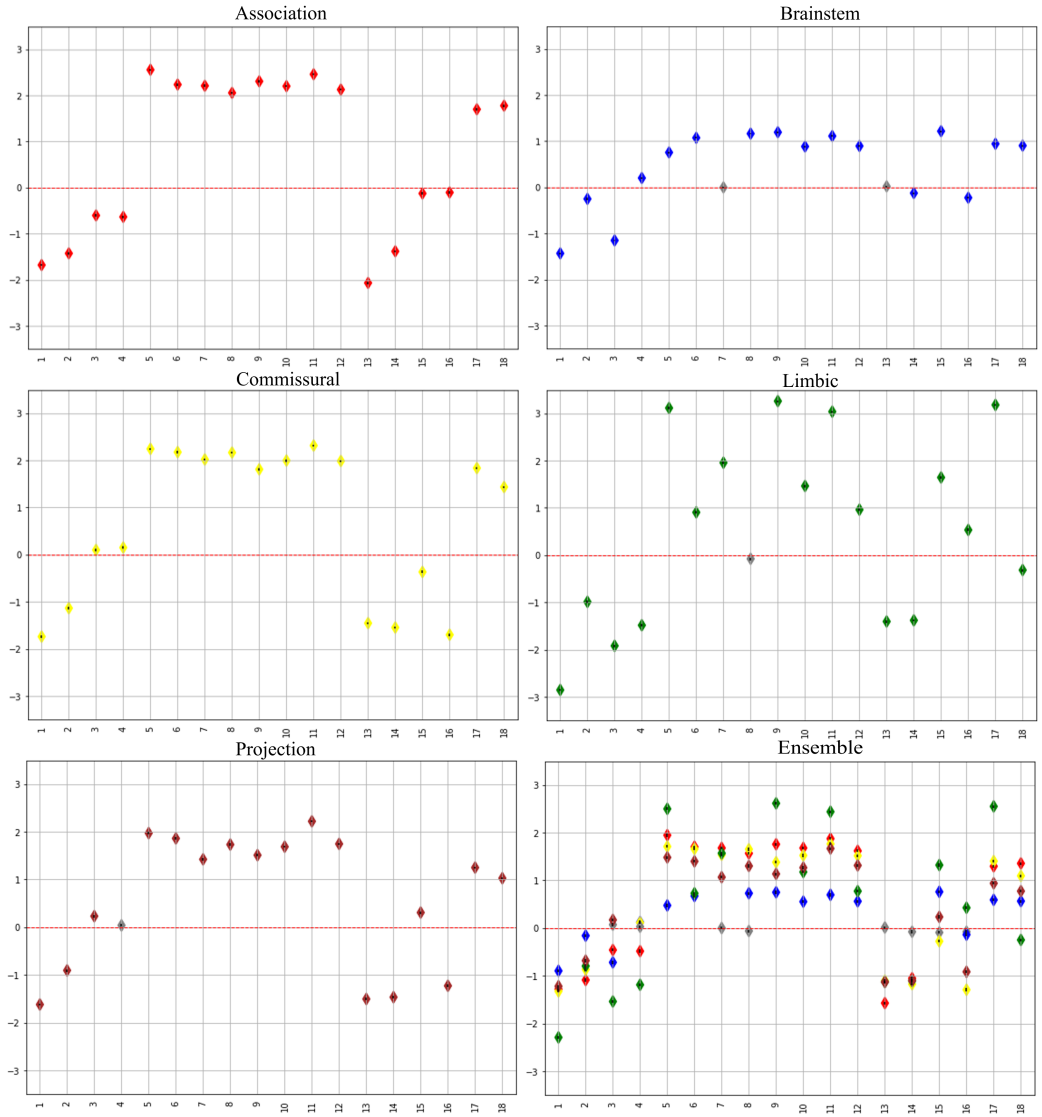


Figure 4.2: Association of the IDPs and brain-PAD for the different models. For each model, the numbers on the x-axis represents the order of the different IDPs summarised in the legend, while the regression coefficient (the diamond shape represents the beta coefficient) values are reported in the y-axis along with their standard error (the small black dot inside the diamond shape). Grey color indicates non-significant association.

association.

### 4.4.4 Lifestyle association with brain-PAD.

Figure 4.4 reports the results of the linear regressions between the bias-adjusted the brain-PAD values and the daily life measures in each of the five FG-based models

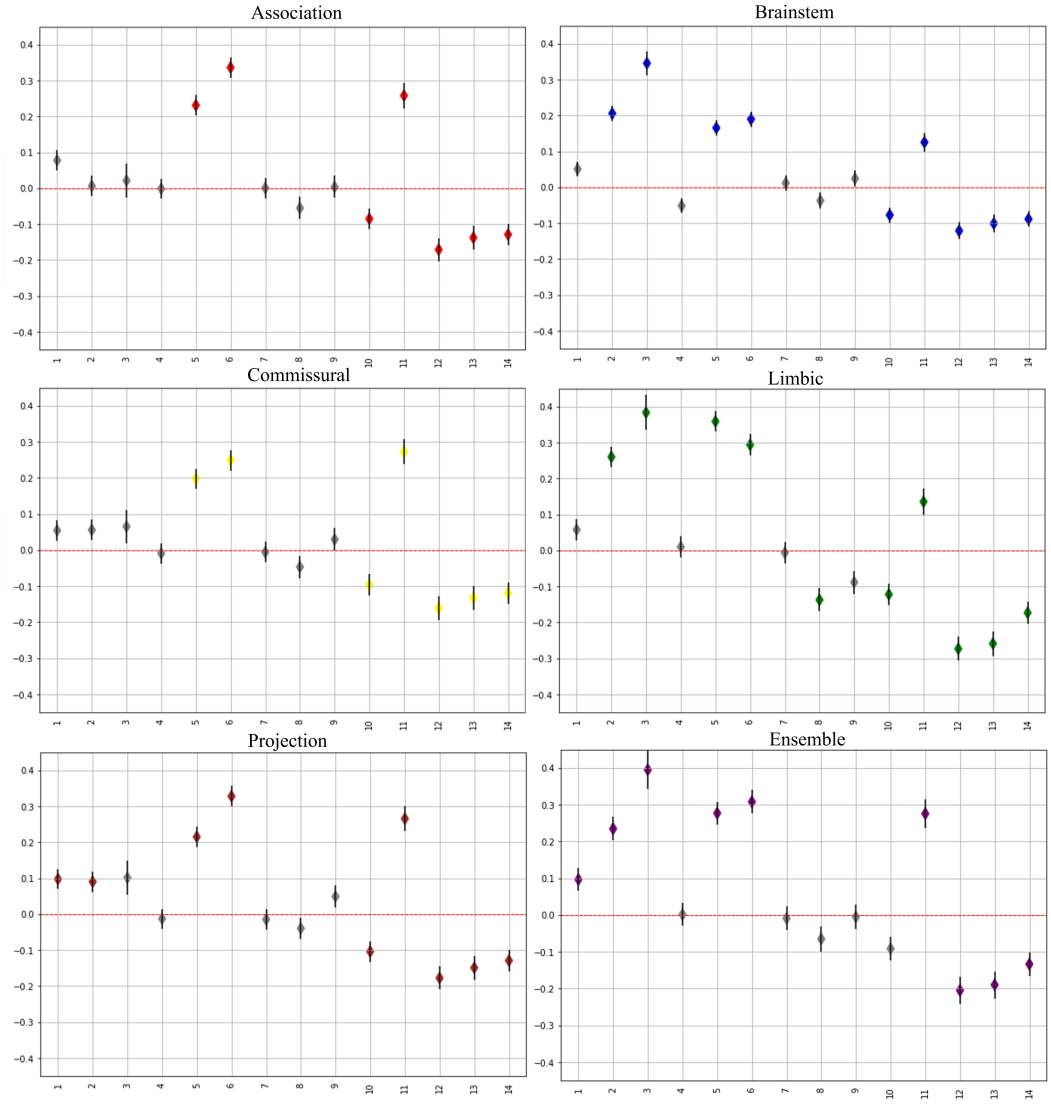


Figure 4.3: Association of the CMR measures, CRFs and brain-PAD. For each model, the numbers on the x-axis represents the order of the different CMR and CRFs measures summarised in the legend, while the regression coefficient (the diamond shape represents the beta coefficient) values are reported in the y-axis along with their standard error. Grey color indicates non-significant association.

plus the Ensemble one. Consistent patterns were visible across the FGs. The highest number of significant associations was observed for the Limbic tracts, while only four measures survived for the Brainstem group, though in agreement with the others. In all cases, increased brain-PAD was associated with ever smoked, smoking status, greater oily fish intake, and tea intake (except for Association fibers). In addition, increased brain-PAD values from Association, Commissural and Limbic fibers were associated with greater lamb/mutton intake and greater frequency

of alcohol intake. Duration of walk for pleasure had a positive impact on brain age, being associated with reduced brain-PAD values in both Limbic and Projection fiber models, while increased brain-PAD was associated with water intake in Commisural and Projection FG models. Finally, seven additional daily life measures, including time spent watching TV or using computer and sleep duration, presented only selective associations in one of the models (4 for Limbic, 2 for Association and 1 for Projection). Check table 6 in the supplementary for more details regarding the association. The coefficient value for all those are significantly associated with brain-PAD in FG is small (less than 0.3) indicating small effect.

### 4.4.5 Association between SNPs and brain-PAD.

Two SNPs located on chromosome 6 showed significant associations ($p < 5E-08$) with brain-PAD values in the Projection FG, namely rs1045537 ($p = 2.87E-08$) and rs16891334 ($p = 4.268E-08$). Figure 4.5 illustrates the Manhattan plot showing the association between the SNPs in all chromosomes and brain-PAD from the Projection FG. Moreover, the Manhattan plots for the other FG and the ensemble model were also reported (Appendix, Figures 1 to 5). The leading SNP (rs1045537) was mapped to *BTN3A* cluster *(BTN3A1 to BTN3A3)*, *SCGN, SLC17A* cluster *(SLC17A1 to SLC17A4)*, *HIST1H1A* group of genes based on FUMA results using positional mapping and eQTL based on GTEx database (version 8.54 and 8.30) and general tissue types. In addition, it is significantly associated with forced vital capacity, BMI, headache and coeliac disease in UKBB cohort.

## 4.5 Discussion

This study focuses on providing a holistic view on the endogenous end exogenous factors shaping brain aging as expressed by brain microstructural features of specific WM tracts, providing hints for the multiscale and multifactorial analysis of the system 'human being'. The challenge being to link heterogeneous information living at different scales, this work takes a step in that direction by linking microscopic (genes), mesoscopic (dMRI IDPs), macroscopic (cardiovascular IDPs) and behavioral (lifestyle) measures through their respective association to the brain age picture provided by dMRI. After investigating the potential of microstructural

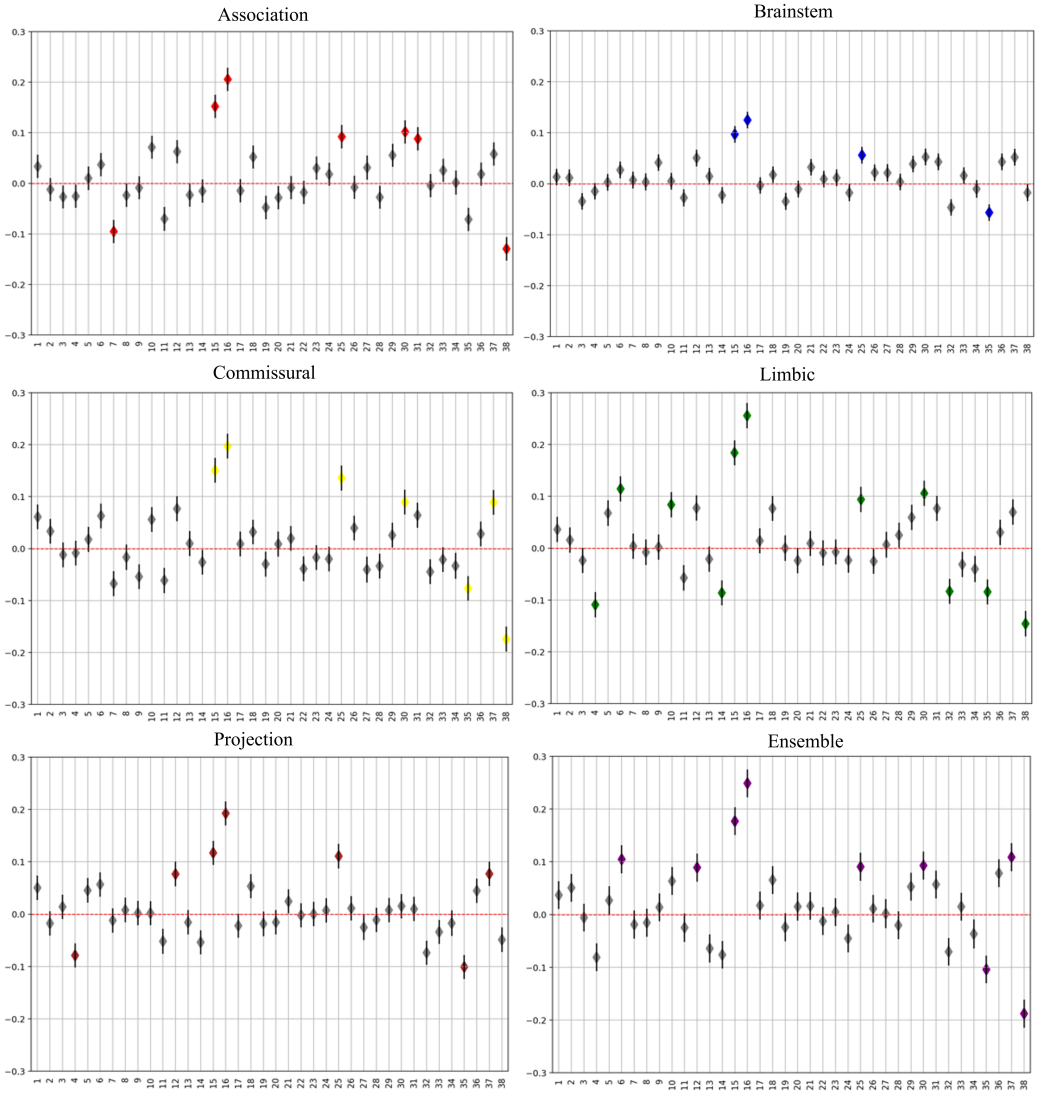


Figure 4.4: Association of daily lifestyle measures and brain-PAD. For each model, the numbers on the x-axis represents the order of the daily lifestyle measures summarised in the legend, while the regression coefficient (the diamond shape represents the beta coefficient) values are reported in the y-axis along with their standard error. Grey color indicates non-significant association. A unique color was assigned to each group measures(e.g physical activity).

measures derived from dMRI in estimating brain-PAD relying on five different FG, the associations of neuroimaging, genetic and cardiovascular IDPs with brain-PAD were assessed and, as a final step, lifestyle and behavioral measures were also con-

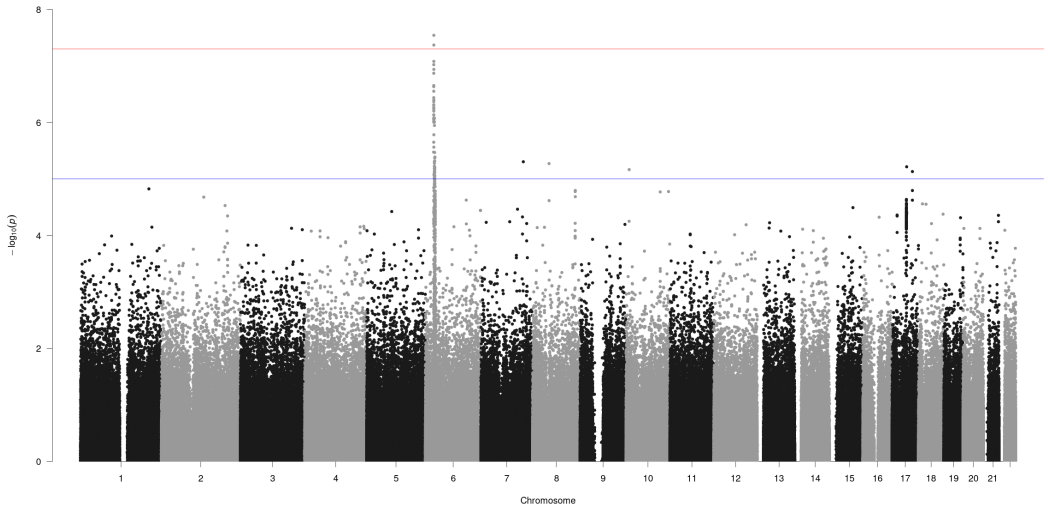


Figure 4.5: Manhattan plot reporting the association results between SNPs and brain-PAD in Projection FG. The red line indicates the GWAS threshold on p-value (i.e.,5E-8), while the blue line indicates the suggestive threshold of p=5E-5.

sidered. The rest of this section will be dedicated to the discussion of the results as well as of the potential consistency of the observed associations across scales while referring to the existing literature.

The estimated brain-PAD was minimized by the Ensemble model, gathering the whole set of $18 \times 5$ microstructural features, leading to the minimum MAE (4.55 years) and the maximum $R^2$ (0.42). On the other end, Brainstem FG led to worst performance, with the highest value for the MAE (5.86 years with std =0.01) and the minimum for $R^2$ (0.11). The Brainstem FG, including the midbrain, pons, and medulla, involves structures with complex WM pathways and GM nuclei that are concentrated in a small area. Intricate Brainstem circuitries are difficult to capture using conventional dMRI measures such as DTI, with the consequence that both the tractography and the estimation of microstructural indices are prone to errors [165]. Among the other single FG-based models, the Limbic one provided the best MAE (5.08 with std = 0.02) and $R^2$ (0.29), closely followed by the others (Association-, Commissural- and Projection-based FG models) showing a similar pattern. The Ensemble model relying on all available IDPs provided the best results compared to single FG-based models, suggesting that the inclusion of multiple features from different WM FG could better depict the modulations related to brain aging and

therefore lead to more accurate estimates.

However, this would impeed to disambiguate the impact of the aging process on the different FGs, that is the main objective of this work. The association of PAD with the dMRI IDPs revealed the path these measures follow in brain aging. Based on the corrected p-value, their association with PAD wes significant in all FGs apart from very few cases. Fractional anisotropy (FA) and ICVF were reduced in all tract groups while L1, L2, L3, MD, ISOVF increased with advancing age. This is in agreement with the expectation since they are consistent with neuronal loss as discussed in [ADD REFS]. The contribution of OD and MO was relatively inconsistent among tract groups featuring an increment in some FGs and a decrement in others. The pattern was similar for the Association, Commissural and Projection FGs, as well as for the Ensemble model. The results for Limbic tract showed a different pattern compared to other FGs. Overall, our results are inline with what have been published before in terms of the direction these IDPs follow in brain aging, as reported, for instance, in Smith, et.al [32]. Their results indicate that FA and ICVF decrease with aging while L1, L2, L3, MD and ISOVF increase. In addition, they showed that the dMRI features are among of those most relevant for the estimation of brain age in Fornix irrespectively of the sex. Our results are consistent with these findings since as the IDPs from the Limbic FG, which is dominant in the Fornix tracts, were on the top of the list of relevant features to model brain age in the Ensemble model.

Another interpretation for such results could be that brain age is more accurately estimated in these regions than other regions which result in reduced error (MAE). In addition, the diffusion indices in the Limbic tracts, specially in the Fornix, might be very sensitive to aging and indicate an atrophy of the tract rather than alterations in WM microstructure [38].

Most of CRFs and CMR measures led to significant associations with brain-PAD in different FGs. The direction of the association was shared by all tract groups. Brain-PAD in the Limbic FG was significantly associated (5 positively and 5 negatively) with most of these measures. Brainstem FG brain-PAD was significantly associated with 4 measures negatively and 5 positively. Brain-PAD in Ensemble

model was significantly and positively associated with 6 measures and significantly and negatively associated with 3 measures. Positive associations was two times compared to negative with brain-PAD in the case when all IDPs were used to model brain age, while association and commissural seem less affected. Among these measures, diabetes, hypertension and LVM were positively associated with brain-PAD in all tract groups while RVEDV, RVESV and RVSV were negatively associated with brain-PAD in all tract groups. The other measures showed inconsistent association with brain-PAD across different tract groups. Body mass index and diabetes were positively associated with brain-PAD which indicates induced acceleration in brain aging. Based on these results, people who suffer from diabetes might experience accelerate brain aging by about half a year, consistently with [36] reporting an acceleration of about 2 years. The difference might be related to the features preprocessing and normalization steps. The body mass index has been associated with risk of developing neurodegeneration or cognitive decline. Increasing in adiposity in overweight and obese individuals might alter the white matter volume that causes faster brain aging up to 10 years [166]. Cardiac index is significantly associated with brain aging even for healthy people. People who present a lower cardiac index or least pumping blood rate appeared almost 2 years older than those having highest cardiac index [117]. Moreover, low cardiac index might be an indication of increase risk of brain disorders. In [167] they have concluded that low cardiac index increase the risk of incident Dementia and AD. Our results demonstrate novel associations between accelerated brain-PAD and vascular risk factors. However, as we do not account for potential co-existence of multiple risk factors we cannot conclude independent associations with individual risk factors. More detailed examination of these relationships including accounting for possible confounding and evaluation of mediating mechanisms is warranted, although beyond the scope of the present work.

Regarding daily lifestyle factors and activities, 11 measures had significant associations with limbic tracts. Among them, 5 measures were negatively associated with brain-PAD meaning that these factors might slow down and preserve from brain aging. Brainstem tracts were significantly associated with only 4 measures,

out of which three were positive (indicating accelerated brain aging) and one was negative (indicating delaied brain aging). Association, Commissural and Projection FG showed close results of 7 significant associations for each one of them. For the Ensemble model, 9 measures were significantly associated with brain-PAD, and mostly were positively associated. Among all these measures, smoking statues and alcohol frequency intake was significant in all cases (apart from alcohol frequency intake in Brainstem). Alcohol frequency intake was negatively associated with brain-PAD which indicates acceleration in brain aging. This has been confirmed before in other studies. Of note, alcohol frequency intake was coded as lower value means higher intake. In [168], alcohol intake history was negatively associated with WM volume specially in corpus callosum. In addition, alcohol frequency intake was associated with deleterious in white matter tracts cause atrophy in ensemble and regional brain [169]. Our findings are inline with previous studies and this was observed in most tract groups. Two variables were considered to define smoking status based on data available in UKBB these included ever smoked (UKBB ID 20160) and smoking status (UKBB ID 20116). Smoking is associated positively with brain-PAD suggesting that smoking has a negative impact on brain aging. It should be noted that smoking habits is being associated with different alterations in both white and grey matter. Moreover, smoking duration linked with reduced total volume of WM . It is also associated with reduction in FA in the cingulate gyrus [170]. Lamb/mutton intake was also positively associated with brain-PAD in some tract groups. Low red meat intake has been associated with better cognitive function [171]. In addition, limited consumption of red meat might reduce risk of AD, slow cognitive decline and reduce AD biomarker such as atrophy [172]. Time spent using computer and sleep duration were positively associated with brain-PAD in Limbic fibers causing acceleration in brain aging. Finally, duration of walk for pleasure was negatively associated pointing to a healthy brain aging as walking stimulates blood circulations and exposition to the sun light.

The association of SNPs and brain-PAD in different FGs led to the identification of one significant locus with leading SNP rs1045537 ($p < 5 \times 10^{-8}$) in Projection fibers. Significant association was observed between rs1045537 SNP and an eQTL of

*BTN3A2* in heart left ventricle, basal ganglia, Frontal Cortex and Cortex. *BTN3A2* gene has been identified as a potential risk gene for schizophrenia [173] [174]. The SNP is also significantly associated with malabsorption/coeliac disease, body mass index and headache. *HIST1H1A* gene was associated with DNA methylation at early AD stages [175]. *SCGN* gene was identified as one of the most common psychostimulants in brain-wide targets [176]. *SLC17A2* is one of the solute carrier family that is membrane protein and transporter. It was associated with neurodegenerative disorders because of its important role in the recovery of neurotransmitters [177].

Estimating brain age for a specific region within brain or using different modes of structural and functional change were proposed before to detect the alterations in brain functions and structures in both healthy and diseased populations. Kaufmann, et al [178] estimated brain age using features from frontal, occipital, temporal, cingulate, parietal, insula, or cerebellar–subcortical regions. They found that the brain-PAD was increased in dementia and multiple sclerosis when the model estimated brain age using features only from cerebellar–subcortical while the largest effect was observed in the frontal lobe in schizophrenia. Smith, et al [38] estimated brain age using 62 modes representing distinct patterns of structural and functional brain alteration and selective association with genetics, cognition, lifestyle, disease and physical measures. They suggested that modelling of distinct pattern of brain alterations would provide more biologically meaningful biomarkers to detect brain aging than one single homogeneous process.

To conclude, in this study we propose to detect the disparity in the alterations of WM FGs through life-course using brain age. Results suggest that brain-PAD holds the potential as an aging biomarker. Moreover, it shows which FGs are more prone to aging than others which could be further investigated and exploited to estimate an aging-driven risk factor and an alert for cognitive decline and brain disorders related to the regions in each fiber group. In addition, we explored the association between daily life style, CRFs and genetic variations and their effects on each FG as well as on the Ensemble model gathering all the considered tracts. Such kind of associations can be employed to examine the influence of environment and ge-

netic factors to shape and control the aging process and related alterations at a FG level, providing a more localized information than the one obtained using the whole white matter. Overall, consistent results were obtained regarding the associations in different FGs. Some FGs showed similar pattern for the different considered associations. One of the main contributions of the study shows which FGs are more affected by the aging process as reflected by the considered IDPs. Furthermore, we were able to show that the Limbic FG plays a prominent role in driving brain aging. In addition, Brainstem FG observed to age faster and lest affected by the used measures in the analysis, precisely with daily life styles and activities This could be explained that Brainstem might age faster as it is more involved in many body functions. Benarroch [179] reported that Brainstem involves tracts that are critically associated with the control of the cardiovascular function, respiration, arousal and wake-sleep cycle. In that matter, brainstem tracts are more prone to alterations due to direct association with body organs. These findings suggest that further research and statistical tests are required to obtain a more comprehensive understanding and confirmation of the role of Limbic and Brainstem tracts in brain aging and their association with both body functions and environmental exposures.

# Chapter Five

# 5 Telomere length and brain IDPs

## 5.1 Introduction

Telomeres are (Deoxyribonucleic acid) DNA-protein complexes which protect the end of chromosomes from fusion and degradation. TL are shortened with time (i.e., during each cell cycle) in most human cell types [180]. Among many phenotypes, TL is associated with central nervous system and brain tumors [181]. Furthermore, TL is considered as a potential biomarker of aging related diseases such as AD [59]. GWAS have identified dozens of SNPs with a significant association to TL [182] [180]. These SNPs were found to play a critical role as regulators of Leukocyte TL through different mechanisms including deoxynucleoside monophosphate biosynthesis [182] and telomere elongation helicase [183]. Furthermore, these SNPs were causally associated through TL shortening with increasing facial skin aging [184], increased risk of AD [59] and coronary heart disease [180]. Confounds factors play a critical role in brain aging and brain IDPs studies [161] which might lead to biased association.

While several studies [185] [50] highlighted correlations between TL and brain IDPs, no study has established the causative link between the two. In fact, in those studies reduced TL may act as a biological proxy for aging and thus creating a correlation between natural aging and brain integrity. Accordingly, examining the causal association between TL and brain IDPs would help to understand the role of TL in the alterations of brain structure and function during aging. Such analysis would include a new biomarker in brain age estimation and would shed the light on one of the causes of the alterations within brain tissues. Therefore, we have performed MR analysis using instrument variables to investigate the casual association between TL and brain IDPs.

## 5.2 Data

To perform MR using instrument variables, we used GWAS summary statistics from two independent studies, one for TL and one for brain IDPs.

### 5.2.1 TL GWAS.

We selected 33 SNPs from different publicly available TL GWAS studies [182, 180]. The first 20 SNPs at 17 genomic loci were from the recent GWAS by Li et al. [182]. They conducted a large-scale GWAS in up to 78,592 European individuals, under the ENGAGE project (European Network for Genetic and Genomic Epidemiology). Polymerase Chain Reaction (PCR) technique was established to measure mean leukocyte TL quantitatively. The TL was presented as the ratio of the telomere repeat number to a single-copy gene. Sex, age and cohort-specific factors including genetic principle components and center were used as covariates in the GWAS. The selected 20 SNPs were significantly and independently associated with leukocyte TL. However, six SNPs were substituted to their proxies as they were palindromic [184]. For that purpose, LDlink was used to select suitable proxies [186].

The remaining 13 SNPs were used previously by Kuo et al. [180] to perform an MR analysis between TL and aging-related diseases in 261,000 older participants in the United Kingdom Biobank (UKB). The authors selected SNPs that were significantly ($P < 5 \times 10^{-8}$) associated with TL from previous GWAS studies. The SNPs used in their study included GWAS results from [183] using European population and six GWAS comprising 9,190 European participants [187]. We added these 13 SNPs to the previously selected 20 SNPs. Ten SNPs were removed because they were in high linkage disequilibrium (LD) with other SNPs ($R^2 > 0.02$). LD was calculated using GBR (British in England and Scotland) samples from Phase 3 (version 5) of the 1,000 Genomes Project using Ensembl 2020 [188]. The final list for our study comprised 23 SNPs (listed in Table 5.1).

Table 5.1: The list of the SNPs used in the MR analysis. rsID, the ID of the SNP; Chr, Chromosome; Pos, Position of the SNP in the genome; EA, effect allele; OA, other allele; EAF, effect allele frequency; Beta, the beta value of the SNP in GWAS; SE, standard error; S, the source of the SNP.

| rsID | Chr | Pos | Gene | EA | OA | EAF | Beta | SE | P-value | Source |
|---|---|---|---|---|---|---|---|---|---|---|
| rs2695242 | 1 | 226594038 | PARP1 | G | T | 0.83 | -0.039 | 0.0064 | 9.31E-11 | [182] |
| rs11125529 | 2 | 54475866 | ACYP2 | A | C | 0.16 | 0.065 | 0.012 | 4.48E-08 | [183] |
| rs6772228 | 3 | 58376019 | PXK | T | A | 0.76 | 0.041 | 0.014 | 3.91E-10 | [189] |
| rs55749605 | 3 | 101232093 | SENP7 | A | C | 0.58 | -0.037 | 0.007 | 2.45E-08 | [182] |
| rs7643115 | 3 | 169512241 | TERC | A | G | 0.243 | -0.0858 | 0.0057 | 6.42E-51 | [182] |
| rs13137667 | 4 | 71774347 | MOB1B | C | T | 0.959 | 0.0765 | 0.0137 | 2.37E-08 | [182] |
| rs7675998 | 4 | 164007820 | NAF1 | G | A | 0.8 | 0.048 | 0.012 | 4.35E-16 | [183] |
| rs7705526 | 5 | 1285974 | TERT | A | C | 0.328 | 0.082 | 0.0058 | 4.82E-45 | [182] |
| rs34991172 | 6 | 25480328 | CARMIL1 | G | T | 0.068 | -0.0608 | 0.0105 | 6.03E-09 | [182] |
| rs805297 | 6 | 31622606 | PRRC2A | A | C | 0.313 | 0.0345 | 0.0055 | 3.41E-10 | [182] |
| rs59294613 | 7 | 124554267 | POT1 | A | C | 0.293 | -0.0407 | 0.0055 | 1.12E-13 | [182] |
| rs9419958 | 10 | 105675946 | STN1 (OBFC1) | C | T | 0.862 | -0.0636 | 0.0071 | 4.77E-19 | [182] |
| rs228595 | 11 | 108105593 | ATM | A | G | 0.417 | -0.0285 | 0.005 | 1.39E-08 | [182] |
| rs76891117 | 14 | 73399837 | DCAF4 | G | A | 0.1 | 0.0476 | 0.0084 | 1.64E-08 | [182] |
| rs3785074 | 16 | 69406986 | TERF2 | G | A | 0.263 | 0.0351 | 0.0056 | 4.5E-10 | [182] |
| rs62053580 | 16 | 74680074 | RFWD3 | G | A | 0.169 | -0.0389 | 0.0071 | 3.96E-08 | [182] |
| rs7194734 | 16 | 82199980 | MPHOSPH6 | T | C | 0.782 | -0.0369 | 0.006 | 6.72E-10 | [182] |
| rs3027234 | 17 | 8136092 | CTC1 | C | T | 0.83 | 0.103 | 0.012 | 2E-08 | [187] |
| rs8105767 | 19 | 22215441 | ZNF208 | G | A | 0.289 | 0.0392 | 0.0054 | 5.21E-13 | [182] |
| rs6028466 | 20 | 38129002 | DHX35 | A | G | 0.17 | 0.058 | 0.013 | 2.57E-08 | [187, 182] |
| rs71325459 | 20 | 62268341 | RTEL1 | T | C | 0.015 | -0.1397 | 0.0227 | 7.04E-10 | [182] |
| rs75691080 | 20 | 62269750 | STMN3 | T | C | 0.091 | -0.0671 | 0.0089 | 5.75E-14 | [182] |
| rs73624724 | 20 | 62436398 | ZBTB46 | C | T | 0.129 | 0.0507 | 0.0074 | 6.08E-12 | [182] |

### 5.2.2 GWAS for Brain IDPs.

GWAS analysis were conducted using IDPs from six modalities covering three main categories that is: diffusion, structural and functional MRI for 40,000 participants (11,000 replication sample) released in early 2020 [190]. 3,913 IDPs was used to conduct GWAS analysis. In addition, 16 quality control and six summary functional connectivity features were used which make the total number 3935 IDPs. More details about the quality control and the used data can be found here [190].

## 5.3 Methods

The TL GWAS included participants from different cohorts such EPIC-CVD and the EPIC-InterAct case-cohort study which was conducted in ten countries including UK [182]. On the other hand, GWAS for brain IDPs was conducted on majority healthy [32] participants (at recruitment time) only from UK. There is a low possibility of overlapping participants between the TL GWAS and the brain IDP GWAS. We conducted MR analysis using the TwoSampleMR [191] package in R. For each brain IDP, we first downloaded the GWAS results and extracted the beta

value, stander error, effect allele, other allele, effect allele frequency and $p$-value for each SNP selected from TL GWAS studies (Table 5.1). Then we harmonised the data from TL GWAS and the brain IDPs GWAS using the `harmonise_data()` function. Finally, we performed MR between TL and brain IDPs. The (random effects) IVW method was adopted as a primary analysis for SNP-specific casual estimate for brain IDPs. $P$-values were corrected for multiple tests using the false discovery rate (FDR) method [192]. IDPs were considered significant at $P_{\text{FDR}} < 0.05$ (corresponding to $P < 0.004409$). Weighted median and weighted mode approaches were also implemented as complementary MR analyses (requiring uncorrected $P < 0.05$). To detect directional pleiotropy and heterogeneity of the genetic instruments, weighted median function [54] and MR-Egger [55] regression were performed. The MR-Egger intercept test ($P > 0.05$), leave-one-SNP-out analyses and the modified Cochran Q statistic methods were implemented as horizontal pleiotropy test and to assess the quality of results. In addition, we used MR–Pleiotropy Residual Sum and Outlier (MR-PRESSO) [193] to detect and correct pleiotropy which affected the overall results. Thus, for IDPs surviving our filtering by IVW ($P_{\text{FDR}} < 0.05$) and complementary analyses ($P < 0.05$), we retained IDPs when they showed either no horizontal pleiotropy in the MR-PRESSO global test ($P > 0.05$) or the IVW adjusted for SNP outliers detected by MR-PRESSO remained significant ($P_{\text{FDR}} < 0.05$). For each brain IDP association with TL, we generated an html file report using the command `mr_report()` in the package. The html file contains on all the results of the methods mentioned earlier. All the html files as the results of the current study will be available online at (`http://mrstudies.org/`).

## 5.4 Results

Figure 5.1 shows the result of the MR causality screen between TL and brain IDPs using the inverse variance weighted (IVW) method. Out of the 3,935 tested IDPs, 347 remained statistically significant after adjusting for multiple testing using the FDR method ($P_{\text{FDR}} < 0.05; P < 0.004409$). However, 119 IDPs were not marginally significant ($P > 0.05$) in the complementary MR analyses (i.e., the weighted mode

and weighted median) leaving 228 IDPs. MR-PRESSO [193] was used to investigate effects of pleiotropy in these MR results. Further 35 IDPs were excluded since MR-PRESSO detected horizontal pleiotropy (MR-PRESSO global test $P < 0.05$), which, after SNP outlier removal, was no longer significant at the FDR-corrected p-value threshold. Thus, the final number of the significant IDPs was 193. P-values of MR Egger-intercept of the 193 IDPs indicate no significant pleiotropy ($P > 0.05$). Therefore, overall, 193 out of 3,935 IDPs showed evidence of being significantly influenced by TL, the majority of which are diffusion metrics in different region of interests. The majority of the significantly associated IDPs (162 of 193) corresponds to different indices from diffusion MRI covering a wide range of white matter tracts (Table 5.2). Three IDPs correspond to resting-state fMRI and the remaining 28 were derived from T1-weighted MRI, with the majority representing gray-white matter intensity contrasts. The direction of association was uniform for each of the modalities: FA, ICVF and gray-white matter intensity contrast were negatively associated with TL (i.e., longer TL causes decreases); axial (L1), radial (L2, L3) and mean diffusivity (MD) were positively associated with TL (i.e., longer TL causes increases in these values)

Table 5.2: The significant IDPs categorized by modality. ED: effect direction whether it is positive (+) or negative (-).

| Category | Number | ED | Category | Number | ED |
|---|---|---|---|---|---|
| FA | 12 | - | ISOVF | 1 | - |
| ICVF | 27 | - | wg intensity-contrast | 18 | + |
| L1 | 18 | + | Thickness | 5 | - |
| L2 | 29 | + | Area | 1 | - |
| L3 | 42 | + | Volume | 4 | - |
| MD | 32 | + | rs-fMRI | 3 | + |
| OD | 1 | - | | | |

Figure 5.2 illustrates for the most prevalent diffusion indices the tracts that are causally influenced by TL according to the MR analysis. Many tracts are found to be associated across the various diffusion indices. For instance, almost all diffusion indices were significant in tracts like posterior thalamic radiation and anterior thalamic radiation in both hemispheres. Furthermore, the grey-white matter intensity contrast in many cortical regions were causally associated with TL (Figure 5.2.

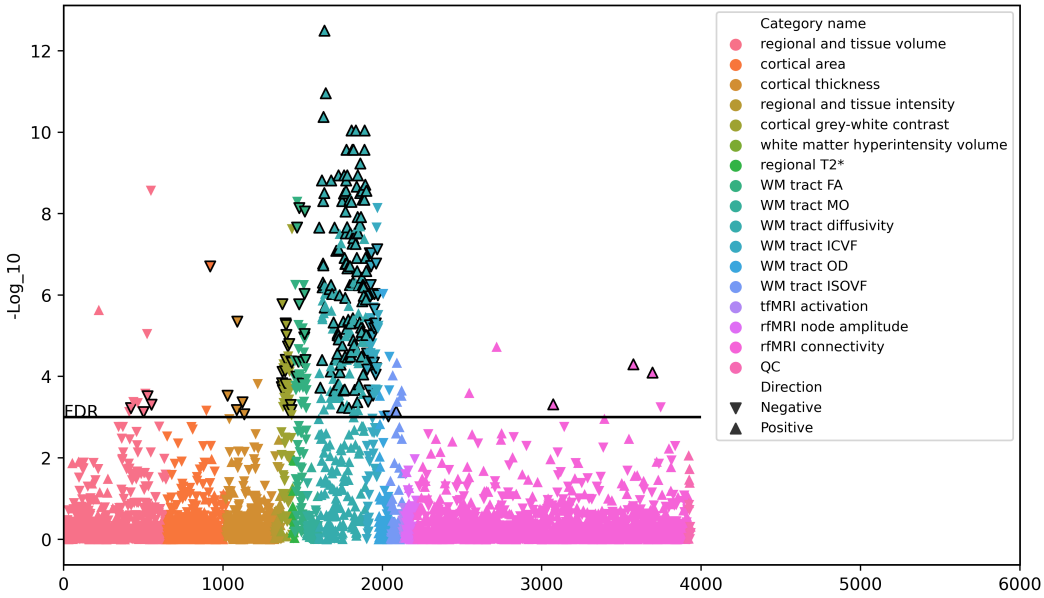


Figure 5.1: The causal association of TL and brain IDPs using the IVW method. The y-axis represents the $-\log_{10}(p-\text{values})$ of the association. The color of each IDP indicates the MRI modality and the triangle shape indicates whether the identified association (IVW $\beta$ value) is positive ($\triangle$) or negative ($\triangledown$). The black horizontal line indicates the FDR-adjusted significance threshold ($P = 0.004409$). The triangles with black border highlight the 193 IDPs that were significantly associated with TL using the IVW method as well as the complementary MR analyses. WM: white matter; FA: fractional anisotropy; MO: diffusion tensor mode; OD: orientation dispersion; ICVF: intracellular volume fraction; ISOVF: isotropic volume fraction; tfMRI: task fMRI; rfMRI: resting-state fMRI; QC: quality control.

## 5.5 Discussion

In this study, we performed casual association of TL and 3,935 brain IDPs using MR. The results indicate that TL casually affect 193 brain IDPs. Interestingly, the majority of the significant IDPs were related to white matter but not to gray matter. Even the measure with the highest number of significant IDPs derived from T1-weighted MRI was the grey-white matter intensity contrast. In the context of aging the diffusion indices can be interpreted in terms of white matter integrity. For instance, high FA values suggest increased diffusion directionality and thereby higher white matter integrity. Contrary, high MD values suggest a higher average rate of diffusion and thus impaired WM integrity [97]. Therefore, with increasing age, FA tends to decline while MD tends to increase in white matter tracts. In previous works some of the IDPs were also identified as informative features to model and estimate

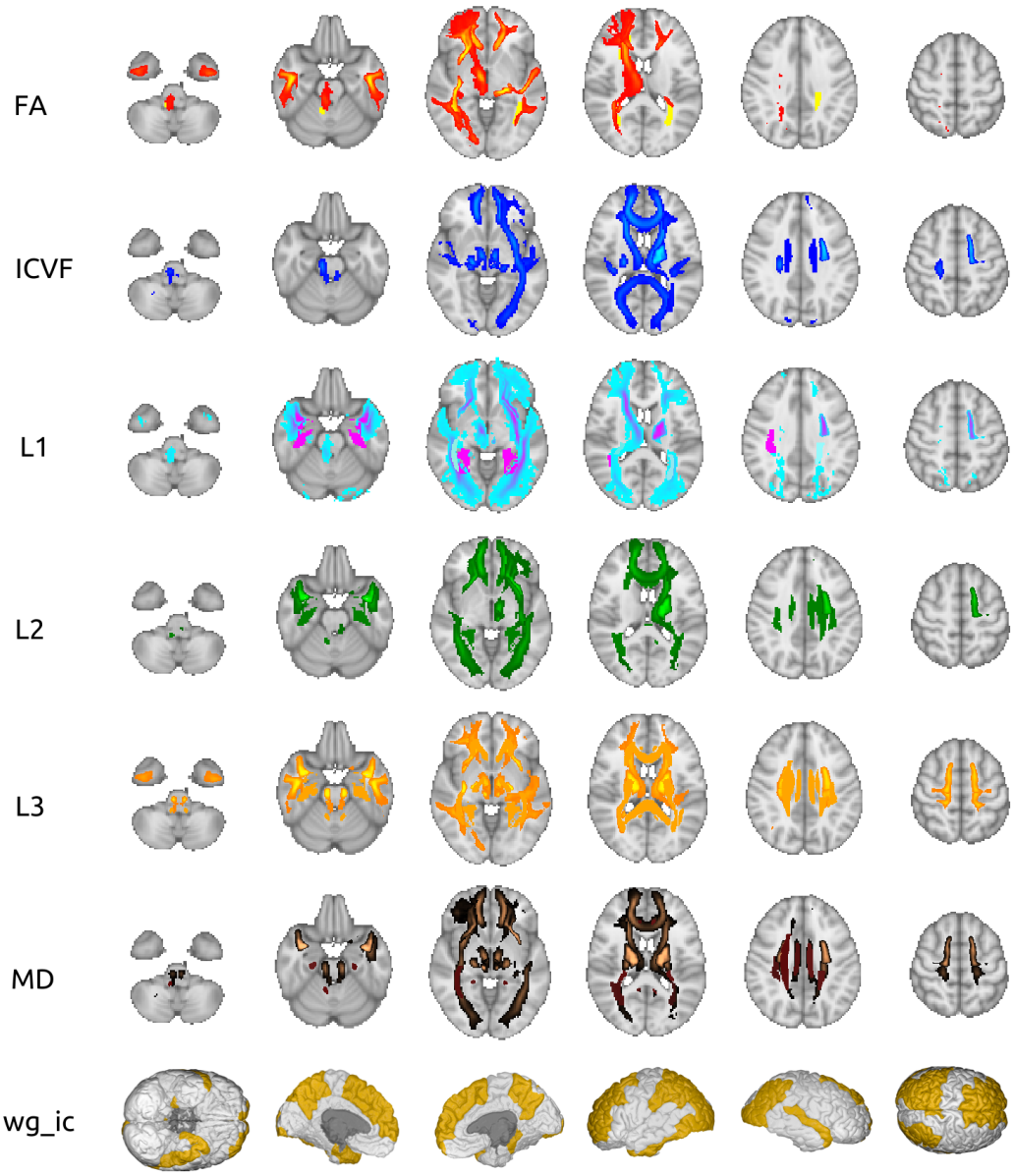


Figure 5.2: Visual representation of the significant IDPs among the seven most prevalent measures. For the six diffusion indices (top six rows) the tracts that are significantly associated with TL are highlighted. The last row shows the cortical regions with a significant effect of TL on gray-white matter intensity contrast. Different colors within a diffusion measure relate to IDPs extracted from two different methods: tract-based spatial statistics (solid colors) and probabilistic tractography (color gradients). The plots were generated by BrainPainter [194] and FSL [195]

brain age. For instance, ten out of the 193 IDPs were previously reported to have a significant association with brain age delta [32] that are: weighted mean anterior thalamic radiation left (L2 and L3), weighted mean posterior thalamic radiation left (L2 and MD), weighted mean uncinate fasciculus left (MD), weighted mean

posterior thalamic radiation right (L2 and MD), weighted mean anterior thalamic radiation right (MD and L3) and TBSS external capsule right (ICVF). Moreover, three other IDPs (i.e., TBSS posterior thalamic radiation right (L3), weighted mean uncinate fasciculus left (L3) and TBSS cingulum hippocampus right (MD)) were also previously reported to be important to estimate brain age [196]. However, despite changes in these IDPs having been reported before as potential biomarkers of brain aging, the driving factor behind these changes was missing. Our MR analysis demonstrated that TL is one key factor that influences the observed values of these IDPs, and by extension brain aging.

Previous studies demonstrated that FA and ICVF decline with aging while axial, radial and MD increase [99], although regional differences have been described [197, 198]. Based on these findings and considering TL as a proxy for cellular aging, we would expect a positive correlations between TL and FA/ICVF as well as negative correlations between TL and axial, radial and mean diffusivity. However, the MR results support the opposite direction, indicating decreasing FA and ICVF with increasing TL as well as increasing L1, L2, L3 and MD with increasing TL. While the expected trend with increasing age for radial and mean diffusivity is quite clear, there are brain regions, such as the midbrain white matter, which show decreases rather than increases in axial diffusivity [197]. Indeed, increased axial diffusivity can be interpreted as a positive marker for white matter integrity since lowered axial diffusivity indicates axon injury; by contrast, increased radial diffusivity has been linked to incomplete or damaged myelination [197]. Furthermore, association between TL and diffusion indices that are reversed compared to the effects of aging have been found in adolescent rats of the same age [199]: axial, radial and mean diffusivity were positively correlated to measured TL. In addition, FA and L1 followed inconsistent pattern in different white matter tracts when brain age was estimated [196]. Regarding the gray-white intensity contrast, previous studies demonstrated that it decreases with ageing [200, 201]. On the other hand, gray-white intensity contrast was found to be increased in people with schizophrenia and bipolar disorder compared to controls [202] although both conditions are linked to

accelerated brain ageing [203, 204, 205]. In addition, increased grey-white matter contrast was observed in Autism Spectrum Disorders [206] which is also linked to accelerated brain ageing [207].

Thus, overall, this MR analysis demonstrated that the association between TL and brain IDPs is not simply the effect of increased cellular aging but there appears to be a more complex relationship underneath.

The instrumental variables used in this MR analysis involved numerous genes, which have been reported in the literature to be associated with regulating TL as well as being involved in brain disorders. The SNP rs2695242 is located within the Poly (ADP-ribose)-polymerase1 (*PARP1*) gene. *PARP1* is known to contribute largely to regulate telomere complex assembly and activity [208]. Additionally, *PARP1* was previously reported to play an essential role in neurodegenerative diseases such as AD and Parkinson's disease [209]. In particular, it was observed that *PARP1* is activated in aging and neurodegenerative diseases leading to autophagy, neuroinflammation and mitochondrial dysfunction and dysregulation [209]. Further instrumental variable (rs7705526) belong to the Telomerase Reverse Transcriptase (*TERT*) gene. The main function of the *TERT* gene is to maintain telomeres by extending them with the telomere repeat sequence [210]. *TERT* was found to have a protective role in brain aging [211]. The authors demonstrated that neurodegenerative symptoms and brain aging were influenced by shorter telomeres, and conversely, that increasing the level of TERT in the brain of mice, and by extension the telomeres, could significantly revert signs of cognitive impairment. Lastly, the SNP rs228595 belongs to the ataxia telangiectasia mutated (*ATM*) gene which contributes telomere maintenance through telomere elongation and telomerase complex assembly [212]. It was reported that in humans, *ATM* function decreased in neurons with increasing progression of AD [213]. Thus, overall, numerous genes that harbor the instrumental variables in our MR analysis exhibit a direct role in maintaining telomeres, and have been, in previous studies, linked to degenerative brain disorders. Our study extends this link to the intermediate level of brain IDPs.

To the best of our knowledge, this is the first study to perform MR between TL and a wide range brain IDPs extracted from different MRI modalities. The results support

the causal link between TL and the brain's micro and macro structure as represented by the IDPs, with a strong emphasis on white-matter related measurements. The second finding of this study was that the direction of TL-IDP associations did not replicate the effect direction of aging-associated changes. However, the diffusion indices are influenced by multiple aspects of the brain's micro and macro structure. For instance, despite showing a decrease in white matter integrity, increased mean diffusivity was found to be associated with increased cell density and axonal density [214]. Furthermore, current studies investigating brain age focus on linking changes in brain IDPs with genetic variations and environment factors [75], but have not considered the potentially driving role of TL. To summarize, our study showed that TL significantly influenced 193 IDPs covering diffusion MRI metrics, cortical grey-white contrast regions, resting state fMRI and morphometric measures making TL a valuable feature to be considered when estimating and investigating brain age.

# Chapter Six

# 6 Alzheimer disease and brain IDPs

Alzheimer's disease (AD) is the most common neurodegenerative disorder and main cause of dementia. AD is characterized by behavioral and cognitive impairment, memory deficits, social deficits and might eventually lead to death [59]. Individuals with AD undergo changes in brain structure and function, especially in terms of atrophy which can be assessed using sMRI. These alterations include cortical thinning, volume loss, morphological changes in grey matter. In particular, hippocampal atrophy has been demonstrated to be an important biomarker of AD and is used to monitor disease progression. In addition to changes in the brain's GM, AD also causes WM structural deterioration that can be captured using diffusion MRI [215]. In particular, diffusion MRI can be used to derive different microstructural indices such as FA and MD related to the motion of water molecules within WM tracts. FA describes the water diffusion directionality and decreased values have been observed in uncinate fasciculus, fornix, superior longitudinal fasciculus and cingulum in AD individuals [216]. Furthermore, increase in MD represents a source of brain pathology and WM degeneration [217] and has been observed in forceps minor, forceps major and projecting fibres in AD patients [218]. In terms of functionality, resting-state fMRI (rs-fMRI) is widely used to map brain connectivity and regional interactions while resting (free-task state). Functional connectivity can be used to assist in diagnosing brain diseases even before brain atrophy occurs [219]. Rs-fMRI has shown to be a valuable tool to identify pathophysiology of functional connectivity in AD patients [220].

Thus far, changes of brain characteristics in AD patients have been assessed using different methods including machine learning [221] and statistical tests such as linear regression, correlation and analysis of variance (ANOVA)[222]. Moreover, the putative causal relations between AD and brain alterations were investigated using Mendelian Randomisation (MR) [65] [49] [223] [224]. MR is a method to inves-

tigate the casual association between modifiable risk factors and a disease using instrument variables obtained from genetics. In brief, a valid instrumental variable should be associated significantly with the exposure, independent from the confounds and associate with the outcome only through the exposure [225]. These are the three core assumptions of choosing a valid instrument variable to perform MR. Single nucleotide polymorphisms (SNPs) are plausible to meet these criteria as they are independent from any confound and the other two assumptions can be applied when performing MR analysis [226].

Recently carried out genome wide association studies (GWAS) detected dozens of SNPs that are linked to AD diagnosis and disease progression. The summary statistics of AD GWAS can be used and exploited to investigate the casual connection between AD with any other exposure or outcome. In a recent study, casual associations between brain imaging endophenotypes and AD were assessed using two-samples MR, transcriptome wide association studies (TWAS), generalized summary statistics based Mendelian randomization (GSMR) and the adaptive sum of powered score (aSPU) approach [65]. In details, the authors used GWAS summary statistics to estimate the casual effect between 1,578 heritable brain phenotypes from UKBB [78] and AD IGAP [227]. Their results indicated casual association of 35 brain phenotypes and AD in aSPU method, while no significant association was detected using the two-samples MR. Using the same summary statistics for brain phenotypes and AD, Katherine A and colleagues [49] conducted a two-samples MR as well as a Multivariate Imaging Wide Association Study (MV-IWAS). They detected several brain phenotypes causally associated with AD in MV-IWAS method, while there was no significant association using the two-samples MR further confirming previous results reported by [65]. Furthermore, MR was recently adopted to assess the causal association between cortical structures and AD [224]. Analyses were conducted using GWAS summary statistics of the thickness of the whole cortex, surface area and 34 cortical regions with AD risk. They detected suggestive causal associations between decreased surface area of the temporal pole and decreased thickness of cuneus with higher risk of AD. However, the association did not pass the Bonferroni-corrected p-value thereshold. More recently, the causal link

was investigated using bi-direction two-samples MR between AD and measures of total intracranial volume, volume of subcortical structures, global/regional cortical thickness and cerebral WM for individuals aged eight to 81 years from five different cohorts [223]. Authors performed GWAS of brain phenotypes using subjects from the different cohorts as follows. For peripubertal period, GWAS was conducted using subjects from Generation R (age range: 8.71- 11.99), the Adolescent Brain Cognitive Development study (age range: 8.92-11.00) and IMAGEN (age range: 12.94-16.04). The Avon Longitudinal Study of Parents and Children (age range: 18-24.5) was used for early adulthood, while UKBB was used for adulthood (age range: 48-81). Their results suggest casual association of AD with cortical and sub-cortical brain measures in mid to late adulthood. In particular, the association of AD was observed with age dependent decreasing in the volume of thalamus, accumbens, hippocampus, thickness of inferior temporal cortices and middle temporal in UKBB cohort.

SNPs selection depends on the tested hypothesis to determine the exposure and the outcome. For instance, if the hypothesis is to test the casual association of AD (exposure) and brain phenotypes (outcome), then SNPs should be significantly associated with AD and independent from brain phenotypes. Conversely, if the tested hypothesis is whether alterations in brain phenotypes cause AD, then the SNPs should be significantly associated with brain phenotypes and independent from AD. In [65] [49] and [224], authors performed SNPs selections and linkage disequilibrium (LD) calculation on brain IDPs GWAS as they were testing the causal influence of brain IDPs on the risk of developing AD (e.g., whether a reduced hippocampus will more likely result in a later AD diagnosis). This led to a different number of SNPs to be considered as instrument variables for each investigated brain IDPs. P-value ($p < 5 \times 10^{-8}$) has become a standard threshold for GWAS to identify a significant association between a genetic variation and a phenotype [228]. In addition, they used a less restrictive p-value threshold ($p < 5 \times 10^{(-6, -5)}$) to select the SNPs associated with brain IDPs from GWAS results. This might include some SNPs that are not significantly associated with brain IDPs based on GWAS standard p-values threshold. Moreover, [223] and [224] considered IDPs from structural MRI

with a focus on GM and brain volumes. However, there are increasing data demonstrating correlations between AD diagnosis and changes in WM and brain function, thus considering IDPs from other MRI modalities such as diffusion and functional MRI can provide the opportunity to detect causal association that was not covered in [223] and [224]. In addition the IDPs extracted from functional MRI were considered as significant features to detect early stage of AD [220]. However, so far no MR studies in AD considered features from dMRI nor from fMRI.

Despite the previous studies performed MR analysis using different number of phenotypes, however two studies [65] [49] used the old GWAS of IGAP while the others used phenotypes obtained only from structural MRI. In this study we used two-samples MRI to assess the casual association of AD and 3,935 brain IDPs extracted from six MRI modal modalities, namely T1 and T2-weighted structural images, dMRI, task fMRI, rs-fMRI and susceptibility-weighted MRI. More in details, we performed SNPs selection and LD calculation on the new AD GWAS from IGAP rather than on brain IDPs GWAS before fitting them into MR analysis. Summery statistics of two independent GWAS that are publicly available were used. Consequently, we do not require data at individual level and therefore, a formal consent is not required to perform such analyses.

## 6.1 Materials

### 6.1.1 Alzheimer disease GWAS

Results from a recent GWAS of clinically diagnosed AD were used to identify suitable instruments to model the exposure in the MR analysis [229]. The GWAS samples were collected from four consortia, Alzheimer Disease Genetics Consortium (ADGC), Cohorts for Heart and Aging Research in Genomic Epidemiology Consortium (CHARGE), The European Alzheimer's Disease Initiative (EADI), and Genetic and Environmental Risk in AD/Defining Genetic, Polygenic and Environmental Risk for Alzheimer's Disease Consortium (GERAD/PERADES). Different quality control steps were performed on the genetic data as described in detail in [229].

### 6.1.2 Brain IDPs GWAS

In our MR analysis brain structure and function were the target. In order to obtain effect size estimates for the genetic instruments, we used results from a GWAS analysis available in the UKBB on 3,935 brain IDPs spanning a range of diffusion, structural, functional MRI summary measures, quality control measures and compact FC features [190]. More details regarding the used methods and quality control criteria can be found in [190]. Of note, the following sets of variables were used as confounds and regressed from brain IDPs for better GWAS interpretability: head size, sex, age, scanner table position, head motion during functional MRI, imaging center and scan date-related slow drifts. The GWAS summary statistics were based on 33K subjects with UK ancestry (22k discovery and 11k replication) and 17,103,079 SNPs. Summary statistics for individual IDPs can be accessed through (`https://open.win.ox.ac.uk/ukbiobank/big40/`)

## 6.2 Methods

First, we downloaded the GWAS results of clinical AD diagnosis [229] that are publicly available at (`https://www.ebi.ac.uk/gwas/studies/GCST007511`). GWAS threshold (P-value $< 5 \times 10^{-8}$) was used to select only the significant association of genetic variants and AD diagnosis. Thereafter, we calculated LD among the SNPs to chose independent genetic variations. PLINK[163] was used to conduct LD clumping using windows size 2 MB, $r^2 = 0.001$ and the 1,000 Genomes Project Phase 3 European datasets as a reference. LDlink [186] was used for SNPs that were not available in the target GWAS or were palindromic. After downloading the GWAS results of the significant SNPs for all 3,935 brain IDPs, we performed MR analysis using TwoSampleMR package in R [230]. The GWAS results for both AD diagnosis and brain IDPs were first harmonized and two-samples MR analysis was performed using inverse-variance weighted (IVW). IVW was adopted as the primary analysis for SNP-specific casual estimate. Weighted mode and weighted median approaches were computed as complementary analysis. IVW assumes all the used genetic variations are valid instrument variables while weighted median assume the majority of used genetic variations are valid instrument variables [231].

The weighted median allows the stronger SNPs to contribute more in the estimation [230]. MR-Egger [55] regression and weighted median function [54] were implemented to detect directional pleiotropy and heterogeneity of the genetic instruments. To test the quality of the results, horizontal pleiotropy test was conducted using the MR Egger intercept test, the modified Cochran Q statistic methods and leave-one-SNP-out analyses. The Bonferroni method (alpha = 0.05) [162] was used to correct p-values for multiple tests across all IDPs.

For each analysis, an HTML file was generated using the TwoSampleMR package in R. The html site reports the results of the main and complementary analyses. Additionally, it features plots to visualize the results such as forest plot and a plot for leave-one-out sensitivity analysis. All html files displaying the results of the current study will be available online at ( `http://mrstudies.org/`).

### 6.3 Results

1,514 SNPs were selected that passed GWAS standard threshold with the majority on chromosome 19. After LD clumping, 28 independent SNPs remained. Among these SNPs, 3 SNPs were not available at GWAS brain IDPs and other 5 were palindromic. 3 SNPs were monoallelic and one did not have sufficient LD $r^2$ (less than 0.04) with any other SNP to be used as proxy. The other 4 SNPs were substituted by their proxies. This left 24 SNPs as the final number to conduct the two-samples MR analysis. Table 6.1 shows the details on the 24 SNPs that were used to conduct the MR analysis. For each brain IDP, we downloaded and extracted the GWAS results of these 24 SNPs from (`https://open.win.ox.ac.uk/ukbiobank/big40/`). The following GWAS results were extracted: beta coefficient, standard error, p-value, effect allele and other allele. A total of 3,935 MR association tests were conducted, one for each brain IDP fixing AD as the exposure and the brain IDPs as the outcome. Thus, significant associations indicate a causal effect of AD on the corresponding brain IDP. AD was significantly associated at $P_{bonferroni} < 0.05$ with 46 IDPs in the main and complementary analysis. However, among these 46 IDPs, eight reported a significant association with one of the 24 SNPs (rs11556505) and therefore violated MR assumptions. We removed that SNP from the set of instru-

Table 6.1: The 24 SNPs used to perform MR causal association. Chr, chromosome; Pos, position; rsID, SNP ID; EA, effect allele; OA, other allele; SE, standard error.

| Chr | Pos | rsID | Gene | EA | OA | Beta | SE | P-value |
|---|---|---|---|---|---|---|---|---|
| 1 | 207750568 | rs679515 | CR1 | T | C | 0.1508 | 0.0183 | 1.555E-16 |
| 2 | 127863029 | rs7583814 | BIN1 | T | C | 0.1212 | 0.0192 | 2.532E-10 |
| 2 | 127892810 | rs6733839 | NIFKP9, BIN1, APOE | T | C | 0.1693 | 0.0154 | 4.022E-28 |
| 6 | 32560306 | rs34665982 | HLA-DRB1 | T | C | 0.0967 | 0.0166 | 5.798E-09 |
| 6 | 41129252 | rs75932628 | TREM2, PLCG2, ABI3 | T | C | 0.6989 | 0.1001 | 2.948E-12 |
| 6 | 47575332 | rs9395286 | CD2AP | T | C | 0.0876 | 0.0157 | 2.232E-08 |
| 7 | 143109139 | rs11767557 | EPHA1-AS1 | T | C | 0.1028 | 0.0182 | 1.561E-08 |
| 8 | 27219987 | rs73223431 | PTK2B | T | C | 0.0936 | 0.0153 | 8.342E-10 |
| 8 | 27468503 | rs867230 | CLU | A | C | 0.1333 | 0.0158 | 3.492E-17 |
| 10 | 11721102 | rs12358692 | ECHDC3, USP6NL-AS1 | C | T | -0.085 | 0.0154 | 3.417E-08 |
| 11 | 121435587 | rs11218343 | SORL1 | T | C | 0.2053 | 0.0369 | 2.633E-08 |
| 11 | 47380340 | rs3740688 | SPI1 | T | G | 0.0935 | 0.0144 | 9.702E-11 |
| 11 | 60021948 | rs1582763 | MS4A4A | A | G | -0.1232 | 0.0149 | 1.186E-16 |
| 11 | 85868640 | rs3851179 | LINC02695, RNU6-560P | T | C | -0.1198 | 0.0148 | 5.809E-16 |
| 14 | 92938855 | rs12590654 | SLC24A4 | A | G | -0.0906 | 0.0157 | 8.729E-09 |
| 19 | 1050874 | rs12151021 | ABCA7 | A | G | 0.1071 | 0.0169 | 2.562E-10 |
| 19 | 45241638 | rs2927437 | CEACAM16-AS1, BCL3 | A | G | 0.2333 | 0.0183 | 3.729E-37 |
| 19 | 45329438 | rs78986976 | BCAM, NECTIN2 | A | G | -0.2519 | 0.039 | 1.045E-10 |
| 19 | 45355288 | rs149661872 | NECTIN2 | T | C | 0.9872 | 0.0762 | 2.164E-38 |
| 19 | 45382675 | rs41290120 | NECTIN2 | A | G | -0.6169 | 0.0411 | 5.197E-51 |
| 19 | 45396144 | rs11556505 | TOMM40 | C | T | -0.9653 | 0.0189 | 0 |
| 19 | 45425460 | rs157595 | APOC1P1,APOC1 | A | G | -0.4329 | 0.017 | 2.43E-143 |
| 19 | 45438554 | rs7254133 | APOC1P1,APOC4 | T | C | 0.2905 | 0.0242 | 4.236E-33 |
| 19 | 45592238 | rs10420562 | GEMIN7-AS1 | C | T | 0.2003 | 0.075633 | 2.742E-13 |

mental variables and repeated the two-samples MR analysis for those eight IDPs. None of the eight IDPs were now significantly influenced by AD. Thus, the final number of the significant causal associations of AD on brain IDPs was 38. The results of heterogeneity test indicated that four of the 38 IDPs exhibited heterogeneity with the full set of 24 independent SNPs in the effect estimates (p-values of MR Egger Q and IVW Q $< 0.05$). This violates the assumptions of valid instrument variables in MR analysis and therefore the four IDPs were no longer considered. Thus, 34 IDPs did not violate MR assumptions and were significantly causally influenced by AD. Moreover, the p-value of Egger_intercept of the 34 IDPs did not suggest any directional horizontal pleiotropy with the 24 SNPs. Figure 6.1 shows the p-values for all IDPs (Figure 1A) and the direction of the association of the 34 IDPs (Figure 1B). Table 6.2 reports the summary results of the 34 brain IDPs. Most of the IDPs are from sMRI followed by rs-fMRI and dMRI. Of note, a key region in this disorder (hippocampus) was significantly associated with AD in both sMRI and dMRI measures. AD was also causally and significantly associated with many measures extracted from fMRI.

**Discussion**

In this study we performed two-samples MR analyses to investigate the causal association of AD and a wide range of brain IDPs. A set of 24 SNPs that are signifi-

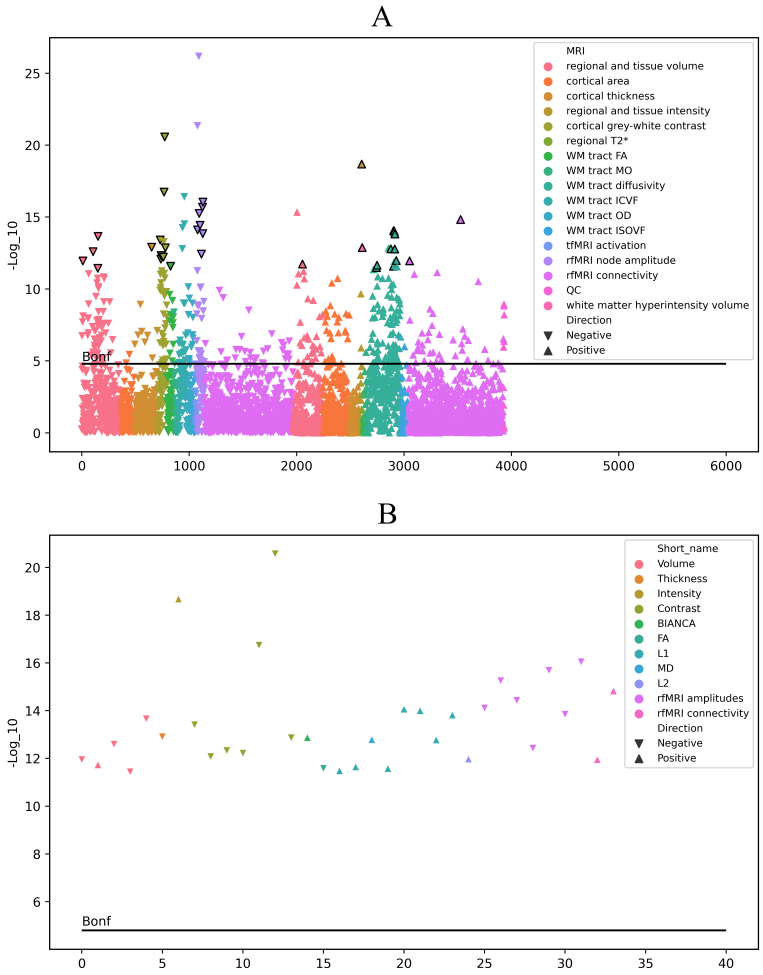


Figure 6.1: The causal association of AD and brain IDPs using the IVW method. The y-axis represents the $-\log_{10}(p-\text{values})$ of the association. The color of each IDP indicates the MRI modality and the triangle shape indicates whether the identified association is positive ($\triangle$) or negative ($\triangledown$). The black horizontal line indicates the Bonferroni-adjusted significance threshold ($P < 0.05/3{,}935$). A) The triangles with black border highlight those 34 IDPs that are significantly associated with AD using the IVW method as well as the complementary MR analyses. B) Focus on the resulting 34 IDPs with their corresponding indices.

cantly associated with AD were included as instrument variables to then perform the causal association with 3,935 brain IDPs from six MRI modalities. After multiple testing correction and ensuring that assumptions of MR analysis were not violated, we found 34 IDPs that were casually driven by AD. The significant IDPs included 15 from sMRI, ten from dMRI and nine from fMRI. The direction of the association matches with the expectations and observations in cross-sectional and longitudinal studies. Among the most prominent: AD causes decline in hippocampal volume and

Table 6.2: List of 34 IDPs causally and significantly associated with AD. The reported p-values are those multiple comparison correction. Lh and rh refer to left and right hemisphere, respectively. The name of the IDPs are extracted from the original paper that performed brain IDPs GWAS [190]).

| IDP short name | Beta | P-value |
|---|---|---|
| IDP T1 FIRST left hippocampus volume | -0.035 | 2.552E-02 |
| aseg global volume WM-hypointensities | 0.042 | 3.157E-02 |
| aseg lh volume Accumbens-area | -0.038 | 1.339E-02 |
| HippSubfield lh volume GC-ML-DG-body | -0.034 | 4.254E-02 |
| HippSubfield lh volume CA4-body | -0.039 | 4.617E-03 |
| aparc-a2009s rh thickness G-cingul-Post-ventral | -0.037 | 9.804E-03 |
| aseg rh intensity Amygdala | 0.047 | 3.033E-05 |
| wg lh intensity-contrast fusiform | -0.044 | 5.933E-03 |
| wg lh intensity-contrast lingual | -0.038 | 2.244E-02 |
| wg lh intensity-contrast parahippocampal | -0.036 | 1.747E-02 |
| wg rh intensity-contrast bankssts | -0.040 | 1.953E-02 |
| wg rh intensity-contrast inferiortemporal | -0.052 | 2.121E-04 |
| wg rh intensity-contrast middletemporal | -0.054 | 4.599E-06 |
| wg rh intensity-contrast pericalcarine | -0.042 | 1.023E-02 |
| IDP T2 FLAIR BIANCA WMH volume | 0.042 | 1.008E-02 |
| IDP dMRI TBSS FA Cingulum hippocampus L | -0.037 | 3.682E-02 |
| IDP dMRI TBSS L1 Posterior limb of internal capsule L | 0.035 | 4.047E-02 |
| IDP dMRI TBSS L1 Superior corona radiata R | 0.041 | 3.430E-02 |
| IDP dMRI ProbtrackX MD fma | 0.040 | 1.099E-02 |
| IDP dMRI ProbtrackX L1 fma | 0.035 | 3.686E-02 |
| IDP dMRI ProbtrackX L1 ifo l | 0.039 | 3.061E-03 |
| IDP dMRI ProbtrackX L1 ptr l | 0.044 | 3.267E-03 |
| IDP dMRI ProbtrackX L1 str l | 0.037 | 1.111E-02 |
| IDP dMRI ProbtrackX L1 str r | 0.039 | 3.908E-03 |
| IDP dMRI ProbtrackX L2 fma | 0.038 | 2.474E-02 |
| rfMRI amplitudes (ICA25 node 9) | -0.039 | 2.948E-03 |
| rfMRI amplitudes (ICA100 node 3) | -0.047 | 9.366E-04 |
| rfMRI amplitudes (ICA100 node 11) | -0.039 | 2.139E-03 |
| rfMRI amplitudes (ICA100 node 24) | -0.039 | 1.586E-02 |
| rfMRI amplitudes (ICA100 node 34) | -0.041 | 6.087E-04 |
| rfMRI amplitudes (ICA100 node 36) | -0.039 | 3.819E-03 |
| rfMRI amplitudes (ICA100 node 39) | -0.043 | 4.252E-04 |
| rfMRI connectivity (ICA25 edge 24) | 0.037 | 2.532E-02 |
| rfMRI connectivity (ICA100 edge 681) | 0.045 | 1.432E-03 |

its subfields [232] [233] as well as increases in WM hyperintensities [234] [235]. In addition, our findings show that both hemispheres are influenced by AD though the left hippocampus is more influenced than the right hippocampus, in agreement with previous studies [236]. Moreover, individuals with AD experience increases in axial, radial and mean diffusivity measures while fractional anisotropy decreases,

both indicating decline of white matter integrety [237]. Furthermore, the MR analysis identified an influence of AD on seven regional amplitudes obtained from rs-fMRI. Studies comparing rs-fMRI amplitudes between healthy controls and people with AD found decreased amplitudes in AD, which matches our results [238] [239]. Thus, our results are inline in terms of the direction of these measures observed in individuals with AD compared to controls [240]. The MR analysis also detected two casual associations of AD and rs-fMRI connectivities, here the direction was positive, i.e., AD causing a stronger coupling between brain regions. Previous work has found decreased as well as increased functional connectivity [241].

Among the 34 significantly influenced IDPs, AD was affecting four measures from both sMRI and dMRI that are related to hippocampus. Decline in hippocampal volume is considered one of the hallmark features of AD [242]. Moreover, alterations in dMRI indices linking the hippocampus to other brain regions might be valuable biomarkers for hippocampal dysfunction that can be exploited to monitor the progress of AD [243]. Our results show that AD causes alterations within brain that can be detected using different IDPs from MRI modalities rather than focusing on one single MRI modality. Further investigations in this direction could focus on the causal influence between brain IDPs from different MRI modalities (e.g., does sMRI influence dMRI or vice versa?), and consequently their effects on cognitive functions. In addition, the results indicate that intensity-contrast in different brain regions including fusiform, lingual, bankssts, inferiorparietal and middletemporal can be used as informative biomarkers to distinguish healthy from AD subjects [244].

rs679515 SNP is located in complement C3b/C4b receptor 1 (*CR1*) gene which was among the top lead SNPs associated with family history of AD in UKBB population [245]. Another SNP (rs6733839) is located upstream of the bridging integrator 1 (*BIN1*) gene. Individuals with 2 copies of this SNP allele (T) experience weak performance in episodic memory, specially in elderly people with type 2 diabetes [246]. The triggering receptor expressed on myeloid cells 2 (*TREM2*) gene on chromosome 6 includes the rs75932628 SNP which is considered as a risk factor of late-onset AD (LOAD) [247]. The rs11767557 variant significantly effects

and regulates gene expression of the erythropoietin-producing hepatoma receptor A1 (*EPHA1*) gene [248] and increase memory decline in LOAD [249]. Early-onset AD (EOAD) was significantly associated with rs73223431 variant through modifying gene expression of the protein tyrosine kinase 2 beta (*PTK2B*) gene [250]. The rs11218343 SNP, belonging to sortilin related receptor 1 (*SORL1*) gene, showed evidence of association with LOAD in many populations including Korean, Japanese and Caucasians. It is also reported that the allele C of the SNP may play a protective role for LOAD in Han Chinese population [251]. Finally, the rs3740688 variant located in the CUGBP elav-like family member 1 (*CELF1*) gene is associated with the processes involved in neurodegeneration and brain amyloidosis [252].

While several significant results were found in our study, the previous works [65] [49] that conducted a two-samples MR did not detect any significant associations. This can be explained by many factors related to the methodology and the quality controls steps. In particular, the main difference is related to the type of association under investigation, indeed in these two works authors assessed the causal association of inherited brain IDPs on AD while we tested the other direction, that is the causal association of AD on brain IDPs. Moreover, we used the extended version of brain IDPs GWAS which was conducted on 3,935 brain IDPs with around 17 millions SNPs from 33k subjects, while these two works used the previous version of 1,578 heritable brain IDPs GWAS for around 11 millions SNPs in 8,428 subjects (discovery dataset). In addition, we performed SNPs selection and LD calculation on AD GWAS while in the two works they performed the steps on brain IDPs GWAS. We also used the standard GWAS threshold (P-value $< 5 \times 10^{-8}$) to select the SNPs that are significantly associated with AD while they used less restrictive 'suggestive' GWAS threshold (P-value $< 5 \times 10^{-5}$). Finally, we also used less instrumental SNPs to perform the two-samples MR, while a different number of SNPs for each IDP was used in the previous studies, ranging from 35 to 112 (mean: 70) for the first work [65] and from 43 to 132 (mean: 81) in the second one [49]. Including a large number of SNPs in the MR analysis might involve invalid instrument variables which consequently affect the outcome of the MR analysis. This could explain why there was no significant associations in the previous studies.

In our study, we used GWAS of brain IDPs from UKBB which is a large-scale biomedical repository and research resource. The vast majority of the subjects are free from neurological diagnoses and mental issues at the time of imaging [32]. Interestingly, despite the UKBB GWAS was for healthy aging control, the genetic factors related to AD play a significant role in brain phenotypes even thought they have not been diagnosed with AD.

One of the main limitation of the MR is that the instrumental variables affect the outcome only through the exposure, as a single gene can influence the outcome through many paths [253]. In addition, despite GWAS is widely used and many genetic variations are linked to a trait or disease, this might violate the MR assumptions as more genetic variations might have significant associations with a trait in future GWAS studies.

In conclusion, the outcome of casual association using MR approach depends heavily on GWAS results, the SNPs selection criteria and LD calculation. The larger samples included in the GWAS of the exposure and the outcomes give more reliable results. These factors play a critical role to identify casual association because they might include relevant or irrelevant SNPs in the topic of interests [254]. In addition, identifying which one of the variables is the exposure and which one is the outcome for the same study has significant impact on the analysis outcome. In our study we selected AD as exposure and the brain IDPs are the outcomes. When we performed the SNPs selection, we followed the three MR assumptions to choose the correct instrumental variables. The instrument variables must be significantly associated with AD based on the GWAS threshold but not with the brain IDPs, otherwise this would be considered pleiotropy. However, if we reversed the exposure to the outcome, then we should select SNPs that were significantly associated with exposure brain IDPs but not with AD. Naturally, this results in very different sets of instrumental variables (SNPs) and leads to diverging outcome. The interpretation of the results would also be different. In our study, we assume that AD causes the alterations in brain structure and function while in the previous works [65] and [49] the outcomes indicate that the inherited alterations within brain phenotypes might cause AD. In addition, including IDPs from wide range of MRI modalities provide

more comprehensive view about the alterations caused by AD within brain's micro and macro structure.

# 7 Conclusions and Future Work

In this thesis, we investigated brain aging using different simple and complex models through brain age estimation using IDPs extracted from brain MRI. We have also applied simple methods and machine learning explainability models to identify the most informative features to model brain age. We further estimated brain age for fiber groups within brain white matter tracts. In addition, we revealed the effects of daily life style, cardiac risk factors and morbidity in brain aging. Finally, we used causal models to explore the role of TL in healthy aging and Alzheimer's disease in unhealthy aging to cause alterations within brain structures and functions.

Initially, our study showed that brain age estimation can be affected with many factors that led to poor model performance. For example, the selected model to estimate brain age has significant impact on the model performance. The used IDPs in the model to estimate brain age have invaluable impact in the model performance. The IDPs extracted from structural MRI have shown to be among the most informative features. In addition, the IDPs extracted from diffusion MRI such as Fractional anisotropy and Mean diffusivity in different tracts groups proved to be among the significant features to estimate brain age. On the contrary, functional MRI IDPs and susceptibility weighted imaging provide less informative phenotypes related to brain aging.

Brain regions might experience different rate of aging. For that matter, we estimated brain age for five groups of white matter tracts. The results showed that Brainstem fibers age faster than the other fiber groups while Limbic fiber groups was the slower in aging. However, statistical test is required to confirm whether the difference in the model's performance among the fiber groups is significant or not. In addition, brain age estimation might be dominated by the IDPs extracted from Limbic fibers. For instance, diffusion measures in Fornix (part of Limbic fiber group) are shown to be the most informative phenotypes to model brain age. The magnitude effects

of daily life style also could be different on different regions of interests. Again, Limbic fibers was more interacted and integrated with daily life style while the result demonstrated Brainstem fibers were less affected.

Due to the observed and unobserved confounds in brain aging that affect both the IDPs and the brain age, causal models might be the most suitable method to assess causal association between any exposure and the alterations within brain structures and functions. This might spot the light on factors that causally change brain characteristics. Our results based on the casual model revealed Telomeres length shortening play significant role in changing brain phenotypes. We therefore suggest considering Telomeres length when brain age is estimated as this might change the rate of aging and consequently decreasing the cognitive functions. However, we do understand such data might not be available in most biomedical data repositories.

Alzheimer's disease is one of the most common brain aging-related diseases. Our results showed that AD causally led to alterations within brain micro and macro structures. These changes can be detected using IDPs extracted from different MRI modalities. We do recommend assessing the causal link of AD and brain using wide range of phenotypes from different MRI modalities without limiting to specific MRI modality. Detecting such association would help to understand the decline of memory and cognitive function related to specific region of interests within brain.

Although we estimated brain age using different models, data, explored the effect of different factors, future works would aim to investigate brain age at tract levels instead of group level. This might help us to understand more deeply the effect of brain aging on each tract group and their consequences in cognitive functions. We would also consider Telomeres length as a new factor to estimate brain age at individuals level.

## Bibliography


[1] Anthony A Mercadante and Prasanna Tadi. “Neuroanatomy, Gray Matter”. In: (2020).

[2] Yishi Wang et al. “Segmentation of gray matter, white matter, and CSF with fluid and white matter suppression using MP2RAGE”. In: *Journal of Magnetic Resonance Imaging* 48.6 (2018), pp. 1540–1550.

[3] Ching-Cheng Chuang et al. “Patient-oriented simulation based on Monte Carlo algorithm by using MRI data”. In: *Biomedical engineering online* 11.1 (2012), pp. 1–16.

[4] Melissa K Edler et al. “Neuron loss associated with age but not Alzheimer’s disease pathology in the chimpanzee brain”. In: *Philosophical Transactions of the Royal Society B* 375.1811 (2020), p. 20190619.

[5] Mohamad Habes et al. “The Brain Chart of Aging: Machine-learning analytics reveals links between brain aging, white matter disease, amyloid burden, and cognition in the iSTAGING consortium of 10,216 harmonized MR scans”. In: *Alzheimer’s & Dementia* 17.1 (2021), pp. 89–102.

[6] Jit Poddar et al. “Biochemical deficits and cognitive decline in brain aging: Intervention by dietary supplements”. In: *Journal of chemical neuroanatomy* 95 (2019), pp. 70–80.

[7] M Ethan MacDonald and G Bruce Pike. “MRI of healthy brain aging: A review”. In: *NMR in Biomedicine* (2021), e4564.

[8] Samprit Chatterjee and Ali S Hadi. *Regression analysis by example*. Vol. 607. John Wiley & Sons, 2006.

[9] John P Nolan and Diana Ojeda-Revah. “Linear and nonlinear regression with stable errors”. In: *Journal of Econometrics* 172.2 (2013), pp. 186–194.

[10] Qi Shi, Mohamed Abdel-Aty, and Jaeyoung Lee. “A Bayesian ridge regression analysis of congestion’s impact on urban expressway safety”. In: *Accident Analysis & Prevention* 88 (2016), pp. 124–137.

[11] A George Assaf, Mike Tsionas, and Anastasios Tasiopoulos. “Diagnosing and correcting the effects of multicollinearity: Bayesian implications of ridge regression”. In: *Tourism Management* 71 (2019), pp. 1–8.

[12] Achmad Efendi and Effrihan. “A simulation study on Bayesian Ridge regression models for several collinearity levels”. In: *AIP Conference Proceedings*. Vol. 1913. 1. AIP Publishing LLC. 2017, p. 020031.

[13] David JC MacKay. “Bayesian interpolation”. In: *Neural computation* 4.3 (1992), pp. 415–447.

[14] Christiane K Kuhl. “Abbreviated magnetic resonance imaging (MRI) for breast cancer screening: rationale, concept, and transfer to clinical practice”. In: *Annual review of medicine* 70 (2019), pp. 501–519.

[15] Cyrus P Zabetian. “Review of Rosenberg’s Molecular and Genetic Basis of Neurological and Psychiatric Disease”. In: *Jama Neurology* 72.12 (2015), pp. 1538–1538.

[16] Sarah Gregory et al. “Longitudinal structural MRI in neurologically healthy adults”. In: *Journal of Magnetic Resonance Imaging* 52.5 (2020), pp. 1385–1399.

[17] Giovanni B Frisoni et al. “The clinical use of structural MRI in Alzheimer disease”. In: *Nature Reviews Neurology* 6.2 (2010), pp. 67–77.

[18] Sarah J Tabrizi et al. “Potential endpoints for clinical trials in premanifest and early Huntington’s disease in the TRACK-HD study: analysis of 24 month observational data”. In: *The Lancet Neurology* 11.1 (2012), pp. 42–53.

[19] Rosa De Micco, Antonio Russo, and Alessandro Tessitore. “Structural MRI in idiopathic Parkinson’s disease”. In: *International review of neurobiology* 141 (2018), pp. 405–438.

[20] Richard G Ellenbogen, Laligam N Sekhar, and Neil Kitchen. *Principles of Neurological Surgery E-Book*. Elsevier Health Sciences, 2017.

[21] Vinit Baliyan et al. “Diffusion weighted imaging: technique and applications”. In: *World journal of radiology* 8.9 (2016), p. 785.

[22] Marta Drake-Pérez et al. “Clinical applications of diffusion weighted imaging in neuroradiology”. In: *Insights into imaging* 9.4 (2018), pp. 535–547.

[23] Rebecca J Broad et al. “Neurite orientation and dispersion density imaging (NODDI) detects cortical and corticospinal tract degeneration in ALS”. In: *Journal of Neurology, Neurosurgery & Psychiatry* 90.4 (2019), pp. 404–411.

[24] Samuel T Nemanich, Bryon A Mueller, and Bernadette T Gillick. “Neurite orientation dispersion and density imaging quantifies corticospinal tract microstructural organization in children with unilateral cerebral palsy”. In: *Human brain mapping* 40.17 (2019), pp. 4888–4900.

[25] Christina Andica et al. “Neurocognitive and psychiatric disorders-related axonal degeneration in Parkinson’s disease”. In: *Journal of neuroscience research* 98.5 (2020), pp. 936–949.

[26] Christina Andica et al. “Neurite orientation dispersion and density imaging reveals white matter microstructural alterations in adults with autism”. In: *Molecular Autism* 12.1 (2021), pp. 1–14.

[27] José M Soares et al. “A hitchhiker’s guide to functional magnetic resonance imaging”. In: *Frontiers in neuroscience* 10 (2016), p. 515.

[28] Dan Pan et al. “Early detection of Alzheimer’s disease using magnetic resonance imaging: a novel approach combining convolutional neural networks and ensemble learning”. In: *Frontiers in neuroscience* 14 (2020), p. 259.

[29] Gemma Lombardi et al. “Structural magnetic resonance imaging for the early diagnosis of dementia due to Alzheimer’s disease in people with mild cognitive impairment”. In: *Cochrane Database of Systematic Reviews* 3 (2020).

[30] Anupama Bhan et al. “Early Diagnosis of Parkinson’s Disease in brain MRI using Deep Learning Algorithm”. In: *2021 Third International Conference on Intelligent Communication Technologies and Virtual Mobile Networks (ICICV)*. IEEE. 2021, pp. 1467–1470.

[31] François Moreau et al. “Early magnetic resonance imaging in transient ischemic attack and minor stroke: do it or lose it”. In: *Stroke* 44.3 (2013), pp. 671–674.

[32] Stephen M Smith et al. “Estimation of brain age delta from brain imaging”. In: *Neuroimage* 200 (2019), pp. 528–539.

[33] Rob J Hyndman and Anne B Koehler. “Another look at measures of forecast accuracy”. In: *International journal of forecasting* 22.4 (2006), pp. 679–688.

[34] Ann-Marie G de Lange and James H Cole. "Commentary: Correction procedures in brain-age prediction". In: *NeuroImage: Clinical* 26 (2020).

[35] Iman Beheshti et al. "Bias-adjustment in neuroimaging-based brain age frameworks: A robust scheme". In: *NeuroImage: Clinical* 24 (2019), p. 102063.

[36] James H Cole. "Multi-modality neuroimaging brain-age in UK Biobank: relationship to biomedical, lifestyle and cognitive factors". In: *Neurobiology of Aging* (2020).

[37] Maxwell L Elliott et al. "Brain-age in midlife is associated with accelerated biological aging and cognitive decline in a longitudinal birth cohort". In: *Molecular psychiatry* (2019), pp. 1–10.

[38] Stephen M Smith et al. "Brain aging comprises many modes of structural and functional change with distinct genetic and biophysical associations". In: *Elife* 9 (2020), e52677. DOI: https://doi.org/10.7554/eLife.52677.

[39] Benedikt Atli Jónsson et al. "Brain age prediction using deep learning uncovers associated sequence variants". In: *Nature communications* 10.1 (2019), pp. 1–10.

[40] Kaida Ning et al. "Association of relative brain age with tobacco smoking, alcohol consumption, and genetic variants". In: *Scientific reports* 10.1 (2020), pp. 1–10.

[41] Dinggang Shen, Guorong Wu, and Heung-Il Suk. "Deep learning in medical image analysis". In: *Annual review of biomedical engineering* 19 (2017), pp. 221–248.

[42] Vaishak Belle and Ioannis Papantonis. "Principles and practice of explainable machine learning". In: *Frontiers in big Data* (2021), p. 39.

[43] Pantelis Linardatos, Vasilis Papastefanopoulos, and Sotiris Kotsiantis. "Explainable ai: A review of machine learning interpretability methods". In: *Entropy* 23.1 (2021), p. 18.

[44] Ramprasaath R Selvaraju et al. "Grad-cam: Visual explanations from deep networks via gradient-based localization". In: *Proceedings of the IEEE international conference on computer vision*. 2017, pp. 618–626.

[45] Aditya Chattopadhay et al. "Grad-cam++: Generalized gradient-based visual explanations for deep convolutional networks". In: *2018 IEEE winter conference on applications of computer vision (WACV)*. IEEE. 2018, pp. 839–847.

[46] Karen Simonyan, Andrea Vedaldi, and Andrew Zisserman. "Deep inside convolutional networks: Visualising image classification models and saliency maps". In: *arXiv preprint arXiv:1312.6034* (2013).

[47] Sebastian Bach et al. "On pixel-wise explanations for non-linear classifier decisions by layer-wise relevance propagation". In: *PloS one* 10.7 (2015), e0130140.

[48] Judea Pearl, Madelyn Glymour, and Nicholas P Jewell. *Causal inference in statistics: A primer*. John Wiley & Sons, 2016.

[49] Katherine A Knutson, Yangqing Deng, and Wei Pan. "Implicating causal brain imaging endophenotypes in Alzheimer's disease using multivariable IWAS and GWAS summary data". In: *NeuroImage* 223 (2020), p. 117347.

[50] Alish B Palmos et al. "Telomere length and human hippocampal neurogenesis". In: *Neuropsychopharmacology* 45.13 (2020), pp. 2239–2247.

[51] David M Evans and George Davey Smith. "Mendelian randomization: new applications in the coming age of hypothesis-free causality". In: *Annual review of genomics and human genetics* 16 (2015), pp. 327–350.

[52] Amy E Taylor et al. "Mendelian randomization in health research: using appropriate genetic variants and avoiding biased estimates". In: *Economics & Human Biology* 13 (2014), pp. 99–106.

[53] Derrick A Bennett. "An introduction to instrumental variables–part 2: Mendelian randomisation". In: *Neuroepidemiology* 35.4 (2010), pp. 307–310.

[54] Jack Bowden et al. "Consistent estimation in Mendelian randomization with some invalid instruments using a weighted median estimator". In: *Genetic epidemiology* 40.4 (2016), pp. 304–314.

[55] Jack Bowden, George Davey Smith, and Stephen Burgess. "Mendelian randomization with invalid instruments: effect estimation and bias detection through Egger regression". In: *International journal of epidemiology* 44.2 (2015), pp. 512–525.

[56] Jerry W Shay and Woodring E Wright. "Telomeres and telomerase: three decades of progress". In: *Nature Reviews Genetics* 20.5 (2019), pp. 299–309.

[57] Deepavali Chakravarti, Kyle A LaBella, and Ronald A DePinho. "Telomeres: history, health, and hallmarks of aging". In: *Cell* (2021).

[58] Alexander Vaiserman and Dmytro Krasnienkov. “Telomere length as a marker of biological age: state-of-the-art, open issues, and future perspectives”. In: *Frontiers in Genetics* 11 (2021), p. 1816.

[59] Kai Gao et al. “Exploring the causal pathway from telomere length to Alzheimer’s disease: an update Mendelian randomization study”. In: *Frontiers in psychiatry* 10 (2019), p. 843.

[60] Ruoqing Chen and Yiqiang Zhan. “Association between telomere length and Parkinson’s disease: a Mendelian randomization study”. In: *Neurobiology of Aging* 97 (2021), 144–e9.

[61] Charleen D Adams and Brian B Boutwell. “A Mendelian randomization study of telomere length and blood-cell traits”. In: *Scientific Reports* 10.1 (2020), pp. 1–9.

[62] Philip C Haycock et al. “Association between telomere length and risk of cancer and non-neoplastic diseases: a Mendelian randomization study”. In: *JAMA oncology* 3.5 (2017), pp. 636–651.

[63] Kathryn Demanelis, Lin Tong, and Brandon L Pierce. “Genetically increased telomere length and aging-related traits in the UK Biobank”. In: *The Journals of Gerontology: Series A* 76.1 (2021), pp. 15–22.

[64] Junhong Yu et al. “Differences between multimodal brain-age and chronological-age are linked to telomere shortening”. In: *Neurobiology of Aging* 115 (2022), pp. 60–69.

[65] Katherine A Knutson and Wei Pan. “Integrating brain imaging endophenotypes with GWAS for Alzheimer’s disease”. In: *Quantitative Biology* (2020), pp. 1–16.

[66] Clare Bycroft et al. “The UK Biobank resource with deep phenotyping and genomic data”. In: *Nature* 562.7726 (2018), pp. 203–209. DOI: https://doi.org/10.1038/s41586-018-0579-z.

[67] Cathie Sudlow et al. “UK biobank: an open access resource for identifying the causes of a wide range of complex diseases of middle and old age”. In: *Plos med* 12.3 (2015), e1001779.

[68] Chloe Fawns-Ritchie and Ian J Deary. “Reliability and validity of the UK Biobank cognitive tests”. In: *PloS one* 15.4 (2020), e0231627.

[69] Rishi Caleyachetty et al. “United Kingdom Biobank (UK Biobank) JACC Focus Seminar 6/8”. In: *Journal of the American College of Cardiology* 78.1 (2021), pp. 56–65.

[70] Fidel Alfaro-Almagro et al. “Image processing and Quality Control for the first 10,000 brain imaging datasets from UK Biobank”. In: *Neuroimage* 166 (2018), pp. 400–424. DOI: https://doi.org/10.1016/j.neuroimage.2017.10.034.

[71] Ahmed Salih et al. “Multi-modal Brain Age Estimation: A Comparative Study Confirms the Importance of Microstructure”. In: *Computational Diffusion MRI*. Springer, 2021, pp. 239–250.

[72] Scott M Lundberg and Su-In Lee. “A unified approach to interpreting model predictions”. In: *Advances in neural information processing systems*. 2017, pp. 4765–4774.

[73] Marco Tulio Ribeiro, Sameer Singh, and Carlos Guestrin. “" Why should I trust you?" Explaining the predictions of any classifier”. In: *Proceedings of the 22nd ACM SIGKDD international conference on knowledge discovery and data mining*. 2016, pp. 1135–1144.

[74] Ahmed Salih et al. “A new scheme for the assessment of the robustness of Explainable Methods Applied to Brain Age estimation”. In: *2021 IEEE 34th International Symposium on Computer-Based Medical Systems (CBMS)*. IEEE. 2021, pp. 492–497. DOI: https://doi.org/10.1109/CBMS52027.2021.00098.

[75] Ahmed Salih et al. “Brain Age Estimation at Tract Group Level and its Association with Daily Life Measures, Cardiac Risk Factors and Genetic Variants”. In: *Scientific Reports* (2021). DOI: https://doi.org/10.1038/s41598-021-99153-8.

[76] Xin Niu et al. “Improved prediction of brain age using multimodal neuroimaging data”. In: *Human Brain Mapping* 41.6 (2020), pp. 1626–1643.

[77] Katja Franke and Christian Gaser. “Ten years of BrainAGE as a neuroimaging biomarker of brain aging: What insights have we gained?” In: *Frontiers in neurology* 10 (2019), p. 789.

[78] Lloyd T Elliott et al. “Genome-wide association studies of brain imaging phenotypes in UK Biobank”. In: *Nature* 562.7726 (2018), pp. 210–216.

[79] UK Biobank. “About UK Biobank”. In: *Available at h ttps://www. ukbiobank. ac. uk/a bout-biobank-uk* (2014).

[80] Kegang Hua et al. “Tract probability maps in stereotaxic spaces: analyses of white matter anatomy and tract-specific quantification”. In: *Neuroimage* 39.1 (2008), pp. 336–347.

[81] Robert Tibshirani. “Regression shrinkage and selection via the lasso”. In: *Journal of the Royal Statistical Society: Series B (Methodological)* 58.1 (1996), pp. 267–288.

[82] John F Kenney and ES Keeping. “Linear regression and correlation”. In: *Mathematics of statistics* 1 (1962), pp. 252–285.

[83] Harris Drucker et al. “Support vector regression machines”. In: *Advances in neural information processing systems*. 1997, pp. 155–161.

[84] F. Pedregosa et al. “Scikit-learn: Machine Learning in Python”. In: *Journal of Machine Learning Research* 12 (2011), pp. 2825–2830.

[85] Lloyd T Elliott et al. “Genome-wide association studies of brain imaging phenotypes in UK Biobank”. In: *Nature* 562.7726 (2018), pp. 210–216.

[86] Karla L Miller et al. “Multimodal population brain imaging in the UK Biobank prospective epidemiological study”. In: *Nature neuroscience* 19.11 (2016), pp. 1523–1536.

[87] Trang T Le et al. “A nonlinear simulation framework supports adjusting for age when analyzing BrainAGE”. In: *Frontiers in aging neuroscience* 10 (2018), p. 317.

[88] Isabelle F van der Velpen et al. “Impaired cardiac function and cognitive brain aging”. In: *Canadian Journal of Cardiology* 33.12 (2017), pp. 1587–1596.

[89] Angela L Jefferson et al. “Cardiac index is associated with brain aging: the Framingham Heart Study”. In: *Circulation* 122.7 (2010), p. 690.

[90] Steffen E Petersen et al. “UK Biobank’s cardiovascular magnetic resonance protocol”. In: *Journal of cardiovascular magnetic resonance* 18.1 (2015), p. 8.

[91] A George Assaf, Mike Tsionas, and Anastasios Tasiopoulos. “Diagnosing and correcting the effects of multicollinearity: Bayesian implications of ridge regression”. In: *Tourism Management* 71 (2019), pp. 1–8.

[92] Achmad Efendi and Effrihan. “A simulation study on Bayesian Ridge regression models for several collinearity levels”. In: *AIP Conference Proceedings*. Vol. 1913. 1. AIP Publishing LLC. 2017, p. 020031.

[93] Han Peng et al. “Accurate brain age prediction with lightweight deep neural networks”. In: *BioRxiv* (2019).

[94] Xufeng Yao et al. “Evaluation of human brain aging via diffusion tensor imaging tract characteristics”. In: *2017 13th International Conference on Natural Computation, Fuzzy Systems and Knowledge Discovery (ICNC-FSKD)*. IEEE. 2017, pp. 2651–2655.

[95] I Driscoll et al. “Longitudinal pattern of regional brain volume change differentiates normal aging from MCI”. In: *Neurology* 72.22 (2009), pp. 1906–1913.

[96] Vanessa Douet and Linda Chang. “Fornix as an imaging marker for episodic memory deficits in healthy aging and in various neurological disorders”. In: *Frontiers in aging neuroscience* 6 (2015), p. 343.

[97] Huan Liu et al. “Aging of cerebral white matter”. In: *Ageing research reviews* 34 (2017), pp. 64–76.

[98] David Qixiang Chen et al. “Age-related changes in diffusion tensor imaging metrics of fornix subregions in healthy humans”. In: *Stereotactic and Functional Neurosurgery* 93.3 (2015), pp. 151–159.

[99] Simon R Cox et al. “Ageing and brain white matter structure in 3,513 UK Biobank participants”. In: *Nature communications* 7.1 (2016), pp. 1–13.

[100] Elizabeth E Moore et al. “Increased left ventricular mass index is associated with compromised white matter microstructure among older adults”. In: *Journal of the American Heart Association* 7.13 (2018), e009041.

[101] James H Cole et al. “Body mass index, but not FTO genotype or major depressive disorder, influences brain structure”. In: *Neuroscience* 252 (2013), pp. 109–117.

[102] Yann LeCun, Yoshua Bengio, and Geoffrey Hinton. “Deep learning”. In: *nature* 521.7553 (2015), pp. 436–444.

[103] Diogo V Carvalho, Eduardo M Pereira, and Jaime S Cardoso. “Machine learning interpretability: A survey on methods and metrics”. In: *Electronics* 8.8 (2019), p. 832.

[104] Richard Li et al. “Machine Learning–Based Interpretation and Visualization of Nonlinear Interactions in Prostate Cancer Survival”. In: *JCO Clinical Cancer Informatics* 4 (2020), pp. 637–646.

[105] Ohad Lewin-Epstein et al. “Predicting antibiotic resistance in hospitalized patients by applying machine learning to electronic medical records”. In: *medRxiv* (2020).

[106] Iam Palatnik de Sousa, Marley Maria Bernardes Rebuzzi Vellasco, and Eduardo Costa da Silva. “Local Interpretable Model-Agnostic Explanations for Classification of Lymph Node Metastases”. In: *Sensors* 19.13 (2019), p. 2969.

[107] Kacper Sokol and Peter Flach. “Explainability fact sheets: a framework for systematic assessment of explainable approaches”. In: *Proceedings of the 2020 Conference on Fairness, Accountability, and Transparency*. 2020, pp. 56–67.

[108] Chin-Fang Lin. “Application-grounded evaluation of predictive model explanation methods”. In: ().

[109] Sina Mohseni and Eric D Ragan. “A human-grounded evaluation benchmark for local explanations of machine learning”. In: *arXiv preprint arXiv:1801.05075* (2018).

[110] Grégoire Montavon, Wojciech Samek, and Klaus-Robert Müller. “Methods for interpreting and understanding deep neural networks”. In: *Digital Signal Processing* 73 (2018), pp. 1–15.

[111] Finale Doshi-Velez and Been Kim. “Towards a rigorous science of interpretable machine learning”. In: *arXiv preprint arXiv:1702.08608* (2017).

[112] Wilson Silva et al. “Towards complementary explanations using deep neural networks”. In: *Understanding and Interpreting Machine Learning in Medical Image Computing Applications*. Springer, 2018, pp. 133–140.

[113] Sarunas J Raudys, Anil K Jain, et al. “Small sample size effects in statistical pattern recognition: Recommendations for practitioners”. In: *IEEE Transactions on pattern analysis and machine intelligence* 13.3 (1991), pp. 252–264.

[114] Andrius Vabalas et al. “Machine learning algorithm validation with a limited sample size”. In: *PloS one* 14.11 (2019), e0224365.

[115] Ahmet Mesrur Halefoglu and David Mark Yousem. “Susceptibility weighted imaging: clinical applications and future directions”. In: *World journal of radiology* 10.4 (2018), p. 30.

[116] Fidel A-A Stephen M. S and Karla L. M. *UK Biobank Brain Imaging Documentation, Version 1.3*. 2017.

[117] Angela L Jefferson. "Cardiac output as a potential risk factor for abnormal brain aging". In: *Journal of Alzheimer's Disease* 20.3 (2010), pp. 813–821. DOI: https://doi.org/10.3233/JAD-2010-100081.

[118] Simon R Cox et al. "Associations between vascular risk factors and brain MRI indices in UK Biobank". In: *European heart journal* 40.28 (2019), pp. 2290–2300.

[119] Thomas V Perneger. "What's wrong with Bonferroni adjustments". In: *Bmj* 316.7139 (1998), pp. 1236–1238.

[120] Weibo Liu et al. "A survey of deep neural network architectures and their applications". In: *Neurocomputing* 234 (2017), pp. 11–26.

[121] Dani Yogatama and Gideon Mann. "Efficient transfer learning method for automatic hyperparameter tuning". In: *Artificial intelligence and statistics*. 2014, pp. 1077–1085.

[122] David Paper and David Paper. "Scikit-Learn Classifier Tuning from Simple Training Sets". In: *Hands-on Scikit-Learn for Machine Learning Applications: Data Science Fundamentals with Python* (2020), pp. 137–163.

[123] Michał Choraś et al. "Machine Learning–the results are not the only thing that matters! What about security, explainability and fairness?" In: *International Conference on Computational Science*. Springer. 2020, pp. 615–628.

[124] Charles Spearman. "The proof and measurement of association between two things." In: (1961).

[125] Haldun Akoglu. "User's guide to correlation coefficients". In: *Turkish journal of emergency medicine* 18.3 (2018), pp. 91–93.

[126] M Sundararajan, A Taly, and Q Yan. "Axiomatic attribution for deep networks". In: *International Conference on Machine Learning*. PMLR. 2017, pp. 3319–3328.

[127] Rory Boyle et al. "Brain-predicted age difference score is related to specific cognitive functions: A multi-site replication analysis". In: *Brain imaging and behavior* 15.1 (2021), pp. 327–345. DOI: http://dx.doi.org/10.1007/s11682-020-00260-3.

[128] Albert C Yang et al. "The association of aging with white matter integrity and functional connectivity hubs". In: *Frontiers in aging neuroscience* 8 (2016), p. 143. DOI: https://doi.org/10.3389/fnagi.2016.00143.

[129] Andrew R Bender, Manuel C Völkle, and Naftali Raz. "Differential aging of cerebral white matter in middle-aged and older adults: a seven-year follow-up". In: *Neuroimage* 125 (2016), pp. 74–83. DOI: https://doi.org/10.1016/j.neuroimage.2015.10.030.

[130] Naftali Raz and Ana M Daugherty. "Pathways to brain aging and their modifiers: free-radical-induced energetic and neural decline in senescence (FRIENDS) model-a mini-review". In: *Gerontology* 64.1 (2018), pp. 49–57. DOI: https://doi.org/10.1159/000479508.

[131] Gwenaëlle Douaud et al. "A common brain network links development, aging, and vulnerability to disease". In: *Proceedings of the National Academy of Sciences* 111.49 (2014), pp. 17648–17653. DOI: https://doi.org/10.1073/pnas.1410378111.

[132] Naftali Raz et al. "Neuroanatomical and cognitive correlates of adult age differences in acquisition of a perceptual-motor skill". In: *Microscopy research and technique* 51.1 (2000), pp. 85–93. DOI: https://doi.org/10.1002/1097-0029(20001001)51:1<85::AID-JEMT9>3.0.CO;2-0.

[133] Tuancheng Feng, Alexander Lacrampe, and Fenghua Hu. "Physiological and pathological functions of TMEM106B: a gene associated with brain aging and multiple brain disorders". In: *Acta neuropathologica* (2021), pp. 1–13. DOI: https://doi.org/10.1007/s00401-020-02246-3.

[134] Sophie R Harding et al. "The TMEM106B risk allele is associated with lower cortical volumes in a clinically diagnosed frontotemporal dementia cohort". In: *Journal of Neurology, Neurosurgery & Psychiatry* 88.11 (2017), pp. 997–998. DOI: http://dx.doi.org/10.1136/jnnp-2017-315641.

[135] Esterina Pascale et al. "Genetic architecture of MAPT gene region in Parkinson disease subtypes". In: *Frontiers in cellular neuroscience* 10 (2016), p. 96. DOI: https://doi.org/10.3389/fncel.2016.00096.

[136] Pouya Tahsili-Fahadan and Romergryko G Geocadin. "Heart–brain axis: effects of neurologic injury on cardiovascular function". In: *Circulation research* 120.3 (2017), pp. 559–572. DOI: https://doi.org/10.1161/CIRCRESAHA.116.308446.

[137] Juliana Rumy Tsuchihashi Takeda, Tatiane Martins Matos, and Juliana Nery de Souza-Talarico. "Cardiovascular risk factors and cognitive performance in aging". In: *Dementia & neuropsychologia* 11.4 (2017), pp. 442–448. DOI: https://doi.org/10.1590/1980-57642016dn11-040015.

[138] Ann-Marie G de Lange et al. "Multimodal brain-age prediction and cardiovascular risk: The Whitehall II MRI sub-study". In: *NeuroImage* 222 (2020), p. 117292. DOI: https://doi.org/10.1016/j.neuroimage.2020.117292.

[139] Katja Franke and Christian Gaser. "Ten years of BrainAGE as a neuroimaging biomarker of brain aging: what insights have we gained?" In: *Frontiers in neurology* 10 (2019), p. 789. DOI: https://doi.org/10.3389/fneur.2019.00789.

[140] Jaroslav Rokicki et al. "Multimodal imaging improves brain age prediction and reveals distinct abnormalities in patients with psychiatric and neurological disorders". In: *Human brain mapping* 42.6 (2021), pp. 1714–1726. DOI: https://doi.org/10.1002/hbm.25323.

[141] Franziskus Liem et al. "Predicting brain-age from multimodal imaging data captures cognitive impairment". In: *Neuroimage* 148 (2017), pp. 179–188. DOI: https://doi.org/10.1016/j.neuroimage.2016.11.005.

[142] Jose Soares et al. "A hitchhiker's guide to diffusion tensor imaging". In: *Frontiers in neuroscience* 7 (2013), p. 31. DOI: https://doi.org/10.3389/fnins.2013.00031.

[143] Daichi Sone. "Neurite orientation and dispersion density imaging: clinical utility, efficacy, and role in therapy". In: *Reports in Medical Imaging* 12 (2019), p. 17. DOI: https://doi.org/10.2147/RMI.S194083.

[144] Mauro Zucchelli et al. "What lies beneath? Diffusion EAP-based study of brain tissue microstructure". In: *Medical image analysis* 32 (2016), pp. 145–156. DOI: https://doi.org/10.1016/j.media.2016.03.008.

[145] Andrew P Merluzzi et al. “Age-dependent differences in brain tissue microstructure assessed with neurite orientation dispersion and density imaging”. In: *Neurobiology of aging* 43 (2016), pp. 79–88. DOI: https://doi.org/10.1016/j.neurobiolaging.2016.03.026.

[146] Dani Beck et al. “White matter microstructure across the adult lifespan: A mixed longitudinal and cross-sectional study using advanced diffusion models and brain-age prediction”. In: *NeuroImage* 224 (2021), p. 117441. DOI: https://doi.org/10.1016/j.neuroimage.2020.117441.

[147] Steffen E Petersen et al. “UK Biobank’s cardiovascular magnetic resonance protocol”. In: *Journal of cardiovascular magnetic resonance* 18.1 (2015), p. 8. DOI: https://doi.org/10.1186/s12968-016-0227-4.

[148] Zahra Raisi-Estabragh et al. “Cardiovascular magnetic resonance imaging in the UK Biobank: a major international health research resource”. In: *European Heart Journal-Cardiovascular Imaging* (2020). DOI: https://doi.org/10.1093/ehjci/jeaa297.

[149] Setsu Wakana et al. “Fiber tract–based atlas of human white matter anatomy”. In: *Radiology* 230.1 (2004), pp. 77–87. DOI: https://doi.org/10.1148/radiol.2301021640.

[150] Susan Standring et al. “Gray’s anatomy: the anatomical basis of clinical practice”. In: *American journal of neuroradiology* 26.10 (2005), p. 2703. DOI: https://doi.org/10.5860/choice.43-1300.

[151] Duane E Haines and Gregory A Mihailoff. *Fundamental Neuroscience for Basic and Clinical Applications E-Book*. Elsevier Health Sciences, 2017.

[152] Hayden Basinger and Jeffery P Hogg. “Neuroanatomy, Brainstem”. In: *StatPearls [Internet]* (2020).

[153] Raluca Pascalau et al. “Anatomy of the limbic white matter tracts as revealed by fiber dissection and tractography”. In: *World neurosurgery* 113 (2018), e672–e689. DOI: https://doi.org/10.1016/j.wneu.2018.02.121.

[154] Marco Catani, Flavio Dell’Acqua, and Michel Thiebaut De Schotten. “A revised limbic system model for memory, emotion and behaviour”. In: *Neuroscience &*

*Biobehavioral Reviews* 37.8 (2013), pp. 1724–1737. DOI: https://doi.org/10.1016/j.neubiorev.2013.07.001.

[155] Yupeng Wu et al. "Segmentation of the cingulum bundle in the human brain: a new perspective based on DSI tractography and fiber dissection study". In: *Frontiers in neuroanatomy* 10 (2016), p. 84. DOI: https://doi.org/10.3389/fnana.2016.00084.

[156] Robert B Daroff and Michael J Aminoff. *Encyclopedia of the neurological sciences*. Academic press, 2014.

[157] Neeta V Kulkarni. *Clinical anatomy (a problem solving approach)*. JP Medical Ltd, 2011.

[158] Rahman Attar et al. "Quantitative CMR population imaging on 20,000 subjects of the UK Biobank imaging study: LV/RV quantification pipeline and its evaluation". In: *Medical image analysis* 56 (2019), pp. 26–42. DOI: https://doi.org/10.1016/j.media.2019.05.006.

[159] D Du Bois. "A formula to estimate the approximate surface area if height and weight be known". In: *Nutrition* 5 (1989), pp. 303–313. DOI: https://doi.org/10.1001/archinte.1916.00080130010002.

[160] Stephane Laurent et al. "Expert consensus document on arterial stiffness: methodological issues and clinical applications". In: *European heart journal* 27.21 (2006), pp. 2588–2605. DOI: https://doi.org/10.1093/eurheartj/ehl254.

[161] Fidel Alfaro-Almagro et al. "Confound modelling in UK Biobank brain imaging". In: *NeuroImage* 224 (2021), p. 117002. DOI: https://doi.org/10.1016/j.neuroimage.2020.117002.

[162] Carlo Bonferroni. "Teoria statistica delle classi e calcolo delle probabilita". In: *Pubblicazioni del R Istituto Superiore di Scienze Economiche e Commericiali di Firenze* 8 (1936), pp. 3–62.

[163] Shaun Purcell et al. "PLINK: a tool set for whole-genome association and population-based linkage analyses". In: *The American journal of human genetics* 81.3 (2007), pp. 559–575. DOI: https://doi.org/10.1086/519795.

[164] Kyoko Watanabe et al. “Functional mapping and annotation of genetic associations with FUMA”. In: *Nature communications* 8.1 (2017), pp. 1–11. DOI: http://dx.doi.org/10.1038/s41467-017-01261-5.

[165] Yu Zhang et al. “Diffusion tensor tractography of brainstem fibers and its application in pain”. In: *PloS one* 15.2 (2020), e0213952. DOI: https://doi.org/10.1371/journal.pone.0213952.

[166] Lisa Ronan et al. “Obesity associated with increased brain age from midlife”. In: *Neurobiology of aging* 47 (2016), pp. 63–70. DOI: https://doi.org/10.1016/j.neurobiolaging.2016.07.010.

[167] Angela L Jefferson et al. “Low cardiac index is associated with incident dementia and Alzheimer disease: the Framingham Heart Study”. In: *Circulation* 131.15 (2015), pp. 1333–1339. DOI: https://doi.org/10.1161/CIRCULATIONAHA.114.012438.

[168] Susan Mosher Ruiz et al. “Drinking history associations with regional white matter volumes in alcoholic men and women”. In: *Alcoholism: Clinical and Experimental Research* 37.1 (2013), pp. 110–122. DOI: https://doi.org/10.1111/j.1530-0277.2012.01862.x.

[169] Linda K McEvoy et al. “Alcohol intake and brain white matter in middle aged men: Microscopic and macroscopic differences”. In: *NeuroImage: Clinical* 18 (2018), pp. 390–398. DOI: https://doi.org/10.1016/j.nicl.2018.02.006.

[170] Joshua C Gray et al. “Associations of cigarette smoking with gray and white matter in the UK Biobank”. In: *Neuropsychopharmacology* 45.7 (2020), pp. 1215–1222. DOI: https://doi.org/10.31234/osf.io/wyvnm.

[171] Janie Corley et al. “Dietary patterns, cognitive function, and structural neuroimaging measures of brain aging”. In: *Experimental Gerontology* (2020), p. 111117. DOI: https://doi.org/10.1016/j.exger.2020.111117.

[172] Michelle Walters et al. “Role of nutrition to promote healthy brain aging and reduce risk of Alzheimer’s disease”. In: *Current Nutrition Reports* 6.2 (2017), pp. 63–71. DOI: https://doi.org/10.1007/s13668-017-0199-5.

[173] Yong Wu et al. “Identification of the primate-specific gene BTN3A2 as an additional schizophrenia risk gene in the MHC loci”. In: *EBioMedicine* 44 (2019), pp. 530–541. DOI: https://doi.org/10.1016/j.ebiom.2019.05.006.

[174] Oneil G Bhalala et al. “Identification of expression quantitative trait loci associated with schizophrenia and affective disorders in normal brain tissue”. In: *PLoS genetics* 14.8 (2018), e1007607. DOI: https://doi.org/10.1371/journal.pgen.1007607.

[175] Idoia Blanco-Luquin et al. “Early epigenetic changes of Alzheimer’s disease in the human hippocampus”. In: *Epigenetics* 15.10 (2020), pp. 1083–1092. DOI: https://doi.org/10.1080/15592294.2020.1748917.

[176] Janos Fuzik et al. “Brain-wide genetic mapping identifies the indusium griseum as a prenatal target of pharmacologically unrelated psychostimulants”. In: *Proceedings of the National Academy of Sciences* 116.51 (2019), pp. 25958–25967. DOI: https://doi.org/10.1073/pnas.1904006116.

[177] Asli Aykaç and Ahmet Ozer Sehirli. “The role of the SLC transporters protein in the neurodegenerative disorders”. In: *Clinical Psychopharmacology and Neuroscience* 18.2 (2020), p. 174. DOI: https://doi.org/10.9758/cpn.2020.18.2.174.

[178] Tobias Kaufmann et al. “Common brain disorders are associated with heritable patterns of apparent aging of the brain”. In: *Nature neuroscience* 22.10 (2019), pp. 1617–1623. DOI: https://doi.org/10.1038/s41593-019-0471-7.

[179] Eduardo E Benarroch. “Brainstem integration of arousal, sleep, cardiovascular, and respiratory control”. In: *Neurology* 91.21 (2018), pp. 958–966. DOI: https://doi.org/10.1212/WNL.0000000000006537.

[180] Chia-Ling Kuo et al. “Telomere length and aging-related outcomes in humans: A Mendelian randomization study in 261,000 older participants”. In: *Aging Cell* 18.6 (2019), e13017.

[181] Meng-Ying Liu, Ashley Nemes, and Qi-Gang Zhou. “The emerging roles for telomerase in the central nervous system”. In: *Frontiers in molecular neuroscience* 11 (2018), p. 160.

[182] Chen Li et al. “Genome-wide association analysis in humans links nucleotide metabolism to leukocyte telomere length”. In: *The American Journal of Human Genetics* 106.3 (2020), pp. 389–404.

[183] Veryan Codd et al. “Identification of seven loci affecting mean telomere length and their association with disease”. In: *Nature genetics* 45.4 (2013), pp. 422–427.

[184] Yiqiang Zhan and Sara Hägg. “Association between genetically predicted telomere length and facial skin aging in the UK Biobank: a Mendelian randomization study”. In: *GeroScience* (2020), pp. 1–7.

[185] Kevin S King et al. “Effect of leukocyte telomere length on total and regional brain volumes in a large population-based cohort”. In: *JAMA neurology* 71.10 (2014), pp. 1247–1254.

[186] Mitchell J Machiela and Stephen J Chanock. “LDlink: a web-based application for exploring population-specific haplotype structure and linking correlated alleles of possible functional variants”. In: *Bioinformatics* 31.21 (2015), pp. 3555–3557.

[187] Massimo Mangino et al. “Genome-wide meta-analysis points to CTC1 and ZNF676 as genes regulating telomere homeostasis in humans”. In: *Human molecular genetics* 21.24 (2012), pp. 5385–5394.

[188] Andrew D Yates et al. “Ensembl 2020”. In: *Nucleic acids research* 48.D1 (2020), pp. D682–D688.

[189] Karen A Pooley et al. “A genome-wide association scan (GWAS) for mean telomere length within the COGS project: identified loci show little association with hormone-related cancer risk”. In: *Human molecular genetics* 22.24 (2013), pp. 5056–5064.

[190] Stephen M Smith et al. “An expanded set of genome-wide association studies of brain imaging phenotypes in UK Biobank”. In: *Nature Neuroscience* (2021), pp. 1–9.

[191] G. Hemani et al. “The MR-Base platform supports systematic causal inference across the human phenome”. In: *eLife* 7 (2018), e34408. URL: `https://elifesciences.org/articles/34408`.

[192] Yoav Benjamini and Yosef Hochberg. "Controlling the false discovery rate: a practical and powerful approach to multiple testing". In: *Journal of the Royal statistical society: series B (Methodological)* 57.1 (1995), pp. 289–300.

[193] Marie Verbanck et al. "Detection of widespread horizontal pleiotropy in causal relationships inferred from Mendelian randomization between complex traits and diseases". In: *Nature genetics* 50.5 (2018), pp. 693–698.

[194] Răzvan V Marinescu et al. "BrainPainter: A software for the visualisation of brain structures, biomarkers and associated pathological processes". In: *Multimodal brain image analysis and mathematical foundations of computational anatomy*. Springer, 2019, pp. 112–120.

[195] Stephen M Smith et al. "Advances in functional and structural MR image analysis and implementation as FSL". In: *Neuroimage* 23 (2004), S208–S219.

[196] James H Cole. "Multimodality neuroimaging brain-age in UK biobank: relationship to biomedical, lifestyle, and cognitive factors". In: *Neurobiology of aging* 92 (2020), pp. 34–42.

[197] Aga Z Burzynska et al. "Age-related differences in white matter microstructure: region-specific patterns of diffusivity". In: *Neuroimage* 49.3 (2010), pp. 2104–2112.

[198] Anna Behler, Jan Kassubek, and Hans-Peter Müller. "Age-related alterations in DTI metrics in the human brain—consequences for age correction". In: *Frontiers in aging neuroscience* 13 (2021).

[199] David K Wright et al. "Telomere length and advanced diffusion MRI as biomarkers for repetitive mild traumatic brain injury in adolescent rats". In: *NeuroImage: Clinical* 18 (2018), pp. 315–324.

[200] Carme Uribe et al. "Gray/white matter contrast in Parkinson's disease". In: *Frontiers in Aging Neuroscience* 10 (2018), p. 89.

[201] Didac Vidal-Piñeiro et al. "Accelerated longitudinal gray/white matter contrast decline in aging in lightly myelinated cortical regions". In: *Human brain mapping* 37.10 (2016), pp. 3669–3684.

[202] KN Jørgensen et al. "Increased MRI-based cortical grey/white-matter contrast in sensory and motor regions in schizophrenia and bipolar disorder". In: *Psychological medicine* 46.9 (2016), pp. 1971–1985.

[203] Saba Shahab et al. “Brain structure, cognition, and brain age in schizophrenia, bipolar disorder, and healthy controls”. In: *Neuropsychopharmacology* 44.5 (2019), pp. 898–906.

[204] Tanya T Nguyen, Lisa T Eyler, and Dilip V Jeste. “Systemic biomarkers of accelerated aging in schizophrenia: a critical review and future directions”. In: *Schizophrenia bulletin* 44.2 (2018), pp. 398–408.

[205] Olaoluwa O Okusaga. “Accelerated aging in schizophrenia patients: the potential role of oxidative stress”. In: *Aging and disease* 5.4 (2014), p. 256.

[206] Marion Fouquet et al. “Increased contrast of the grey-white matter boundary in the motor, visual and auditory areas in Autism Spectrum Disorders”. In: *bioRxiv* (2019). DOI: 10.1101/750117. eprint: https://www.biorxiv.org/content/early/2019/09/05/750117.full.pdf. URL: https://www.biorxiv.org/content/early/2019/09/05/750117.

[207] David Mason et al. “Autistic traits are associated with faster pace of aging: Evidence from the Dunedin study at age 45”. In: *Autism Research* 14.8 (2021), pp. 1684–1694.

[208] Nikita V Savelyev et al. “PARP1 regulates the biogenesis and activity of telomerase complex through modification of H/ACA-proteins”. In: *Frontiers in cell and developmental biology* 9 (2021).

[209] Kanmin Mao and Guo Zhang. “The role of PARP1 in neurodegenerative diseases and aging”. In: *The FEBS Journal* (2021).

[210] Gabriele Saretzki and Tengfei Wan. “Telomerase in Brain: The New Kid on the Block and Its Role in Neurodegenerative Diseases”. In: *Biomedicines* 9.5 (2021), p. 490.

[211] Kurt Whittemore et al. “Telomerase gene therapy ameliorates the effects of neurodegeneration associated to short telomeres in mice”. In: *Aging (Albany NY)* 11.10 (2019), p. 2916.

[212] Adrian S Tong et al. “ATM and ATR signaling regulate the recruitment of human telomerase to telomeres”. In: *Cell reports* 13.8 (2015), pp. 1633–1646.

[213] Xuting Shen et al. “Neurons in vulnerable regions of the Alzheimer’s disease brain display reduced ATM signaling”. In: *Eneuro* 3.1 (2016).

[214] HB Stolp et al. "Voxel-wise comparisons of cellular microstructure and diffusion-MRI in mouse hippocampus using 3D Bridging of Optically-clear histology with Neuroimaging Data (3D-BOND)". In: *Scientific reports* 8.1 (2018), pp. 1–12.

[215] Lorenzo Pini et al. "Brain atrophy in Alzheimer's disease and aging". In: *Ageing research reviews* 30 (2016), pp. 25–48.

[216] Josué Luiz Dalboni da Rocha et al. "Fractional Anisotropy changes in parahippocampal cingulum due to Alzheimer's Disease". In: *Scientific reports* 10.1 (2020), pp. 1–8.

[217] Farshid Sepehrband et al. "Nonparenchymal fluid is the source of increased mean diffusivity in preclinical Alzheimer's disease". In: *Alzheimer's & Dementia: Diagnosis, Assessment & Disease Monitoring* 11 (2019), pp. 348–354.

[218] Miguel Ángel Araque Caballero et al. "White matter diffusion alterations precede symptom onset in autosomal dominant Alzheimer's disease". In: *Brain* 141.10 (2018), pp. 3065–3080.

[219] Seyed Hani Hojjati et al. "Predicting conversion from MCI to AD by integrating rs-fMRI and structural MRI". In: *Computers in biology and medicine* 102 (2018), pp. 30–39.

[220] Seyed Hani Hojjati, Ata Ebrahimzadeh, and Abbas Babajani-Feremi. "Identification of the early stage of Alzheimer's disease using structural MRI and resting-state fMRI". In: *Frontiers in neurology* 10 (2019), p. 904.

[221] Qing Li et al. "Classification of Alzheimer's disease, mild cognitive impairment, and cognitively unimpaired individuals using multi-feature kernel discriminant dictionary learning". In: *Frontiers in computational neuroscience* 11 (2018), p. 117.

[222] Fulvia Palesi et al. "Exploring patterns of alteration in Alzheimer's disease brain networks: a combined structural and functional connectomics analysis". In: *Frontiers in neuroscience* 10 (2016), p. 380.

[223] Roxanna Korologou-Linden et al. "The bidirectional causal effects of brain morphology across the life course and risk of Alzheimer's disease: A cross-cohort comparison and Mendelian randomization meta-analysis". In: *medRxiv* (2021).

[224] Bang-Sheng Wu et al. “Cortical structure and the risk for Alzheimer’s disease: a bidirectional Mendelian randomization study”. In: *Translational Psychiatry* 11.1 (2021), pp. 1–7.

[225] Sarah A Gagliano Taliun and David M Evans. *Ten simple rules for conducting a mendelian randomization study*. 2021.

[226] Neil M Davies, Michael V Holmes, and George Davey Smith. “Reading Mendelian randomisation studies: a guide, glossary, and checklist for clinicians”. In: *Bmj* 362 (2018).

[227] Jean-Charles Lambert et al. “Meta-analysis of 74,046 individuals identifies 11 new susceptibility loci for Alzheimer’s disease”. In: *Nature genetics* 45.12 (2013), pp. 1452–1458.

[228] João Fadista et al. “The (in) famous GWAS P-value threshold revisited and updated for low-frequency variants”. In: *European Journal of Human Genetics* 24.8 (2016), pp. 1202–1205.

[229] Brian W Kunkle et al. “Genetic meta-analysis of diagnosed Alzheimer’s disease identifies new risk loci and implicates A$\beta$, tau, immunity and lipid processing”. In: *Nature genetics* 51.3 (2019), pp. 414–430.

[230] Gibran Hemani et al. “The MR-Base platform supports systematic causal inference across the human phenome”. In: *elife* 7 (2018), e34408.

[231] Stephen Burgess et al. “A robust and efficient method for Mendelian randomization with hundreds of genetic variants”. In: *Nature communications* 11.1 (2020), pp. 1–11.

[232] Lisa Nobis et al. “Hippocampal volume across age: Nomograms derived from over 19,700 people in UK Biobank”. In: *NeuroImage: Clinical* 23 (2019), p. 101904.

[233] Louis Nadal et al. “Differential annualized rates of hippocampal subfields atrophy in aging and future Alzheimer’s clinical syndrome”. In: *Neurobiology of Aging* 90 (2020), pp. 75–83.

[234] Antoine Garnier-Crussard et al. “White matter hyperintensity topography in Alzheimer’s disease and links to cognition”. In: *Alzheimer’s & Dementia* (2021).

[235] Anja Soldan et al. “White matter hyperintensities and CSF Alzheimer disease biomarkers in preclinical Alzheimer disease”. In: *Neurology* 94.9 (2020), e950–e960.

[236] Feng Shi et al. *Hippocampal volume and asymmetry in mild cognitive impairment and Alzheimer's disease: Meta-analyses of MRI studies*. 2009.

[237] Tommaso Maggipinto et al. "DTI measurements for Alzheimer's classification". In: *Physics in Medicine & Biology* 62.6 (2017), p. 2361.

[238] Xuena Liu et al. "Abnormal amplitude of low-frequency fluctuations of intrinsic brain activity in Alzheimer's disease". In: *Journal of Alzheimer's Disease* 40.2 (2014), pp. 387–397.

[239] Zhiqun Wang et al. "Spatial patterns of intrinsic brain activity in mild cognitive impairment and Alzheimer's disease: A resting-state functional MRI study". In: *Human brain mapping* 32.10 (2011), pp. 1720–1740.

[240] Chantel D Mayo et al. "Relationship between DTI metrics and cognitive function in Alzheimer's disease". In: *Frontiers in aging neuroscience* 10 (2019), p. 436.

[241] Kun Wang et al. "Altered functional connectivity in early Alzheimer's disease: A resting-state fMRI study". In: *Human brain mapping* 28.10 (2007), pp. 967–978.

[242] Glenda Halliday. "Pathology and hippocampal atrophy in Alzheimer's disease". In: *The Lancet Neurology* 16.11 (2017), pp. 862–864.

[243] Andreas Fellgiebel and Igor Yakushev. "Diffusion tensor imaging of the hippocampus in MCI and early Alzheimer's disease". In: *Journal of Alzheimer's Disease* 26.s3 (2011), pp. 257–262.

[244] Håkon Grydeland et al. "Improved prediction of Alzheimer's disease with longitudinal white matter/gray matter contrast changes". In: *Human brain mapping* 34.11 (2013), pp. 2775–2785.

[245] Riccardo E Marioni et al. "GWAS on family history of Alzheimer's disease". In: *Translational psychiatry* 8.1 (2018), pp. 1–7.

[246] Lior Greenbaum et al. "Potential contribution of the Alzheimer's disease risk locus BIN1 to episodic memory performance in cognitively normal Type 2 diabetes elderly". In: *European Neuropsychopharmacology* 26.4 (2016), pp. 787–795.

[247] Josue D Gonzalez Murcia et al. "Assessment of TREM2 rs75932628 association with Alzheimer's disease in a population-based sample: the Cache County Study". In: *Neurobiology of aging* 34.12 (2013), 2889–e11.

[248] Guiyou Liu et al. “Alzheimer’s disease rs11767557 variant regulates EPHA1 gene expression specifically in human whole blood”. In: *Journal of Alzheimer’s Disease* 61.3 (2018), pp. 1077–1088.

[249] Minerva M Carrasquillo et al. “Late-onset Alzheimer’s risk variants in memory decline, incident mild cognitive impairment, and Alzheimer’s disease”. In: *Neurobiology of aging* 36.1 (2015), pp. 60–67.

[250] Yi Yan et al. “Genetic Association of FERMT2, HLA-DRB1, CD2AP, and PTK2B Polymorphisms With Alzheimer’s Disease Risk in the Southern Chinese Population”. In: *Frontiers in aging neuroscience* 12 (2020), p. 16.

[251] Cheng-Cheng Zhang et al. “SORL1 is associated with the risk of late-onset Alzheimer’s disease: a replication study and meta-analyses”. In: *Molecular neurobiology* 54.3 (2017), pp. 1725–1732.

[252] Meng-Shan Tan et al. “Associations of Alzheimer’s disease risk variants with gene expression, amyloidosis, tauopathy, and neurodegeneration”. In: *Alzheimer’s Research & Therapy* 13.1 (2021), pp. 1–11.

[253] Robert J Glynn. “Promises and limitations of mendelian randomization for evaluation of biomarkers”. In: *Clinical chemistry* 56.3 (2010), pp. 388–390.

[254] Alexander Teumer. “Common methods for performing Mendelian randomization”. In: *Frontiers in cardiovascular medicine* 5 (2018), p. 51.

# Appendix

# A Appendix

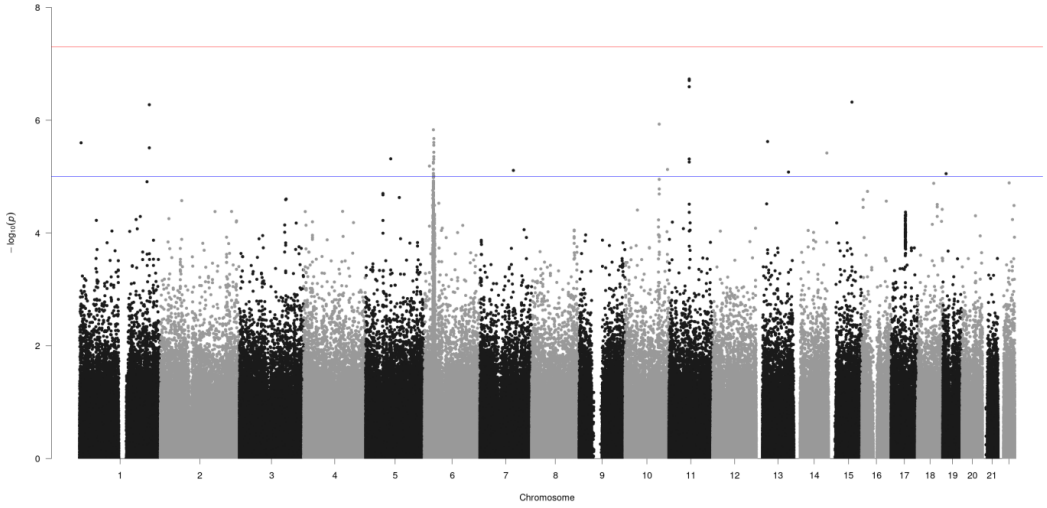


Figure 1 –Manhattan plot reporting the association results between SNPs and brain-PAD in Association FG. The red line indicates the GWAS threshold on p-value (i.e.,5E-8), while the blue line indicates the suggestive threshold of p=5E-5.

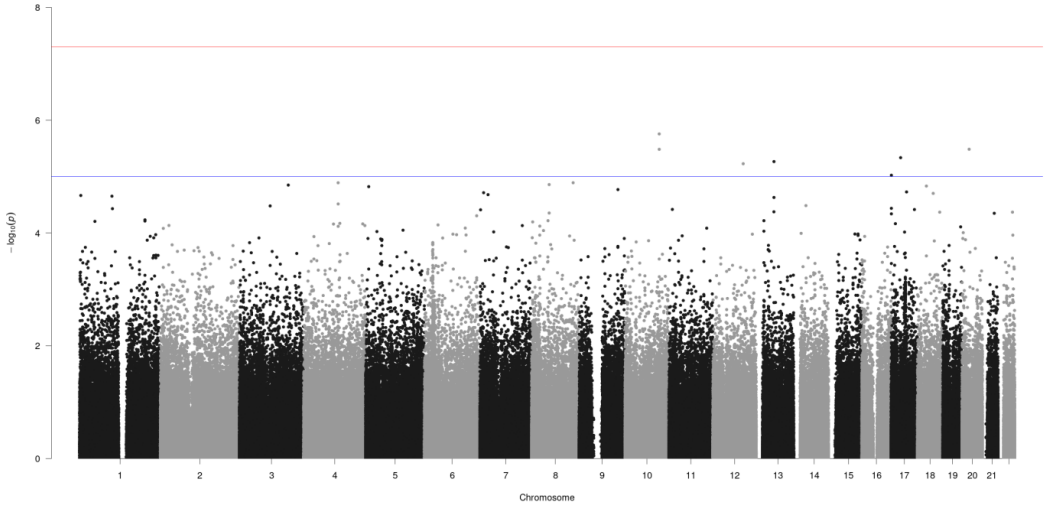


Figure 2 –Manhattan plot reporting the association results between SNPs and brain-PAD in Brainstem FG. The red line indicates the GWAS threshold on p-value (i.e.,5E-8), while the blue line indicates the suggestive threshold of p=5E-5.

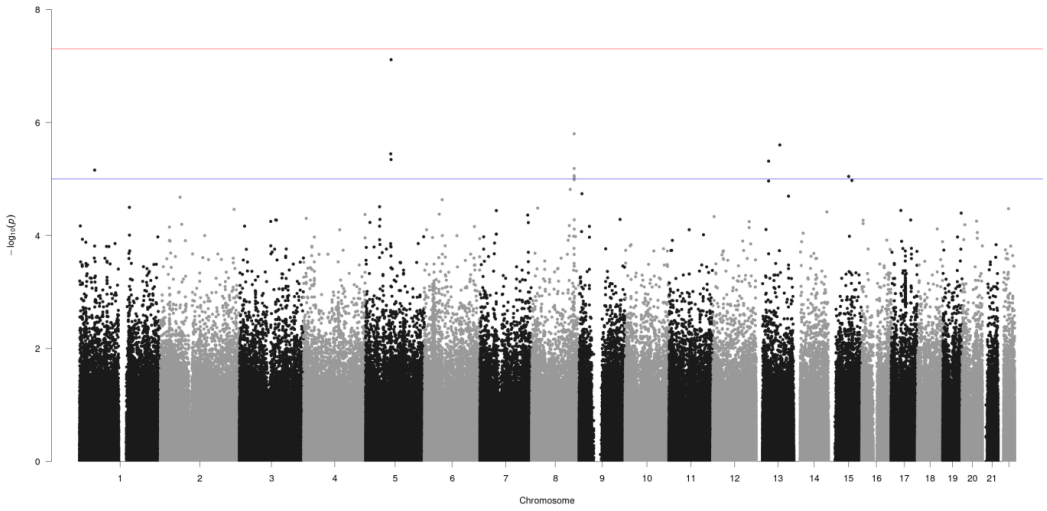


Figure 3 –Manhattan plot reporting the association results between SNPs and brain-PAD in Commissural FG. The red line indicates the GWAS threshold on p-value (i.e.,5E-8), while the blue line indicates the suggestive threshold of p=5E-5.

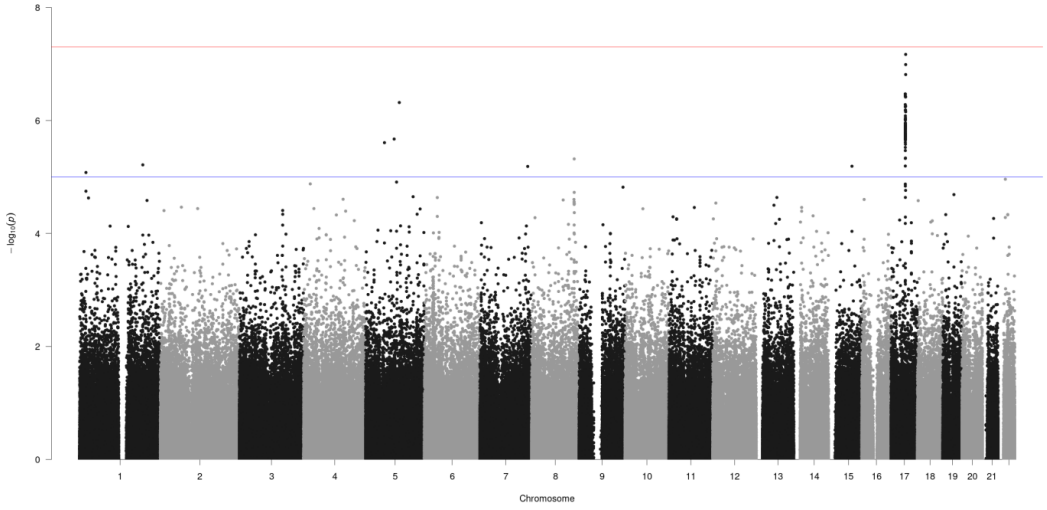


Figure 4 –Manhattan plot reporting the association results between SNPs and brain-PAD in Limbic FG. The red line indicates the GWAS threshold on p-value (i.e.,5E-8), while the blue line indicates the suggestive threshold of p=5E-5.

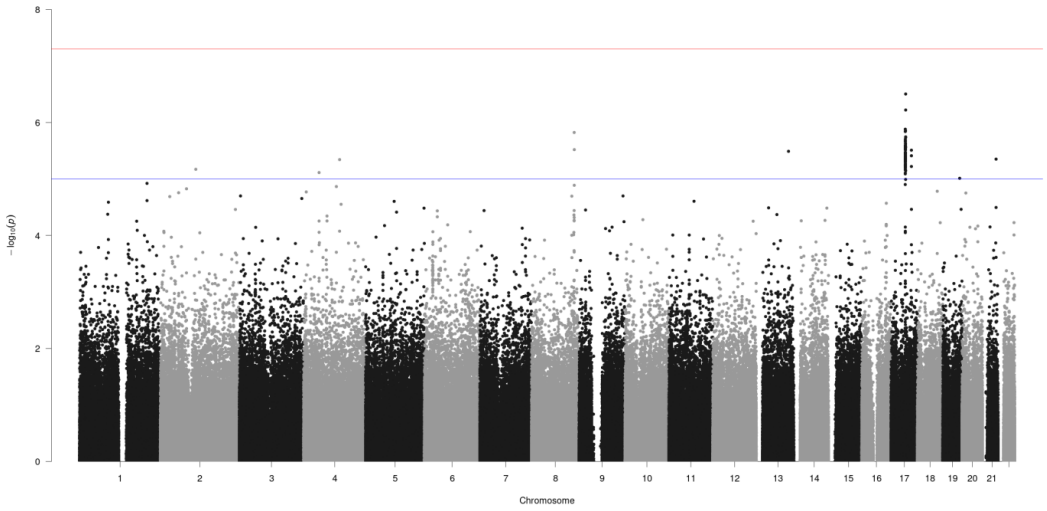


Figure 5 –Manhattan plot reporting the association results between SNPs and brain-PAD in Ensemble FG. The red line indicates the GWAS threshold on p-value (i.e.,5E-8), while the blue line indicates the suggestive threshold of p=5E-5.

Table 1 – The complete list of conditions used as exclusion criteria. ID is the Data-Field at UKB

| Non-cancer illness code, self-reported | | | |
|---|---|---|---|
| **ID** | **Condition** | **ID** | **Condition** |
| 1244 | infection of nervous system | 1267 | spinal injury |
| 1245 | brain abscess/intracranial abscess | 1394 | peripheral nerve injury |
| 1246 | encephalitis | 1242 | eye/eyelid problem |
| 1247 | meningitis | 1274 | eye infection |
| 1248 | spinal abscess | 1275 | retinal problem |
| 1249 | cranial nerve problem/palsy | 1281 | retinal detachment |
| 1523 | trigemminal neuralgia | 1282 | retinal artery/vein occlusion |
| 1251 | spinal cord disorder | 1527 | retinitis pigmentosa |
| 1252 | paraplegia | 1528 | macular degeneration |
| 1524 | spina bifida | 1276 | diabetic eye disease |
| 1254 | peripheral nerve disorder | 1277 | glaucoma |
| 1255 | peripheral neuropathy | 1278 | cataract |
| 1256 | acute infective polyneuritis/guillain-barre syndrome | 1279 | eye trauma |
| 1257 | trapped nerve/compressed nerve | 1435 | optic neuritis |
| 1468 | diabetic neuropathy/ulcers | 1529 | dry eyes |
| 258 | chronic/degenerative neurological problem | 1530 | iritis |
| 1259 | motor neurone disease | 1613 | blepharitis / eyelid infection |
| 1260 | myasthenia gravis | 1243 | psychological/psychiatric problem |
| 1261 | multiple sclerosis | 286 | depression |
| 1262 | parkinsons disease | 1531 | post-natal depression |
| 1263 | dementia/alzheimers/cognitive impairment | 1287 | anxiety/panic attacks |
| 1397 | other demyelinating disease (not multiple sclerosis) | 1288 | nervous breakdown |
| 1264 | epilepsy | 1289 | schizophrenia |
| 1265 | migraine | 1290 | deliberate self-harm/suicide attempt |
| 1433 | cerebral palsy | 1291 | mania/bipolar disorder/manic depression |
| 1434 | other neurological problem | 408 | alcohol dependency |
| 1436 | headaches (not migraine) | 1409 | opioid dependency |
| 1437 | myasthenia gravis | 1410 | other substance abuse/dependency |
| 1525 | benign / essential tremor | 1469 | post-traumatic stress disorder |
| 1526 | polio / poliomyelitis | 1470 | anorexia/bulimia/other eating disorder |
| 1659 | meningioma / benign meningeal tumour | 1614 | stress |
| 1683 | benign neuroma | 1615 | obsessive compulsive disorder (ocd) |
| 1240 | neurological injury/trauma | 1616 | insomnia |
| 1266 | head injury | 1267 | spinal injury |
| **ICD10** | | | |
| G000 | G00.0 Haemophilus meningitis | I688 | I68.8 Other cerebrovascular disorders in diseases classified elsewhere |
| G001 | G00.1 Pneumococcal meningitis | G20 | G20 Parkinson's disease |
| G002 | G00.2 Streptococcal meningitis | G21 | G21 Secondary Parkinsonism |
| G003 | G00.3 Staphylococcal meningitis | G210 | G21.0 Malignant neuroleptic syndrome |
| G008 | G00.8 Other bacterial meningitis | G211 | G21.1 Other drug-induced secondary Parkinsonism |
| G009 | G00.9 Bacterial meningitis, unspecified | G212 | G21.2 Secondary Parkinsonism due to other external agents |
| G01 | G01 Meningitis in bacterial diseases classified elsewhere | G213 | G21.3 Postencephalitic Parkinsonism |
| G020 | G02.0 Meningitis in viral diseases classified elsewhere | G214 | G21.4 Vascular parkinsonism |
| G021 | G02.1 Meningitis in mycoses | G218 | G21.8 Other secondary Parkinsonism |
| G030 | G03.0 Nonpyogenic meningitis | G219 | G21.9 Secondary Parkinsonism, unspecified |
| G031 | G03.1 Chronic meningitis | G22 | G22 Parkinsonism in diseases classified elsewhere |

| | | | |
|---|---|---|---|
| G032 | G03.2 Benign recurrent meningitis [Mollaret] | G300 | G30.0 Alzheimer's disease with early onset |
| G038 | G03.8 Meningitis due to other specified causes | G301 | G30.1 Alzheimer's disease with late onset |
| G039 | G03.9 Meningitis, unspecified | G308 | G30.8 Other Alzheimer's disease |
| G040 | G04.0 Acute disseminated encephalitis | F000 | F00.0 Dementia in Alzheimer's disease with early onset |
| G042 | G04.2 Bacterial meningoencephalitis and meningomyelitis, not elsewhere classified | F001 | F00.1 Dementia in Alzheimer's disease with late onset |
| G048 | G04.8 Other encephalitis, myelitis and encephalomyelitis | F002 | F00.2 Dementia in Alzheimer's disease, atypical or mixed type |
| G049 | G04.9 Encephalitis, myelitis and encephalomyelitis, unspecified | F009 | F00.9 Dementia in Alzheimer's disease, unspecified |
| G050 | G05.0 Encephalitis, myelitis and encephalomyelitis in bacterial diseases classified elsewhere | G310 | G31.0 Circumscribed brain atrophy |
| G051 | G05.1 Encephalitis, myelitis and encephalomyelitis in viral diseases classified elsewhere | G311 | G31.1 Senile degeneration of brain, not elsewhere classified |
| G052 | G05.2 Encephalitis, myelitis and encephalomyelitis in other infectious and parasitic diseases classified elsewhere | G312 | G31.2 Degeneration of nervous system due to alcohol |
| G058 | G05.8 Encephalitis, myelitis and encephalomyelitis in other diseases classified elsewhere | G318 | G31.8 Other specified degenerative diseases of nervous system |
| G06 | G06 Intracranial and intraspinal abscess and granuloma | G319 | G31.9 Degenerative disease of nervous system, unspecified |
| G060 | G06.0 Intracranial abscess and granuloma | G320 | G32.0 Subacute combined degeneration of spinal cord in diseases classified elsewhere |
| G061 | G06.1 Intraspinal abscess and granuloma | G328 | G32.8 Other specified degenerative disorders of nervous system in diseases classified elsewhere |
| G062 | G06.2 Extradural and subdural abscess, unspecified | G230 | G23.0 Hallervorden-Spatz disease |
| G07 | G07 Intracranial and intraspinal abscess and granuloma in diseases classified elsewhere | G231 | G23.1 Progressive supranuclear ophthalmoplegia [Steele-Richardson-Olszewski] |
| G08 | G08 Intracranial and intraspinal phlebitis and thrombophlebitis | G232 | G23.2 Striatonigral degeneration |
| G09 | G09 Sequelae of inflammatory diseases of central nervous system | G233 | G23.3 Multiple system atrophy, cerebellar type |
| G35 | G35 Multiple sclerosis | G238 | G23.8 Other specified degenerative diseases of basal ganglia |
| G360 | G36.0 Neuromyelitis optica [Devic] | G239 | G23.9 Degenerative disease of basal ganglia, unspecified |
| G368 | G36.8 Other specified acute disseminated demyelination | G240 | G24.0 Drug-induced dystonia |
| G369 | G36.9 Acute disseminated demyelination, unspecified | G241 | G24.1 Idiopathic familial dystonia |
| G370 | G37.0 Diffuse sclerosis | G242 | G24.2 Idiopathic nonfamilial dystonia |
| G371 | G37.1 Central demyelination of corpus callosum | G248 | G24.8 Other dystonia |
| G372 | G37.2 Central pontine myelinolysis | G249 | G24.9 Dystonia, unspecified |
| G373 | G37.3 Acute transverse myelitis in demyelinating disease of central nervous system | G253 | G25.3 Myoclonus |
| G374 | G37.4 Subacute necrotising myelitis | G254 | G25.4 Drug-induced chorea |
| G378 | G37.8 Other specified demyelinating diseases of central nervous system | G255 | G25.5 Other chorea |
| G379 | G37.9 Demyelinating disease of central nervous system, unspecified | G258 | G25.8 Other specified extrapyramidal and movement disorders |
| G400 | G40.0 Localisation-related (focal) (partial) idiopathic epilepsy and epileptic syndromes with seizures of localised onset | G259 | G25.9 Extrapyramidal and movement disorder, unspecified |

| | | | |
|---|---|---|---|
| G401 | G40.1 Localisation-related (focal) (partial) symptomatic epilepsy and epileptic syndromes with simple partial seizures | F010 | F01.0 Vascular dementia of acute onset |
| G402 | G40.2 Localisation-related (focal) (partial) symptomatic epilepsy and epileptic syndromes with complex partial seizures | F011 | F01.1 Multi-infarct dementia |
| G403 | G40.3 Generalised idiopathic epilepsy and epileptic syndromes | F012 | F01.2 Subcortical vascular dementia |
| G404 | G40.4 Other generalised epilepsy and epileptic syndromes | F013 | F01.3 Mixed cortical and subcortical vascular dementia |
| G405 | G40.5 Special epileptic syndromes | F018 | F01.8 Other vascular dementia |
| G406 | G40.6 Grand mal seizures, unspecified (with or without petit mal) | F019 | F01.9 Vascular dementia, unspecified |
| G407 | G40.7 Petit mal, unspecified, without grand mal seizures | F020 | F02.0 Dementia in Pick's disease |
| G408 | G40.8 Other epilepsy | F021 | F02.1 Dementia in Creutzfeldt-Jakob disease |
| G409 | G40.9 Epilepsy, unspecified | F022 | F02.2 Dementia in Huntington's disease |
| G410 | G41.0 Grand mal status epilepticus | F023 | F02.3 Dementia in Parkinson's disease |
| G411 | G41.1 Petit mal status epilepticus | F024 | F02.4 Dementia in human immunodeficiency virus [HIV] disease |
| G412 | G41.2 Complex partial status epilepticus | F028 | F02.8 Dementia in other specified diseases classified elsewhere |
| G418 | G41.8 Other status epilepticus | F03 | F03 Unspecified dementia |
| G419 | G41.9 Status epilepticus, unspecified | F04 | F04 Organic amnesic syndrome, not induced by alcohol and other psychoactive substances |
| G450 | G45.0 Vertebro-basilar artery syndrome | G10 | G10 Huntington's disease |
| G451 | G45.1 Carotid artery syndrome (hemispheric) | G110 | G11.0 Congenital nonprogressive ataxia |
| G453 | G45.3 Amaurosis fugax | G111 | G11.1 Early-onset cerebellar ataxia |
| G454 | G45.4 Transient global amnesia | G112 | G11.2 Late-onset cerebellar ataxia |
| G458 | G45.8 Other transient cerebral ischaemic attacks and related syndromes | G113 | G11.3 Cerebellar ataxia with defective DNA repair |
| G459 | G45.9 Transient cerebral ischaemic attack, unspecified | G114 | G11.4 Hereditary spastic paraplegia |
| G700 | G70.0 Myasthenia gravis | G118 | G11.8 Other hereditary ataxias |
| G702 | G70.2 Congenital and developmental myasthenia | G119 | G11.9 Hereditary ataxia, unspecified |
| G708 | G70.8 Other specified myoneural disorders | G120 | G12.0 Infantile spinal muscular atrophy, type I [Werdnig-Hoffman] |
| G709 | G70.9 Myoneural disorder, unspecified | G121 | G12.1 Other inherited spinal muscular atrophy |
| G800 | G80.0 Spastic cerebral palsy | G122 | G12.2 Motor neuron disease |
| G801 | G80.1 Spastic diplegia | G128 | G12.8 Other spinal muscular atrophies and related syndromes |
| G802 | G80.2 Infantile hemiplegia | G129 | G12.9 Spinal muscular atrophy, unspecified |
| G803 | G80.3 Dyskinetic cerebral palsy | G130 | G13.0 Paraneoplastic neuromyopathy and neuropathy |
| G808 | G80.8 Other infantile cerebral palsy | G131 | G13.1 Other systemic atrophy primarily affecting central nervous system in neoplastic disease |
| G809 | G80.9 Infantile cerebral palsy, unspecified | G138 | G13.8 Systemic atrophy primarily affecting central nervous system in other diseases classified elsewhere |
| D320 | D32.0 Cerebral meninges | F050 | F05.0 Delirium not superimposed on dementia, so described |
| D321 | D32.1 Spinal meninges | F051 | F05.1 Delirium superimposed on dementia |
| D329 | D32.9 Meninges, unspecified | F058 | F05.8 Other delirium |
| D330 | D33.0 Brain, supratentorial | F059 | F05.9 Delirium, unspecified |
| D331 | D33.1 Brain, infratentorial | F060 | F06.0 Organic hallucinosis |

| | | | |
|---|---|---|---|
| D332 | D33.2 Brain, unspecified | F062 | F06.2 Organic delusional [schizophrenia-like] disorder |
| D333 | D33.3 Cranial nerves | F063 | F06.3 Organic mood [affective] disorders |
| D334 | D33.4 Spinal cord | F064 | F06.4 Organic anxiety disorder |
| D339 | D33.9 Central nervous system, unspecified | F066 | F06.6 Organic emotionally labile [asthenic] disorder |
| G122 | G12.2 Motor neuron disease | F067 | F06.7 Mild cognitive disorder |
| S06 | S06 Intracranial injury | F068 | F06.8 Other specified mental disorders due to brain damage and dysfunction and to physical disease |
| I600 | I60.0 Subarachnoid haemorrhage from carotid siphon and bifurcation | F069 | F06.9 Unspecified mental disorder due to brain damage and dysfunction and to physical disease |
| I601 | I60.1 Subarachnoid haemorrhage from middle cerebral artery | F070 | F07.0 Organic personality disorder |
| I602 | I60.2 Subarachnoid haemorrhage from anterior communicating artery | F071 | F07.1 Postencephalitic syndrome |
| I603 | I60.3 Subarachnoid haemorrhage from posterior communicating artery | F072 | F07.2 Postconcussional syndrome |
| I604 | I60.4 Subarachnoid haemorrhage from basilar artery | F078 | F07.8 Other organic personality and behavioural disorders due to brain disease, damage and dysfunction |
| I605 | I60.5 Subarachnoid haemorrhage from vertebral artery | F079 | F07.9 Unspecified organic personality and behavioural disorder due to brain disease, damage and dysfunction |
| I606 | I60.6 Subarachnoid haemorrhage from other intracranial arteries | F09 | F09 Unspecified organic or symptomatic mental disorder |
| I607 | I60.7 Subarachnoid haemorrhage from intracranial artery, unspecified | Block F70-F79 | F70-F79 Mental retardation |
| I608 | I60.8 Other subarachnoid haemorrhage | F20 | F20 Schizophrenia |
| I609 | I60.9 Subarachnoid haemorrhage, unspecified | F21 | F21 Schizotypal disorder |
| I610 | I61.0 Intracerebral haemorrhage in hemisphere, subcortical | F42 | F42 Obsessive-compulsive disorder |
| I611 | I61.1 Intracerebral haemorrhage in hemisphere, cortical | F30 | F30 Manic episode |
| I612 | I61.2 Intracerebral haemorrhage in hemisphere, unspecified | F31 | F31 Bipolar affective disorder |
| I613 | I61.3 Intracerebral haemorrhage in brain stem | F323 | F32.3 Severe depressive episode with psychotic symptoms |
| I614 | I61.4 Intracerebral haemorrhage in cerebellum | F333 | F33.3 Recurrent depressive disorder, current episode severe with psychotic symptoms |
| I615 | I61.5 Intracerebral haemorrhage, intraventricular | F50 | F50 Eating disorders |
| I616 | I61.6 Intracerebral haemorrhage, multiple localised | Block Q00-Q07 | Q00-Q07 Congenital malformations of the nervous system |
| I618 | I61.8 Other intracerebral haemorrhage | G91 | G91 Hydrocephalus |
| I619 | I61.9 Intracerebral haemorrhage, unspecified | G92 | G92 Toxic encephalopathy |
| I620 | I62.0 Subdural haemorrhage (acute) (nontraumatic) | G931 | G93.1 Anoxic brain damage, not elsewhere classified |
| I621 | I62.1 Nontraumatic extradural haemorrhage | G932 | G93.2 Benign intracranial hypertension |
| I629 | I62.9 Intracranial haemorrhage (nontraumatic), unspecified | G934 | G93.4 Encephalopathy, unspecified |
| I630 | I63.0 Cerebral infarction due to thrombosis of precerebral arteries | G935 | G93.5 Compression of brain |
| I631 | I63.1 Cerebral infarction due to embolism of precerebral arteries | G936 | G93.6 Cerebral oedema |

| | | | |
|---|---|---|---|
| I632 | I63.2 Cerebral infarction due to unspecified occlusion or stenosis of precerebral arteries | G94 | G94 Other disorders of brain in diseases classified elsewhere |
| I633 | I63.3 Cerebral infarction due to thrombosis of cerebral arteries | G95 | G95 Other diseases of spinal cord |
| I634 | I63.4 Cerebral infarction due to embolism of cerebral arteries | C710 | C71.0 Cerebrum, except lobes and ventricles |
| I635 | I63.5 Cerebral infarction due to unspecified occlusion or stenosis of cerebral arteries | C711 | C71.1 Frontal lobe |
| I636 | I63.6 Cerebral infarction due to cerebral venous thrombosis, nonpyogenic | C712 | C71.2 Temporal lobe |
| I638 | I63.8 Other cerebral infarction | C713 | C71.3 Parietal lobe |
| I639 | I63.9 Cerebral infarction, unspecified | C714 | C71.4 Occipital lobe |
| I64 | I64 Stroke, not specified as haemorrhage or infarction | C715 | C71.5 Cerebral ventricle |
| I672 | I67.2 Cerebral atherosclerosis | C716 | C71.6 Cerebellum |
| I673 | I67.3 Progressive vascular leukoencephalopathy | C717 | C71.7 Brain stem |
| I674 | I67.4 Hypertensive encephalopathy | C718 | C71.8 Overlapping lesion of brain |
| I675 | I67.5 Moyamoya disease | C719 | C71.9 Brain, unspecified |
| I680 | I68.0 Cerebral amyloid angiopathy | C720 | C72.0 Spinal cord |
| G410 | G41.0 Grand mal status epilepticus | I611 | I61.1 Intracerebral haemorrhage in hemisphere, cortical |
| G411 | G41.1 Petit mal status epilepticus | I612 | I61.2 Intracerebral haemorrhage in hemisphere, unspecified |
| G412 | G41.2 Complex partial status epilepticus | I613 | I61.3 Intracerebral haemorrhage in brain stem |
| G418 | G41.8 Other status epilepticus | I614 | I61.4 Intracerebral haemorrhage in cerebellum |
| G419 | G41.9 Status epilepticus, unspecified | I615 | I61.5 Intracerebral haemorrhage, intraventricular |
| G450 | G45.0 Vertebro-basilar artery syndrome | I616 | I61.6 Intracerebral haemorrhage, multiple localised |
| G451 | G45.1 Carotid artery syndrome (hemispheric) | I618 | I61.8 Other intracerebral haemorrhage |
| G453 | G45.3 Amaurosis fugax | I619 | I61.9 Intracerebral haemorrhage, unspecified |
| G454 | G45.4 Transient global amnesia | I620 | I62.0 Subdural haemorrhage (acute) (nontraumatic) |
| G458 | G45.8 Other transient cerebral ischaemic attacks and related syndromes | I621 | I62.1 Nontraumatic extradural haemorrhage |
| G459 | G45.9 Transient cerebral ischaemic attack, unspecified | I629 | I62.9 Intracranial haemorrhage (nontraumatic), unspecified |
| G700 | G70.0 Myasthenia gravis | I630 | I63.0 Cerebral infarction due to thrombosis of precerebral arteries |
| G702 | G70.2 Congenital and developmental myasthenia | I631 | I63.1 Cerebral infarction due to embolism of precerebral arteries |
| G708 | G70.8 Other specified myoneural disorders | I632 | I63.2 Cerebral infarction due to unspecified occlusion or stenosis of precerebral arteries |
| G709 | G70.9 Myoneural disorder, unspecified | I633 | I63.3 Cerebral infarction due to thrombosis of cerebral arteries |
| G800 | G80.0 Spastic cerebral palsy | I634 | I63.4 Cerebral infarction due to embolism of cerebral arteries |
| G801 | G80.1 Spastic diplegia | I635 | I63.5 Cerebral infarction due to unspecified occlusion or stenosis of cerebral arteries |
| G802 | G80.2 Infantile hemiplegia | I636 | I63.6 Cerebral infarction due to cerebral venous thrombosis, nonpyogenic |

| | | | |
|---|---|---|---|
| G803 | G80.3 Dyskinetic cerebral palsy | I638 | I63.8 Other cerebral infarction |
| G808 | G80.8 Other infantile cerebral palsy | I639 | I63.9 Cerebral infarction, unspecified |
| G809 | G80.9 Infantile cerebral palsy, unspecified | I64 | I64 Stroke, not specified as haemorrhage or infarction |
| D320 | D32.0 Cerebral meninges | I672 | I67.2 Cerebral atherosclerosis |
| D321 | D32.1 Spinal meninges | I673 | I67.3 Progressive vascular leukoencephalopathy |
| D329 | D32.9 Meninges, unspecified | I674 | I67.4 Hypertensive encephalopathy |
| D330 | D33.0 Brain, supratentorial | I675 | I67.5 Moyamoya disease |
| D331 | D33.1 Brain, infratentorial | I680 | I68.0 Cerebral amyloid angiopathy |
| D332 | D33.2 Brain, unspecified | I605 | I60.5 Subarachnoid haemorrhage from vertebral artery |
| D333 | D33.3 Cranial nerves | I606 | I60.6 Subarachnoid haemorrhage from other intracranial arteries |
| D334 | D33.4 Spinal cord | I607 | I60.7 Subarachnoid haemorrhage from intracranial artery, unspecified |
| D339 | D33.9 Central nervous system, unspecified | I608 | I60.8 Other subarachnoid haemorrhage |
| G122 | G12.2 Motor neuron disease | I609 | I60.9 Subarachnoid haemorrhage, unspecified |
| S06 | S06 Intracranial injury | I610 | I61.0 Intracerebral haemorrhage in hemisphere, subcortical |
| I600 | I60.0 Subarachnoid haemorrhage from carotid siphon and bifurcation | I603 | I60.3 Subarachnoid haemorrhage from posterior communicating artery |
| I601 | I60.1 Subarachnoid haemorrhage from middle cerebral artery | I604 | I60.4 Subarachnoid haemorrhage from basilar artery |
| I602 | I60.2 Subarachnoid haemorrhage from anterior communicating artery | | |
| **Algorithmically-defined outcomes** | | | |
| 42006 | Date of stroke | 42018 | Date of all cause dementia report |
| 42008 | Date of ischaemic stroke (should be covered by 42006) | 42022 | Date of vascular dementia report |
| 42010 | Date of intracerebral haemorrhage (should be covered by 42006) | 42024 | Date of frontotemporal dementia report |
| 42012 | Date of subarachnoid haemorrhage (should be covered by 42006) | 42021 | Date of alzheimer's disease report |
| 42030 | Date of all cause parkinsonism report | | |

Table 2 – The 27 major tracts using probabilistic tractography approach and their fiber group

| **IDPs** | **Fiber group** |
|---|---|
| tract acoustic radiation (left) | Projection |
| tract acoustic radiation (right) | Projection |
| anterior thalamic radiation (left) | Projection |
| anterior thalamic radiation (right) | Projection |
| tract cingulate gyrus part of cingulum (left) | Limbic |
| tract cingulate gyrus part of cingulum (right) | Limbic |
| tract parahippocampal part of cingulum (left) | Limbic |
| tract parahippocampal part of cingulum (right) | Limbic |
| tract corticospinal tract (left) | Projection |
| tract corticospinal tract (right) | Projection |
| tract forceps major | Commissural |
| tract forceps minor | Commissural |
| tract inferior fronto-occipital fasciculus (left) | Association |
| tract inferior fronto-occipital fasciculus (right) | Association |
| tract inferior longitudinal fasciculus (left) | Association |
| tract inferior longitudinal fasciculus (right) | Association |
| tract middle cerebellar peduncle | Brainstem |
| tract medial lemniscus (left) | Brainstem |
| tract medial lemniscus (right) | Brainstem |
| tract posterior thalamic radiation (left) | Projection |
| tract posterior thalamic radiation (right) | Projection |
| tract superior longitudinal fasciculus (left) | Association |
| tract superior longitudinal fasciculus (right) | Association |
| tract superior thalamic radiation (left) | Projection |
| tract superior thalamic radiation (right) | Projection |
| tract uncinate fasciculus (left) | Association |
| tract uncinate fasciculus (right) | Association |

Table 3 – The daily life measures that are used to perform association with brain predicted age delta.

| **The measure** | **Category** |
|---|---|
| Duration of heavy DIY | Physical activity |
| Duration of light DIY | Physical activity |
| Duration of walk | Physical activity |
| duration of walk for pleasuer | Physical activity |
| Time spent driving | Physical activity |
| Time spent using computer | Physical activity |
| Time spent watching TV | Physical activity |
| Length of mobile phone use | Electronic device |
| Plays computer games | Electronic device |
| Sleep duration | Sleeping habits |
| Getting up in morning | Sleeping habits |
| Nap during day | Sleeping habits |
| Sleeplessness / insomnia | Sleeping habits |
| Snoring | Sleeping habits |
| Ever smoked | Smoking |
| Smoking status | Smoking |
| Alcohol drinker status | Alcohol |
| Alcohol frequency intake | Alcohol |
| Former alcohol drinker | Alcohol |
| Time spend outdoors in summer | Sun exposure |
| Time spent outdoors in winter | Sun exposure |
| Cooked vegetable intake | Diet |
| Salad / raw vegetable intake | Diet |
| Fresh fruit intake | Diet |
| Dried fruit intake | Diet |
| Oily fish intake | Diet |
| Non-oily fish intake | Diet |
| Processed meat intake | Diet |
| Poultry intake | Diet |

| | |
|---|---|
| Beef intake | Diet |
| Lamb/mutton intake | Diet |
| Pork intake | Diet |
| Never eat eggs, dairy, wheat, sugar | Diet |
| Cheese intake | Diet |
| Bread intake | Diet |
| Tea intake | Diet |
| Coffee intake | Diet |
| Water intake | Diet |

Table 4 – The association of brain predicted age delta and brain phenotypes for each model sorted by p-value. IDPs refer to image-derived phenotype. For ensemble model extra letter is added to the name of the IDP to show from which fiber (model) group it is.

| **Association model** | | | | | | |
|---|---|---|---|---|---|---|
| IDP | Coefficient | std err | T value | coefficient interval_S | coefficient interval_E | corrected_pvalue |
| Mean_fa | -1.6811 | 0.0241 | -69.6434 | -1.7284 | -1.6338 | 0.0000 |
| Weighted_mean_fa | -1.4280 | 0.0251 | -56.8855 | -1.4772 | -1.3788 | 0.0000 |
| Mean_md_A | 2.5560 | 0.0210 | 121.4856 | 2.5148 | 2.5972 | 0.0000 |
| Weighted_mean_md | 2.2347 | 0.0222 | 100.4946 | 2.1911 | 2.2783 | 0.0000 |
| Mean_l1_A | 2.2083 | 0.0235 | 93.9742 | 2.1623 | 2.2544 | 0.0000 |
| Weighted_mean_l1 | 2.0557 | 0.0237 | 86.6103 | 2.0091 | 2.1022 | 0.0000 |
| Mean_l2_A | 2.3050 | 0.0219 | 105.3755 | 2.2621 | 2.3479 | 0.0000 |
| Weighted_mean_l2 | 2.2003 | 0.0222 | 99.0235 | 2.1568 | 2.2439 | 0.0000 |
| Mean_l3_A | 2.4587 | 0.0213 | 115.2263 | 2.4169 | 2.5005 | 0.0000 |
| Weighted_mean_l3 | 2.1265 | 0.0226 | 94.2058 | 2.0822 | 2.1707 | 0.0000 |
| Mean_icvf_A | -2.0701 | 0.0231 | -89.7290 | -2.1154 | -2.0249 | 0.0000 |
| Weighted_mean_icvf | -1.3834 | 0.0249 | -55.6356 | -1.4321 | -1.3347 | 0.0000 |
| Mean_isovf_A | 1.6983 | 0.0243 | 69.9553 | 1.6507 | 1.7459 | 0.0000 |
| Weighted_mean_isovf | 1.7763 | 0.0240 | 73.9643 | 1.7292 | 1.8234 | 0.0000 |
| Weighted_mean_mo | -0.6364 | 0.0275 | -23.1851 | -0.6902 | -0.5826 | 0.0000 |
| Mean_mo | -0.6047 | 0.0264 | -22.8948 | -0.6565 | -0.5530 | 0.0000 |
| Mean_od | -0.1277 | 0.0272 | -4.6940 | -0.1810 | -0.0744 | 0.0000 |
| Weighted_mean_od | -0.1065 | 0.0281 | -3.7887 | -0.1616 | -0.0514 | 0.0027 |
| **Brainstem model** | | | | | | |
| IDP | Coefficient | std err | T value | coefficient interval_S | coefficient interval_E | corrected_pvalue |
| Mean_fa | -1.4347 | 0.0166 | -86.3267 | -1.4673 | -1.4021 | 0.0000 |
| Mean_mo | -1.1532 | 0.0174 | -66.1220 | -1.1874 | -1.1191 | 0.0000 |
| Mean_md | 0.7561 | 0.0185 | 40.7778 | 0.7197 | 0.7924 | 0.0000 |
| Weighted_mean_md | 1.0745 | 0.0174 | 61.6719 | 1.0404 | 1.1087 | 0.0000 |
| Weighted_mean_l1 | 1.1649 | 0.0174 | 66.8147 | 1.1307 | 1.1991 | 0.0000 |
| Mean_l2 | 1.1952 | 0.0172 | 69.3096 | 1.1614 | 1.2290 | 0.0000 |
| Weighted_mean_l2 | 0.8853 | 0.0182 | 48.6925 | 0.8497 | 0.9210 | 0.0000 |
| Mean_l3 | 1.1125 | 0.0179 | 61.9856 | 1.0774 | 1.1477 | 0.0000 |
| Weighted_mean_l3 | 0.8957 | 0.0181 | 49.3855 | 0.8601 | 0.9312 | 0.0000 |
| Mean_od | 1.2175 | 0.0170 | 71.5308 | 1.1842 | 1.2509 | 0.0000 |
| Mean_isovf | 0.9430 | 0.0178 | 52.9441 | 0.9081 | 0.9780 | 0.0000 |
| Weighted_mean_isovf | 0.9040 | 0.0181 | 49.9920 | 0.8686 | 0.9395 | 0.0000 |
| Weighted_mean_fa | -0.2521 | 0.0203 | -12.4515 | -0.2918 | -0.2125 | 0.0000 |
| Weighted_mean_od | -0.2266 | 0.0200 | -11.3071 | -0.2659 | -0.1873 | 0.0000 |
| Weighted_mean_mo | 0.2013 | 0.0198 | 10.1734 | 0.1625 | 0.2400 | 0.0000 |
| Weighted_mean_icvf | -0.1262 | 0.0200 | -6.3158 | -0.1654 | -0.0870 | 0.0000 |
| Mean_l1 | -0.0022 | 0.0193 | -0.1122 | -0.0400 | 0.0356 | 1.0000 |
| Mean_icvf | 0.0202 | 0.0203 | 0.9961 | -0.0196 | 0.0600 | 1.0000 |
| **Commissural model** | | | | | | |
| IDP | Coefficient | std err | T value | coefficient interval_S | coefficient interval_E | corrected_pvalue |
| Mean_fa | -1.7403 | 0.0243 | -71.7110 | -1.7879 | -1.6927 | 0.0000 |
| Weighted_mean_fa | -1.1361 | 0.0255 | -44.5788 | -1.1861 | -1.0862 | 0.0000 |
| Mean_md | 2.2439 | 0.0225 | 99.8921 | 2.1998 | 2.2879 | 0.0000 |
| Weighted_mean_md | 2.1749 | 0.0227 | 95.9544 | 2.1305 | 2.2194 | 0.0000 |
| Mean_l1 | 2.0197 | 0.0234 | 86.4106 | 1.9739 | 2.0655 | 0.0000 |
| Weighted_mean_l1 | 2.1660 | 0.0236 | 91.8566 | 2.1198 | 2.2122 | 0.0000 |
| Mean_l2 | 1.8096 | 0.0239 | 75.8039 | 1.7628 | 1.8564 | 0.0000 |
| Weighted_mean_l2 | 1.9965 | 0.0231 | 86.5350 | 1.9513 | 2.0417 | 0.0000 |
| Mean_l3 | 2.3152 | 0.0223 | 103.8275 | 2.2715 | 2.3589 | 0.0000 |
| Weighted_mean_l3 | 1.9872 | 0.0232 | 85.7796 | 1.9418 | 2.0326 | 0.0000 |
| Mean_icvf | -1.4558 | 0.0256 | -56.8630 | -1.5059 | -1.4056 | 0.0000 |
| Weighted_mean_icvf | -1.5483 | 0.0247 | -62.7045 | -1.5967 | -1.4999 | 0.0000 |
| Weighted_mean_od | -1.7011 | 0.0279 | -61.0182 | -1.7558 | -1.6465 | 0.0000 |

| | | | | | | |
|---|---|---|---|---|---|---|
| Mean_isovf | 1.8364 | 0.0236 | 77.6768 | 1.7901 | 1.8828 | 0.0000 |
| Weighted_mean_isovf | 1.4334 | 0.0248 | 57.8090 | 1.3848 | 1.4821 | 0.0000 |
| Mean_od | -0.3689 | 0.0265 | -13.9254 | -0.4208 | -0.3170 | 0.0000 |
| Weighted_mean_mo | 0.1489 | 0.0284 | 5.2402 | 0.0932 | 0.2045 | 0.0000 |
| Mean_mo | 0.0985 | 0.0267 | 3.6871 | 0.0461 | 0.1508 | 0.0041 |
| **Limbic model** | | | | | | |
| IDP | Coefficient | std err | T value | coefficient interval_S | coefficient interval_E | corrected_pvalue |
| Mean_fa | -2.8571 | 0.0206 | -138.8892 | -2.8974 | -2.8168 | 0.0000 |
| Mean_mo | -1.9210 | 0.0248 | -77.5291 | -1.9695 | -1.8724 | 0.0000 |
| Weighted_mean_mo | -1.4861 | 0.0260 | -57.2268 | -1.5371 | -1.4352 | 0.0000 |
| Mean_md | 3.1136 | 0.0201 | 154.7092 | 3.0742 | 3.1531 | 0.0000 |
| Mean_l1 | 1.9548 | 0.0264 | 74.1213 | 1.9031 | 2.0065 | 0.0000 |
| Mean_l2 | 3.2599 | 0.0185 | 176.2969 | 3.2237 | 3.2962 | 0.0000 |
| Weighted_mean_l2 | 1.4627 | 0.0259 | 56.4058 | 1.4119 | 1.5136 | 0.0000 |
| Mean_l3 | 3.0363 | 0.0202 | 150.2191 | 2.9967 | 3.0759 | 0.0000 |
| Mean_icvf | -1.4071 | 0.0261 | -53.9439 | -1.4582 | -1.3560 | 0.0000 |
| Weighted_mean_icvf | -1.3828 | 0.0262 | -52.8570 | -1.4341 | -1.3315 | 0.0000 |
| Mean_od | 1.6430 | 0.0257 | 63.9326 | 1.5926 | 1.6934 | 0.0000 |
| Mean_isovf | 3.1784 | 0.0205 | 155.2579 | 3.1383 | 3.2185 | 0.0000 |
| Weighted_mean_fa | -0.9910 | 0.0270 | -36.6575 | -1.0440 | -0.9380 | 0.0000 |
| Weighted_mean_l3 | 0.9606 | 0.0269 | 35.6850 | 0.9079 | 1.0134 | 0.0000 |
| Weighted_mean_md | 0.9042 | 0.0268 | 33.6989 | 0.8516 | 0.9568 | 0.0000 |
| Weighted_mean_od | 0.5310 | 0.0275 | 19.2921 | 0.4771 | 0.5850 | 0.0000 |
| Weighted_mean_isovf | -0.3176 | 0.0274 | -11.5771 | -0.3714 | -0.2638 | 0.0000 |
| Weighted_mean_l1 | -0.0790 | 0.0275 | -2.8686 | -0.1330 | -0.0250 | 0.0743 |
| **Projection model** | | | | | | |
| IDP | Coefficient | std err | T value | coefficient interval_S | coefficient interval_E | corrected_pvalue |
| Mean_fa | -1.6217 | 0.0241 | -67.4044 | -1.6689 | -1.5746 | 0.0000 |
| Mean_md | 1.9715 | 0.0227 | 86.9868 | 1.9271 | 2.0159 | 0.0000 |
| Weighted_mean_md | 1.8609 | 0.0231 | 80.7287 | 1.8157 | 1.9061 | 0.0000 |
| Mean_l1 | 1.4220 | 0.0251 | 56.6829 | 1.3728 | 1.4712 | 0.0000 |
| Weighted_mean_l1 | 1.7320 | 0.0242 | 71.6298 | 1.6846 | 1.7794 | 0.0000 |
| Mean_l2 | 1.5094 | 0.0241 | 62.5543 | 1.4621 | 1.5567 | 0.0000 |
| Weighted_mean_l2 | 1.6865 | 0.0236 | 71.3470 | 1.6402 | 1.7328 | 0.0000 |
| Mean_l3 | 2.2189 | 0.0215 | 103.1246 | 2.1767 | 2.2611 | 0.0000 |
| Weighted_mean_l3 | 1.7458 | 0.0235 | 74.3703 | 1.6998 | 1.7919 | 0.0000 |
| Mean_icvf | -1.5062 | 0.0241 | -62.4418 | -1.5535 | -1.4589 | 0.0000 |
| Weighted_mean_icvf | -1.4683 | 0.0242 | -60.5818 | -1.5158 | -1.4208 | 0.0000 |
| Weighted_mean_od | -1.2296 | 0.0271 | -45.3222 | -1.2828 | -1.1764 | 0.0000 |
| Mean_isovf | 1.2492 | 0.0247 | 50.5267 | 1.2007 | 1.2976 | 0.0000 |
| Weighted_mean_isovf | 1.0264 | 0.0252 | 40.7574 | 0.9771 | 1.0758 | 0.0000 |
| Weighted_mean_fa | -0.9067 | 0.0263 | -34.4539 | -0.9582 | -0.8551 | 0.0000 |
| Mean_od | 0.3060 | 0.0269 | 11.3718 | 0.2532 | 0.3587 | 0.0000 |
| Mean_mo | 0.2305 | 0.0266 | 8.6606 | 0.1784 | 0.2827 | 0.0000 |
| Weighted_mean_mo | 0.0381 | 0.0263 | 1.4464 | -0.0135 | 0.0897 | 1.0000 |
| **Ensemble model** | | | | | | |
| IDP | Coefficient | std err | T value | coefficient interval_S | coefficient interval_E | corrected_pvalue |
| Mean_fa_A | -1.2818 | 0.0289 | -44.3711 | -1.3384 | -1.2251 | 0.0000 |
| Mean_md_A | 1.9464 | 0.0286 | 67.9942 | 1.8903 | 2.0026 | 0.0000 |
| Weighted_mean_md_A | 1.7028 | 0.0286 | 59.5416 | 1.6467 | 1.7588 | 0.0000 |
| Mean_l1_A | 1.6788 | 0.0297 | 56.4430 | 1.6205 | 1.7371 | 0.0000 |
| Weighted_mean_l1_A | 1.5664 | 0.0295 | 53.1076 | 1.5086 | 1.6242 | 0.0000 |
| Mean_l2_A | 1.7565 | 0.0285 | 61.6554 | 1.7007 | 1.8123 | 0.0000 |
| Weighted_mean_l2_A | 1.6783 | 0.0285 | 58.9661 | 1.6225 | 1.7341 | 0.0000 |
| Mean_l3_A | 1.8742 | 0.0285 | 65.6935 | 1.8183 | 1.9301 | 0.0000 |
| Weighted_mean_l3_A | 1.6186 | 0.0286 | 56.6340 | 1.5625 | 1.6746 | 0.0000 |
| Mean_icvf_A | -1.5740 | 0.0289 | -54.4710 | -1.6307 | -1.5174 | 0.0000 |
| Mean_isovf_A | 1.2948 | 0.0291 | 44.5382 | 1.2378 | 1.3518 | 0.0000 |
| Weighted_mean_isovf_A | 1.3551 | 0.0290 | 46.7276 | 1.2982 | 1.4119 | 0.0000 |
| Mean_fa_C | -1.3263 | 0.0292 | -45.4895 | -1.3835 | -1.2692 | 0.0000 |
| Mean_md_C | 1.7095 | 0.0288 | 59.2903 | 1.6529 | 1.7660 | 0.0000 |

| | | | | | | |
|---|---|---|---|---|---|---|
| Weighted_mean_md_C | 1.6591 | 0.0288 | 57.6128 | 1.6026 | 1.7155 | 0.0000 |
| Mean_l1_C | 1.5370 | 0.0290 | 52.9527 | 1.4801 | 1.5939 | 0.0000 |
| Weighted_mean_l1_C | 1.6516 | 0.0297 | 55.6885 | 1.5935 | 1.7097 | 0.0000 |
| Mean_l2_C | 1.3800 | 0.0289 | 47.7020 | 1.3233 | 1.4367 | 0.0000 |
| Weighted_mean_l2_C | 1.5225 | 0.0286 | 53.1414 | 1.4663 | 1.5786 | 0.0000 |
| Mean_l3_C | 1.7640 | 0.0289 | 61.0120 | 1.7073 | 1.8207 | 0.0000 |
| Weighted_mean_l3_C | 1.5170 | 0.0287 | 52.8381 | 1.4607 | 1.5732 | 0.0000 |
| Weighted_mean_icvf_C | -1.1763 | 0.0291 | -40.3585 | -1.2334 | -1.1192 | 0.0000 |
| Weighted_mean_od_C | -1.2944 | 0.0328 | -39.4650 | -1.3587 | -1.2301 | 0.0000 |
| Mean_isovf_C | 1.4022 | 0.0288 | 48.7488 | 1.3458 | 1.4585 | 0.0000 |
| Mean_fa_L | -2.2932 | 0.0274 | -83.5811 | -2.3470 | -2.2394 | 0.0000 |
| Mean_mo_L | -1.5405 | 0.0287 | -53.6261 | -1.5968 | -1.4842 | 0.0000 |
| Weighted_mean_mo_L | -1.1897 | 0.0291 | -40.8975 | -1.2467 | -1.1327 | 0.0000 |
| Mean_md_L | 2.4990 | 0.0280 | 89.3511 | 2.4442 | 2.5538 | 0.0000 |
| Mean_l1_L | 1.5689 | 0.0304 | 51.6461 | 1.5094 | 1.6285 | 0.0000 |
| Mean_l2_L | 2.6146 | 0.0272 | 96.0507 | 2.5613 | 2.6680 | 0.0000 |
| Weighted_mean_l2_L | 1.1752 | 0.0290 | 40.5222 | 1.1183 | 1.2320 | 0.0000 |
| Mean_l3_L | 2.4386 | 0.0278 | 87.8721 | 2.3842 | 2.4930 | 0.0000 |
| Mean_icvf_L | -1.1292 | 0.0291 | -38.8429 | -1.1861 | -1.0722 | 0.0000 |
| Mean_od_L | 1.3201 | 0.0291 | 45.3979 | 1.2631 | 1.3771 | 0.0000 |
| Mean_isovf_L | 2.5501 | 0.0285 | 89.4927 | 2.4943 | 2.6060 | 0.0000 |
| Mean_fa_P | -1.2209 | 0.0291 | -41.8994 | -1.2780 | -1.1638 | 0.0000 |
| Mean_md_P | 1.4803 | 0.0287 | 51.5540 | 1.4241 | 1.5366 | 0.0000 |
| Weighted_mean_md_P | 1.3981 | 0.0288 | 48.6037 | 1.3417 | 1.4544 | 0.0000 |
| Weighted_mean_l1_P | 1.3011 | 0.0296 | 44.0211 | 1.2432 | 1.3591 | 0.0000 |
| Mean_l2_P | 1.1345 | 0.0289 | 39.1977 | 1.0777 | 1.1912 | 0.0000 |
| Weighted_mean_l2_P | 1.2659 | 0.0289 | 43.8333 | 1.2093 | 1.3225 | 0.0000 |
| Mean_l3_P | 1.6670 | 0.0284 | 58.6613 | 1.6113 | 1.7227 | 0.0000 |
| Weighted_mean_l3_P | 1.3129 | 0.0289 | 45.4847 | 1.2563 | 1.3695 | 0.0000 |
| Mean_icvf_P | -1.1301 | 0.0289 | -39.0612 | -1.1868 | -1.0734 | 0.0000 |
| Weighted_mean_icvf_L | -1.1075 | 0.0291 | -38.0359 | -1.1646 | -1.0504 | 0.0000 |
| Weighted_mean_icvf_P | -1.1016 | 0.0290 | -38.0347 | -1.1584 | -1.0448 | 0.0000 |
| Weighted_mean_isovf_C | 1.0949 | 0.0290 | 37.7663 | 1.0381 | 1.1517 | 0.0000 |
| Weighted_mean_fa_A | -1.0896 | 0.0293 | -37.1658 | -1.1470 | -1.0321 | 0.0000 |
| Mean_icvf_C | -1.1072 | 0.0299 | -37.0364 | -1.1658 | -1.0486 | 0.0000 |
| Weighted_mean_icvf_A | -1.0535 | 0.0290 | -36.3515 | -1.1103 | -0.9967 | 0.0000 |
| Mean_l1_P | 1.0662 | 0.0298 | 35.8223 | 1.0078 | 1.1245 | 0.0000 |
| Mean_isovf_P | 0.9374 | 0.0290 | 32.3109 | 0.8806 | 0.9943 | 0.0000 |
| Mean_fa_B | -0.8977 | 0.0300 | -29.9704 | -0.9564 | -0.8390 | 0.0000 |
| Weighted_mean_fa_C | -0.8676 | 0.0292 | -29.7423 | -0.9248 | -0.8104 | 0.0000 |
| Weighted_mean_od_P | -0.9177 | 0.0316 | -29.0546 | -0.9796 | -0.8557 | 0.0000 |
| Weighted_mean_fa_L | -0.7961 | 0.0295 | -26.9894 | -0.8539 | -0.7383 | 0.0000 |
| Weighted_mean_isovf_P | 0.7737 | 0.0291 | 26.5777 | 0.7166 | 0.8307 | 0.0000 |
| Weighted_mean_l3_L | 0.7733 | 0.0293 | 26.3562 | 0.7158 | 0.8309 | 0.0000 |
| Mean_od_B | 0.7595 | 0.0293 | 25.9523 | 0.7021 | 0.8169 | 0.0000 |
| Mean_l2_B | 0.7490 | 0.0294 | 25.4366 | 0.6913 | 0.8067 | 0.0000 |
| Weighted_mean_md_L | 0.7280 | 0.0292 | 24.9409 | 0.6708 | 0.7853 | 0.0000 |
| Weighted_mean_l1_B | 0.7285 | 0.0296 | 24.6498 | 0.6706 | 0.7865 | 0.0000 |
| Mean_mo_B | -0.7206 | 0.0295 | -24.4204 | -0.7784 | -0.6627 | 0.0000 |
| Mean_l3_B | 0.6962 | 0.0300 | 23.1990 | 0.6374 | 0.7550 | 0.0000 |
| Weighted_mean_md_B | 0.6721 | 0.0291 | 23.0902 | 0.6150 | 0.7291 | 0.0000 |
| Weighted_mean_fa_P | -0.6838 | 0.0302 | -22.6624 | -0.7429 | -0.6246 | 0.0000 |
| Mean_isovf_B | 0.5900 | 0.0291 | 20.2903 | 0.5330 | 0.6470 | 0.0000 |
| Weighted_mean_isovf_B | 0.5643 | 0.0293 | 19.2506 | 0.5068 | 0.6217 | 0.0000 |
| Weighted_mean_l3_B | 0.5609 | 0.0294 | 19.1073 | 0.5033 | 0.6184 | 0.0000 |
| Weighted_mean_l2_B | 0.5532 | 0.0294 | 18.8289 | 0.4956 | 0.6108 | 0.0000 |
| Mean_md_B | 0.4740 | 0.0294 | 16.0981 | 0.4163 | 0.5317 | 0.0000 |
| Weighted_mean_mo_A | -0.4849 | 0.0307 | -15.7983 | -0.5451 | -0.4247 | 0.0000 |
| Mean_mo_A | -0.4605 | 0.0295 | -15.5943 | -0.5184 | -0.4026 | 0.0000 |
| Weighted_mean_od_L | 0.4253 | 0.0296 | 14.3537 | 0.3672 | 0.4834 | 0.0000 |
| Mean_od_C | -0.2774 | 0.0294 | -9.4234 | -0.3351 | -0.2197 | 0.0000 |

| | | | | | | |
|---|---|---|---|---|---|---|
| Weighted_mean_isovf_L | -0.2496 | 0.0294 | -8.4788 | -0.3073 | -0.1919 | 0.0000 |
| Mean_od_P | 0.2327 | 0.0303 | 7.6849 | 0.1734 | 0.2921 | 0.0000 |
| Mean_mo_P | 0.1702 | 0.0299 | 5.6875 | 0.1116 | 0.2289 | 0.0000 |
| Weighted_mean_fa_B | -0.1599 | 0.0309 | -5.1697 | -0.2205 | -0.0993 | 0.0000 |
| Weighted_mean_od_B | -0.1387 | 0.0306 | -4.5341 | -0.1987 | -0.0788 | 0.0005 |
| Weighted_mean_mo_B | 0.1224 | 0.0302 | 4.0569 | 0.0633 | 0.1816 | 0.0045 |
| Weighted_mean_mo_C | 0.1128 | 0.0315 | 3.5822 | 0.0511 | 0.1745 | 0.0308 |
| Mean_od_A | -0.0932 | 0.0302 | -3.0898 | -0.1523 | -0.0341 | 0.1806 |
| Weighted_mean_icvf_B | -0.0788 | 0.0304 | -2.5892 | -0.1384 | -0.0191 | 0.8666 |
| Weighted_mean_od_A | -0.0785 | 0.0312 | -2.5196 | -0.1395 | -0.0174 | 1.0000 |
| Mean_l1_B | -0.0002 | 0.0293 | -0.0065 | -0.0577 | 0.0573 | 1.0000 |
| Mean_icvf_B | 0.0106 | 0.0309 | 0.3448 | -0.0499 | 0.0711 | 1.0000 |
| Mean_mo_C | 0.0705 | 0.0296 | 2.3817 | 0.0125 | 0.1285 | 1.0000 |
| Weighted_mean_l1_L | -0.0618 | 0.0295 | -2.0965 | -0.1196 | -0.0040 | 1.0000 |
| Weighted_mean_mo_P | 0.0280 | 0.0296 | 0.9474 | -0.0299 | 0.0859 | 1.0000 |

Table 5 – The association of cardiac risk factors and vascular measures association with brain predicted age delta sorted by p-value for each model.

| **Association model** | | | | | | |
|---|---|---|---|---|---|---|
| The measure | Coefficient | std err | T value | coefficient interval_S | coefficient interval_E | corrected_pvalue |
| Hypertens | 0.3359 | 0.0287 | 11.7021 | 0.2796 | 0.3921 | 0.0000 |
| Diabetes | 0.2306 | 0.0280 | 8.2244 | 0.1756 | 0.2856 | 0.0000 |
| cmr_LVM_i | 0.2578 | 0.0353 | 7.2965 | 0.1885 | 0.3270 | 0.0000 |
| cmr_RVEDV_i | -0.1716 | 0.0325 | -5.2829 | -0.2352 | -0.1079 | 0.0000 |
| cmr_RVSV_i | -0.1294 | 0.0295 | -4.3891 | -0.1872 | -0.0716 | 0.0002 |
| cmr_RVESV_i | -0.1380 | 0.0332 | -4.1632 | -0.2030 | -0.0730 | 0.0004 |
| cmr_LVSV_i | -0.0856 | 0.0292 | -2.9354 | -0.1427 | -0.0284 | 0.0467 |
| Deprivation | 0.0774 | 0.0282 | 2.7386 | 0.0220 | 0.1327 | 0.0865 |
| BMI | 0.0059 | 0.0284 | 0.2059 | -0.0499 | 0.0616 | 1.0000 |
| BSA | 0.0210 | 0.0467 | 0.4499 | -0.0706 | 0.1127 | 1.0000 |
| IPAQ | -0.0016 | 0.0281 | -0.0565 | -0.0566 | 0.0534 | 1.0000 |
| ASI0 | 0.0002 | 0.0285 | 0.0081 | -0.0557 | 0.0562 | 1.0000 |
| cmr_LVEDV_i | -0.0556 | 0.0308 | -1.8024 | -0.1160 | 0.0049 | 1.0000 |
| cmr_LVESV_i | 0.0033 | 0.0308 | 0.1056 | -0.0571 | 0.0636 | 1.0000 |
| **Brainstem model** | | | | | | |
| The measure | Coefficient | std err | T value | coefficient interval_S | coefficient interval_E | corrected_pvalue |
| BSA | 0.3450 | 0.0338 | 10.2229 | 0.2789 | 0.4112 | 0.0000 |
| BMI | 0.2050 | 0.0206 | 9.9739 | 0.1647 | 0.2453 | 0.0000 |
| Hypertens | 0.1894 | 0.0209 | 9.0743 | 0.1485 | 0.2303 | 0.0000 |
| Diabetes | 0.1650 | 0.0203 | 8.1145 | 0.1252 | 0.2049 | 0.0000 |
| cmr_RVEDV_i | -0.1215 | 0.0236 | -5.1586 | -0.1677 | -0.0753 | 0.0000 |
| cmr_LVM_i | 0.1249 | 0.0257 | 4.8686 | 0.0746 | 0.1752 | 0.0000 |
| cmr_RVESV_i | -0.1013 | 0.0241 | -4.2060 | -0.1485 | -0.0541 | 0.0004 |
| cmr_RVSV_i | -0.0890 | 0.0214 | -4.1617 | -0.1309 | -0.0471 | 0.0004 |
| cmr_LVSV_i | -0.0777 | 0.0211 | -3.6762 | -0.1191 | -0.0363 | 0.0033 |
| IPAQ | -0.0519 | 0.0203 | -2.5523 | -0.0918 | -0.0120 | 0.1500 |
| Deprivation | 0.0502 | 0.0205 | 2.4487 | 0.0100 | 0.0903 | 0.2009 |
| ASI0 | 0.0114 | 0.0207 | 0.5515 | -0.0292 | 0.0520 | 1.0000 |
| cmr_LVEDV_i | -0.0376 | 0.0224 | -1.6817 | -0.0815 | 0.0062 | 1.0000 |
| cmr_LVESV_i | 0.0240 | 0.0224 | 1.0718 | -0.0199 | 0.0678 | 1.0000 |
| **Commissural model** | | | | | | |
| The measure | Coefficient | std err | T value | coefficient interval_S | coefficient interval_E | corrected_pvalue |
| Hypertens | 0.2487 | 0.0286 | 8.6859 | 0.1926 | 0.3048 | 0.0000 |
| cmr_LVM_i | 0.2727 | 0.0351 | 7.7607 | 0.2039 | 0.3416 | 0.0000 |
| Diabetes | 0.1971 | 0.0279 | 7.0617 | 0.1424 | 0.2518 | 0.0000 |
| cmr_RVEDV_i | -0.1615 | 0.0323 | -4.9948 | -0.2248 | -0.0981 | 0.0000 |
| cmr_RVSV_i | -0.1194 | 0.0293 | -4.0695 | -0.1769 | -0.0619 | 0.0007 |
| cmr_RVESV_i | -0.1326 | 0.0330 | -4.0214 | -0.1973 | -0.0680 | 0.0008 |
| cmr_LVSV_i | -0.0967 | 0.0290 | -3.3331 | -0.1536 | -0.0398 | 0.0121 |
| BMI | 0.0553 | 0.0283 | 1.9554 | -0.0001 | 0.1107 | 0.7079 |
| Deprivation | 0.0541 | 0.0281 | 1.9246 | -0.0010 | 0.1091 | 0.7602 |
| BSA | 0.0649 | 0.0466 | 1.3946 | -0.0263 | 0.1562 | 1.0000 |
| IPAQ | -0.0095 | 0.0279 | -0.3404 | -0.0642 | 0.0452 | 1.0000 |
| ASI0 | -0.0062 | 0.0284 | -0.2186 | -0.0618 | 0.0494 | 1.0000 |
| cmr_LVEDV_i | -0.0469 | 0.0307 | -1.5279 | -0.1071 | 0.0133 | 1.0000 |
| cmr_LVESV_i | 0.0293 | 0.0306 | 0.9545 | -0.0308 | 0.0893 | 1.0000 |
| **Limbic model** | | | | | | |
| The measure | Coefficient | std err | T value | coefficient interval_S | coefficient interval_E | corrected_pvalue |
| Diabetes | 0.3585 | 0.0288 | 12.4471 | 0.3020 | 0.4149 | 0.0000 |
| Hypertens | 0.2934 | 0.0296 | 9.9051 | 0.2353 | 0.3514 | 0.0000 |
| BMI | 0.2599 | 0.0292 | 8.8982 | 0.2026 | 0.3171 | 0.0000 |
| cmr_RVEDV_i | -0.2732 | 0.0334 | -8.1715 | -0.3388 | -0.2077 | 0.0000 |
| BSA | 0.3831 | 0.0482 | 7.9449 | 0.2886 | 0.4776 | 0.0000 |
| cmr_RVESV_i | -0.2587 | 0.0341 | -7.5807 | -0.3256 | -0.1918 | 0.0000 |
| cmr_RVSV_i | -0.1731 | 0.0304 | -5.6969 | -0.2327 | -0.1135 | 0.0000 |
| cmr_LVEDV_i | -0.1374 | 0.0318 | -4.3263 | -0.1996 | -0.0751 | 0.0002 |

| | | | | | | |
|---|---|---|---|---|---|---|
| cmr_LVSV_i | -0.1222 | 0.0301 | -4.0658 | -0.1811 | -0.0633 | 0.0007 |
| cmr_LVM_i | 0.1354 | 0.0365 | 3.7142 | 0.0639 | 0.2068 | 0.0029 |
| cmr_LVESV_i | -0.0885 | 0.0317 | -2.7907 | -0.1506 | -0.0263 | 0.0737 |
| Deprivation | 0.0577 | 0.0291 | 1.9807 | 0.0006 | 0.1147 | 0.6670 |
| IPAQ | 0.0098 | 0.0289 | 0.3376 | -0.0469 | 0.0664 | 1.0000 |
| ASI0 | -0.0066 | 0.0294 | -0.2242 | -0.0643 | 0.0511 | 1.0000 |
| **Projection model** | | | | | | |
| The measure | Coefficient | std err | T value | coefficient interval_S | coefficient interval_E | corrected_pvalue |
| Hypertens | 0.3274 | 0.0283 | 11.5799 | 0.2720 | 0.3828 | 0.0000 |
| Diabetes | 0.2146 | 0.0276 | 7.7736 | 0.1605 | 0.2687 | 0.0000 |
| cmr_LVM_i | 0.2652 | 0.0348 | 7.6176 | 0.1969 | 0.3334 | 0.0000 |
| cmr_RVEDV_i | -0.1776 | 0.0320 | -5.5550 | -0.2403 | -0.1149 | 0.0000 |
| cmr_RVESV_i | -0.1491 | 0.0327 | -4.5599 | -0.2132 | -0.0850 | 0.0001 |
| cmr_RVSV_i | -0.1291 | 0.0290 | -4.4494 | -0.1860 | -0.0722 | 0.0001 |
| cmr_LVSV_i | -0.1040 | 0.0287 | -3.6232 | -0.1603 | -0.0478 | 0.0041 |
| Deprivation | 0.0975 | 0.0278 | 3.5064 | 0.0430 | 0.1520 | 0.0064 |
| BMI | 0.0901 | 0.0280 | 3.2180 | 0.0352 | 0.1450 | 0.0181 |
| BSA | 0.1013 | 0.0463 | 2.1887 | 0.0106 | 0.1920 | 0.4009 |
| IPAQ | -0.0128 | 0.0276 | -0.4624 | -0.0669 | 0.0414 | 1.0000 |
| ASI0 | -0.0149 | 0.0281 | -0.5295 | -0.0699 | 0.0402 | 1.0000 |
| cmr_LVEDV_i | -0.0397 | 0.0304 | -1.3045 | -0.0992 | 0.0199 | 1.0000 |
| cmr_LVESV_i | 0.0491 | 0.0303 | 1.6174 | -0.0104 | 0.1086 | 1.0000 |
| **Ensemble model** | | | | | | |
| The measure | Coefficient | std err | T value | coefficient interval_S | coefficient interval_E | corrected_pvalue |
| Hypertens | 0.3074 | 0.0318 | 9.6783 | 0.2451 | 0.3697 | 0.0000 |
| Diabetes | 0.2765 | 0.0309 | 8.9359 | 0.2159 | 0.3372 | 0.0000 |
| BSA | 0.3945 | 0.0516 | 7.6500 | 0.2934 | 0.4956 | 0.0000 |
| BMI | 0.2343 | 0.0313 | 7.4784 | 0.1729 | 0.2958 | 0.0000 |
| cmr_LVM_i | 0.2752 | 0.0391 | 7.0461 | 0.1986 | 0.3517 | 0.0000 |
| cmr_RVEDV_i | -0.2052 | 0.0359 | -5.7218 | -0.2755 | -0.1349 | 0.0000 |
| cmr_RVESV_i | -0.1900 | 0.0366 | -5.1909 | -0.2617 | -0.1182 | 0.0000 |
| cmr_RVSV_i | -0.1337 | 0.0326 | -4.1047 | -0.1975 | -0.0698 | 0.0006 |
| Deprivation | 0.0963 | 0.0312 | 3.0859 | 0.0351 | 0.1575 | 0.0285 |
| cmr_LVSV_i | -0.0918 | 0.0322 | -2.8523 | -0.1549 | -0.0287 | 0.0609 |
| cmr_LVEDV_i | -0.0653 | 0.0340 | -1.9165 | -0.1320 | 0.0015 | 0.7744 |
| IPAQ | 0.0012 | 0.0310 | 0.0389 | -0.0595 | 0.0619 | 1.0000 |
| ASI0 | -0.0093 | 0.0315 | -0.2962 | -0.0711 | 0.0524 | 1.0000 |
| cmr_LVESV_i | -0.0054 | 0.0340 | -0.1600 | -0.0721 | 0.0612 | 1.0000 |

Table 6 – The association of brain predicted age delta and daily life measures for each model.

| **Association model** | | | | | | |
|---|---|---|---|---|---|---|
| The measure | Coefficient | std err | T value | coefficient interval_S | coefficient interval_E | corrected_pvalue |
| Smoking status | 0.2056 | 0.0228 | 9.0046 | 0.1608 | 0.2503 | 0.0000 |
| Ever smoked | 0.1522 | 0.0229 | 6.6426 | 0.1073 | 0.1971 | 0.0000 |
| Alcohol frequency intake | -0.1296 | 0.0232 | -5.5763 | -0.1752 | -0.0840 | 0.0000 |
| Lamb/mutton intake | 0.1017 | 0.0230 | 4.4133 | 0.0565 | 0.1469 | 0.0004 |
| Time spent watching TV | -0.0955 | 0.0231 | -4.1300 | -0.1408 | -0.0502 | 0.0014 |
| Oily fish intake | 0.0921 | 0.0232 | 3.9781 | 0.0467 | 0.1375 | 0.0027 |
| Pork intake | 0.0880 | 0.0230 | 3.8339 | 0.0430 | 0.1330 | 0.0048 |
| Tea intake | -0.0714 | 0.0228 | -3.1331 | -0.1161 | -0.0267 | 0.0659 |
| Sleep duration | 0.0712 | 0.0229 | 3.1097 | 0.0263 | 0.1160 | 0.0713 |
| Getting up in morning | -0.0703 | 0.0234 | -2.9975 | -0.1162 | -0.0243 | 0.1036 |
| Nap during day | 0.0626 | 0.0231 | 2.7109 | 0.0173 | 0.1079 | 0.2553 |
| Water intake | 0.0579 | 0.0230 | 2.5125 | 0.0127 | 0.1030 | 0.4560 |
| Beef intake | 0.0554 | 0.0229 | 2.4228 | 0.0106 | 0.1003 | 0.5857 |
| Former alcohol drinker | 0.0522 | 0.0228 | 2.2869 | 0.0075 | 0.0968 | 0.8441 |
| Duration of heavy DIY | 0.0334 | 0.0230 | 1.4523 | -0.0117 | 0.0784 | 1.0000 |
| Duration of light DIY | -0.0123 | 0.0229 | -0.5371 | -0.0573 | 0.0326 | 1.0000 |
| Duration of walk | -0.0268 | 0.0228 | -1.1738 | -0.0715 | 0.0179 | 1.0000 |
| duration of walk for pleasure | -0.0256 | 0.0229 | -1.1190 | -0.0705 | 0.0193 | 1.0000 |
| Time spent driving | 0.0101 | 0.0232 | 0.4355 | -0.0354 | 0.0556 | 1.0000 |
| Time spent using computer | 0.0370 | 0.0230 | 1.6076 | -0.0081 | 0.0820 | 1.0000 |
| Length of mobile phone use | -0.0237 | 0.0233 | -1.0194 | -0.0693 | 0.0219 | 1.0000 |
| Plays computer games | -0.0089 | 0.0228 | -0.3888 | -0.0537 | 0.0359 | 1.0000 |
| Sleeplessness / insomnia | -0.0231 | 0.0231 | -1.0021 | -0.0684 | 0.0221 | 1.0000 |
| Snoring | -0.0154 | 0.0228 | -0.6735 | -0.0601 | 0.0294 | 1.0000 |
| Alcohol drinker status | -0.0147 | 0.0228 | -0.6418 | -0.0594 | 0.0301 | 1.0000 |
| Time spend outdoors in summer | -0.0478 | 0.0233 | -2.0539 | -0.0934 | -0.0022 | 1.0000 |
| Time spent outdoors in winter | -0.0283 | 0.0231 | -1.2207 | -0.0736 | 0.0171 | 1.0000 |
| Cooked vegetable intake | -0.0086 | 0.0229 | -0.3755 | -0.0534 | 0.0362 | 1.0000 |
| Salad / raw vegetable intake | -0.0180 | 0.0229 | -0.7868 | -0.0629 | 0.0269 | 1.0000 |
| Fresh fruit intake | 0.0299 | 0.0230 | 1.3005 | -0.0151 | 0.0749 | 1.0000 |
| Dried fruit intake | 0.0179 | 0.0229 | 0.7842 | -0.0269 | 0.0627 | 1.0000 |
| Non-oily fish intake | -0.0078 | 0.0229 | -0.3423 | -0.0526 | 0.0370 | 1.0000 |
| Processed meat intake | 0.0310 | 0.0238 | 1.3051 | -0.0156 | 0.0776 | 1.0000 |
| Poultry intake | -0.0275 | 0.0228 | -1.2052 | -0.0723 | 0.0172 | 1.0000 |
| Never eat eggs, dairy, wheat, sugar | -0.0045 | 0.0229 | -0.1989 | -0.0494 | 0.0403 | 1.0000 |
| Cheese intake | 0.0254 | 0.0229 | 1.1068 | -0.0196 | 0.0703 | 1.0000 |
| Bread intake | 0.0015 | 0.0240 | 0.0615 | -0.0455 | 0.0485 | 1.0000 |
| Coffee intake | 0.0181 | 0.0229 | 0.7926 | -0.0267 | 0.0629 | 1.0000 |
| **Brainstem model** | | | | | | |
| The measure | Coefficient | std err | T value | coefficient interval_S | coefficient interval_E | corrected_pvalue |
| Smoking status | 0.1249 | 0.0163 | 7.6708 | 0.0930 | 0.1568 | 0.0000 |
| Ever smoked | 0.0969 | 0.0163 | 5.9387 | 0.0650 | 0.1289 | 0.0000 |
| Tea intake | -0.0567 | 0.0162 | -3.4875 | -0.0885 | -0.0248 | 0.0186 |
| Oily fish intake | 0.0560 | 0.0165 | 3.3958 | 0.0237 | 0.0884 | 0.0261 |
| Lamb/mutton intake | 0.0525 | 0.0164 | 3.2002 | 0.0203 | 0.0846 | 0.0523 |
| Water intake | 0.0519 | 0.0164 | 3.1629 | 0.0197 | 0.0841 | 0.0595 |
| Nap during day | 0.0504 | 0.0165 | 3.0616 | 0.0181 | 0.0827 | 0.0838 |
| Never eat eggs, dairy, wheat, sugar | -0.0465 | 0.0163 | -2.8554 | -0.0785 | -0.0146 | 0.1635 |
| Coffee intake | 0.0430 | 0.0163 | 2.6394 | 0.0111 | 0.0749 | 0.3159 |
| Pork intake | 0.0430 | 0.0164 | 2.6257 | 0.0109 | 0.0750 | 0.3289 |
| Plays computer games | 0.0414 | 0.0163 | 2.5444 | 0.0095 | 0.0733 | 0.4163 |
| Beef intake | 0.0386 | 0.0163 | 2.3689 | 0.0067 | 0.0705 | 0.6784 |
| Duration of heavy DIY | 0.0132 | 0.0164 | 0.8051 | -0.0189 | 0.0453 | 1.0000 |
| Duration of light DIY | 0.0115 | 0.0163 | 0.7057 | -0.0205 | 0.0436 | 1.0000 |
| Duration of walk | -0.0346 | 0.0163 | -2.1289 | -0.0665 | -0.0027 | 1.0000 |
| duration of walk for pleasure | -0.0148 | 0.0163 | -0.9089 | -0.0468 | 0.0172 | 1.0000 |

| | | | | | | |
|---|---|---|---|---|---|---|
| Time spent driving | 0.0027 | 0.0165 | 0.1659 | -0.0297 | 0.0351 | 1.0000 |
| Time spent using computer | 0.0269 | 0.0164 | 1.6426 | -0.0052 | 0.0590 | 1.0000 |
| Time spent watching TV | 0.0071 | 0.0165 | 0.4292 | -0.0252 | 0.0394 | 1.0000 |
| Length of mobile phone use | 0.0034 | 0.0166 | 0.2047 | -0.0291 | 0.0358 | 1.0000 |
| Sleep duration | 0.0049 | 0.0163 | 0.2992 | -0.0271 | 0.0368 | 1.0000 |
| Getting up in morning | -0.0276 | 0.0167 | -1.6510 | -0.0604 | 0.0052 | 1.0000 |
| Sleeplessness / insomnia | 0.0144 | 0.0165 | 0.8754 | -0.0178 | 0.0466 | 1.0000 |
| Snoring | -0.0228 | 0.0163 | -1.3997 | -0.0546 | 0.0091 | 1.0000 |
| Alcohol drinker status | -0.0035 | 0.0163 | -0.2155 | -0.0354 | 0.0284 | 1.0000 |
| Former alcohol drinker | 0.0176 | 0.0163 | 1.0854 | -0.0142 | 0.0495 | 1.0000 |
| Time spend outdoors in summer | -0.0347 | 0.0166 | -2.0909 | -0.0672 | -0.0022 | 1.0000 |
| Time spent outdoors in winter | -0.0107 | 0.0165 | -0.6490 | -0.0430 | 0.0216 | 1.0000 |
| Cooked vegetable intake | 0.0324 | 0.0163 | 1.9890 | 0.0005 | 0.0643 | 1.0000 |
| Salad / raw vegetable intake | 0.0091 | 0.0163 | 0.5598 | -0.0228 | 0.0411 | 1.0000 |
| Fresh fruit intake | 0.0117 | 0.0164 | 0.7121 | -0.0204 | 0.0437 | 1.0000 |
| Dried fruit intake | -0.0178 | 0.0163 | -1.0946 | -0.0498 | 0.0141 | 1.0000 |
| Non-oily fish intake | 0.0217 | 0.0163 | 1.3292 | -0.0103 | 0.0536 | 1.0000 |
| Processed meat intake | 0.0212 | 0.0169 | 1.2532 | -0.0120 | 0.0544 | 1.0000 |
| Poultry intake | 0.0033 | 0.0163 | 0.2049 | -0.0286 | 0.0352 | 1.0000 |
| Cheese intake | 0.0159 | 0.0163 | 0.9765 | -0.0161 | 0.0480 | 1.0000 |
| Bread intake | -0.0102 | 0.0171 | -0.5964 | -0.0437 | 0.0233 | 1.0000 |
| Alcohol frequency intake | -0.0177 | 0.0166 | -1.0666 | -0.0501 | 0.0148 | 1.0000 |
| **Commissural model** | | | | | | |
| The measure | Coefficient | std err | T value | coefficient interval_S | coefficient interval_E | corrected_pvalue |
| Smoking status | 0.1971 | 0.0238 | 8.2854 | 0.1505 | 0.2438 | 0.0000 |
| Alcohol frequency intake | -0.1743 | 0.0242 | -7.2064 | -0.2217 | -0.1269 | 0.0000 |
| Ever smoked | 0.1505 | 0.0239 | 6.3088 | 0.1038 | 0.1973 | 0.0000 |
| Oily fish intake | 0.1359 | 0.0241 | 5.6346 | 0.0886 | 0.1831 | 0.0000 |
| Lamb/mutton intake | 0.0895 | 0.0240 | 3.7308 | 0.0425 | 0.1365 | 0.0073 |
| Water intake | 0.0890 | 0.0240 | 3.7075 | 0.0419 | 0.1360 | 0.0080 |
| Tea intake | -0.0766 | 0.0237 | -3.2248 | -0.1231 | -0.0300 | 0.0480 |
| Nap during day | 0.0766 | 0.0241 | 3.1801 | 0.0294 | 0.1238 | 0.0561 |
| Time spent watching TV | -0.0674 | 0.0241 | -2.7989 | -0.1147 | -0.0202 | 0.1951 |
| Pork intake | 0.0641 | 0.0239 | 2.6794 | 0.0172 | 0.1110 | 0.2806 |
| Time spent using computer | 0.0629 | 0.0240 | 2.6272 | 0.0160 | 0.1099 | 0.3275 |
| Duration of heavy DIY | 0.0610 | 0.0239 | 2.5497 | 0.0141 | 0.1079 | 0.4100 |
| Getting up in morning | -0.0613 | 0.0244 | -2.5122 | -0.1092 | -0.0135 | 0.4563 |
| Sleep duration | 0.0561 | 0.0238 | 2.3525 | 0.0094 | 0.1028 | 0.7091 |
| Plays computer games | -0.0542 | 0.0238 | -2.2772 | -0.1008 | -0.0075 | 0.8659 |
| Duration of light DIY | 0.0332 | 0.0239 | 1.3916 | -0.0136 | 0.0801 | 1.0000 |
| Duration of walk | -0.0120 | 0.0238 | -0.5052 | -0.0586 | 0.0346 | 1.0000 |
| duration of walk for pleasure | -0.0086 | 0.0239 | -0.3611 | -0.0554 | 0.0382 | 1.0000 |
| Time spent driving | 0.0176 | 0.0242 | 0.7283 | -0.0298 | 0.0650 | 1.0000 |
| Length of mobile phone use | -0.0167 | 0.0242 | -0.6877 | -0.0642 | 0.0308 | 1.0000 |
| Sleeplessness / insomnia | 0.0097 | 0.0241 | 0.4039 | -0.0374 | 0.0569 | 1.0000 |
| Snoring | -0.0264 | 0.0238 | -1.1091 | -0.0729 | 0.0202 | 1.0000 |
| Alcohol drinker status | 0.0089 | 0.0238 | 0.3751 | -0.0377 | 0.0556 | 1.0000 |
| Former alcohol drinker | 0.0319 | 0.0238 | 1.3416 | -0.0147 | 0.0785 | 1.0000 |
| Time spend outdoors in summer | -0.0299 | 0.0242 | -1.2333 | -0.0773 | 0.0176 | 1.0000 |
| Time spent outdoors in winter | 0.0086 | 0.0241 | 0.3570 | -0.0386 | 0.0559 | 1.0000 |
| Cooked vegetable intake | 0.0196 | 0.0238 | 0.8218 | -0.0271 | 0.0663 | 1.0000 |
| Salad / raw vegetable intake | -0.0390 | 0.0238 | -1.6380 | -0.0857 | 0.0077 | 1.0000 |
| Fresh fruit intake | -0.0171 | 0.0239 | -0.7156 | -0.0640 | 0.0298 | 1.0000 |
| Dried fruit intake | -0.0200 | 0.0238 | -0.8416 | -0.0667 | 0.0266 | 1.0000 |
| Non-oily fish intake | 0.0396 | 0.0238 | 1.6647 | -0.0070 | 0.0863 | 1.0000 |
| Processed meat intake | -0.0405 | 0.0248 | -1.6356 | -0.0891 | 0.0080 | 1.0000 |
| Poultry intake | -0.0336 | 0.0238 | -1.4126 | -0.0802 | 0.0130 | 1.0000 |
| Beef intake | 0.0256 | 0.0238 | 1.0756 | -0.0211 | 0.0723 | 1.0000 |
| Never eat eggs, dairy, wheat, sugar | -0.0447 | 0.0238 | -1.8738 | -0.0914 | 0.0021 | 1.0000 |
| Cheese intake | -0.0212 | 0.0239 | -0.8879 | -0.0680 | 0.0256 | 1.0000 |
| Bread intake | -0.0334 | 0.0250 | -1.3353 | -0.0824 | 0.0156 | 1.0000 |

| | | | | | | |
|---|---|---|---|---|---|---|
| Coffee intake | 0.0284 | 0.0238 | 1.1915 | -0.0183 | 0.0750 | 1.0000 |
| **Limbic model** | | | | | | |
| The measure | Coefficient | std err | T value | coefficient interval_S | coefficient interval_E | corrected_pvalue |
| Smoking status | 0.2558 | 0.0241 | 10.5944 | 0.2084 | 0.3031 | 0.0000 |
| Ever smoked | 0.1840 | 0.0242 | 7.5945 | 0.1365 | 0.2315 | 0.0000 |
| Alcohol frequency intake | -0.1459 | 0.0246 | -5.9318 | -0.1941 | -0.0977 | 0.0000 |
| Time spent using computer | 0.1145 | 0.0243 | 4.7080 | 0.0668 | 0.1621 | 0.0001 |
| duration of walk for pleasure | -0.1092 | 0.0242 | -4.5051 | -0.1567 | -0.0617 | 0.0003 |
| Lamb/mutton intake | 0.1058 | 0.0244 | 4.3416 | 0.0580 | 0.1535 | 0.0005 |
| Oily fish intake | 0.0939 | 0.0245 | 3.8307 | 0.0459 | 0.1420 | 0.0049 |
| Snoring | -0.0864 | 0.0241 | -3.5788 | -0.1337 | -0.0391 | 0.0132 |
| Tea intake | -0.0844 | 0.0241 | -3.4970 | -0.1317 | -0.0371 | 0.0179 |
| Sleep duration | 0.0838 | 0.0242 | 3.4583 | 0.0363 | 0.1313 | 0.0207 |
| Never eat eggs, dairy, wheat, sugar | -0.0835 | 0.0242 | -3.4485 | -0.1309 | -0.0360 | 0.0215 |
| Former alcohol drinker | 0.0766 | 0.0241 | 3.1756 | 0.0293 | 0.1239 | 0.0569 |
| Nap during day | 0.0774 | 0.0245 | 3.1625 | 0.0294 | 0.1253 | 0.0596 |
| Pork intake | 0.0766 | 0.0243 | 3.1535 | 0.0290 | 0.1242 | 0.0614 |
| Water intake | 0.0694 | 0.0244 | 2.8494 | 0.0217 | 0.1172 | 0.1667 |
| Time spent driving | 0.0677 | 0.0246 | 2.7542 | 0.0195 | 0.1158 | 0.2239 |
| Beef intake | 0.0594 | 0.0242 | 2.4518 | 0.0119 | 0.1068 | 0.5405 |
| Getting up in morning | -0.0573 | 0.0248 | -2.3110 | -0.1060 | -0.0087 | 0.7923 |
| Duration of heavy DIY | 0.0361 | 0.0243 | 1.4866 | -0.0115 | 0.0838 | 1.0000 |
| Duration of light DIY | 0.0157 | 0.0243 | 0.6452 | -0.0319 | 0.0633 | 1.0000 |
| Duration of walk | -0.0238 | 0.0241 | -0.9867 | -0.0711 | 0.0235 | 1.0000 |
| Time spent watching TV | 0.0039 | 0.0245 | 0.1583 | -0.0441 | 0.0519 | 1.0000 |
| Length of mobile phone use | -0.0077 | 0.0246 | -0.3138 | -0.0559 | 0.0405 | 1.0000 |
| Plays computer games | 0.0021 | 0.0242 | 0.0849 | -0.0453 | 0.0495 | 1.0000 |
| Sleeplessness / insomnia | -0.0211 | 0.0245 | -0.8633 | -0.0691 | 0.0268 | 1.0000 |
| Alcohol drinker status | 0.0143 | 0.0242 | 0.5916 | -0.0331 | 0.0617 | 1.0000 |
| Time spend outdoors in summer | -0.0001 | 0.0246 | -0.0045 | -0.0484 | 0.0482 | 1.0000 |
| Time spent outdoors in winter | -0.0240 | 0.0245 | -0.9797 | -0.0721 | 0.0240 | 1.0000 |
| Cooked vegetable intake | 0.0093 | 0.0242 | 0.3833 | -0.0382 | 0.0567 | 1.0000 |
| Salad / raw vegetable intake | -0.0092 | 0.0242 | -0.3817 | -0.0567 | 0.0382 | 1.0000 |
| Fresh fruit intake | -0.0073 | 0.0243 | -0.2987 | -0.0549 | 0.0404 | 1.0000 |
| Dried fruit intake | -0.0233 | 0.0242 | -0.9622 | -0.0707 | 0.0242 | 1.0000 |
| Non-oily fish intake | -0.0254 | 0.0242 | -1.0501 | -0.0728 | 0.0220 | 1.0000 |
| Processed meat intake | 0.0066 | 0.0251 | 0.2612 | -0.0427 | 0.0559 | 1.0000 |
| Poultry intake | 0.0251 | 0.0242 | 1.0378 | -0.0223 | 0.0725 | 1.0000 |
| Cheese intake | -0.0314 | 0.0243 | -1.2955 | -0.0790 | 0.0161 | 1.0000 |
| Bread intake | -0.0404 | 0.0254 | -1.5899 | -0.0901 | 0.0094 | 1.0000 |
| Coffee intake | 0.0304 | 0.0242 | 1.2568 | -0.0170 | 0.0778 | 1.0000 |
| **Projection model** | | | | | | |
| The measure | Coefficient | std err | T value | coefficient interval_S | coefficient interval_E | corrected_pvalue |
| Smoking status | 0.1926 | 0.0231 | 8.3357 | 0.1473 | 0.2379 | 0.0000 |
| Ever smoked | 0.1170 | 0.0232 | 5.0469 | 0.0716 | 0.1625 | 0.0000 |
| Oily fish intake | 0.1108 | 0.0234 | 4.7290 | 0.0649 | 0.1567 | 0.0001 |
| Tea intake | -0.1009 | 0.0231 | -4.3777 | -0.1461 | -0.0557 | 0.0005 |
| duration of walk for pleasure | -0.0789 | 0.0232 | -3.4039 | -0.1243 | -0.0335 | 0.0253 |
| Water intake | 0.0770 | 0.0233 | 3.3045 | 0.0313 | 0.1227 | 0.0362 |
| Nap during day | 0.0766 | 0.0234 | 3.2730 | 0.0307 | 0.1224 | 0.0405 |
| Never eat eggs, dairy, wheat, sugar | -0.0738 | 0.0231 | -3.1919 | -0.1192 | -0.0285 | 0.0538 |
| Time spent using computer | 0.0567 | 0.0233 | 2.4391 | 0.0111 | 0.1023 | 0.5600 |
| Snoring | -0.0538 | 0.0231 | -2.3324 | -0.0990 | -0.0086 | 0.7483 |
| Former alcohol drinker | 0.0532 | 0.0231 | 2.3066 | 0.0080 | 0.0984 | 0.8014 |
| Duration of heavy DIY | 0.0503 | 0.0232 | 2.1665 | 0.0048 | 0.0958 | 1.0000 |
| Duration of light DIY | -0.0177 | 0.0232 | -0.7621 | -0.0632 | 0.0278 | 1.0000 |
| Duration of walk | 0.0140 | 0.0231 | 0.6055 | -0.0313 | 0.0592 | 1.0000 |
| Time spent driving | 0.0454 | 0.0235 | 1.9330 | -0.0006 | 0.0914 | 1.0000 |
| Time spent watching TV | -0.0120 | 0.0234 | -0.5146 | -0.0579 | 0.0338 | 1.0000 |
| Length of mobile phone use | 0.0078 | 0.0235 | 0.3304 | -0.0383 | 0.0539 | 1.0000 |
| Plays computer games | 0.0020 | 0.0231 | 0.0857 | -0.0433 | 0.0473 | 1.0000 |

| | | | | | | |
|---|---|---|---|---|---|---|
| Sleep duration | 0.0018 | 0.0232 | 0.0790 | -0.0436 | 0.0472 | 1.0000 |
| Getting up in morning | -0.0520 | 0.0237 | -2.1937 | -0.0985 | -0.0055 | 1.0000 |
| Sleeplessness / insomnia | -0.0157 | 0.0234 | -0.6743 | -0.0615 | 0.0300 | 1.0000 |
| Alcohol drinker status | -0.0221 | 0.0231 | -0.9573 | -0.0674 | 0.0232 | 1.0000 |
| Time spend outdoors in summer | -0.0184 | 0.0235 | -0.7829 | -0.0646 | 0.0277 | 1.0000 |
| Time spent outdoors in winter | -0.0155 | 0.0234 | -0.6631 | -0.0614 | 0.0304 | 1.0000 |
| Cooked vegetable intake | 0.0244 | 0.0231 | 1.0524 | -0.0210 | 0.0697 | 1.0000 |
| Salad / raw vegetable intake | -0.0022 | 0.0232 | -0.0943 | -0.0476 | 0.0432 | 1.0000 |
| Fresh fruit intake | 0.0001 | 0.0232 | 0.0047 | -0.0454 | 0.0457 | 1.0000 |
| Dried fruit intake | 0.0071 | 0.0231 | 0.3061 | -0.0382 | 0.0524 | 1.0000 |
| Non-oily fish intake | 0.0111 | 0.0231 | 0.4821 | -0.0342 | 0.0565 | 1.0000 |
| Processed meat intake | -0.0254 | 0.0240 | -1.0564 | -0.0725 | 0.0217 | 1.0000 |
| Poultry intake | -0.0111 | 0.0231 | -0.4793 | -0.0563 | 0.0342 | 1.0000 |
| Beef intake | 0.0077 | 0.0231 | 0.3334 | -0.0377 | 0.0531 | 1.0000 |
| Lamb/mutton intake | 0.0153 | 0.0233 | 0.6573 | -0.0304 | 0.0610 | 1.0000 |
| Pork intake | 0.0099 | 0.0232 | 0.4255 | -0.0357 | 0.0554 | 1.0000 |
| Cheese intake | -0.0340 | 0.0232 | -1.4679 | -0.0795 | 0.0114 | 1.0000 |
| Bread intake | -0.0174 | 0.0243 | -0.7171 | -0.0650 | 0.0302 | 1.0000 |
| Coffee intake | 0.0447 | 0.0231 | 1.9323 | -0.0006 | 0.0900 | 1.0000 |
| Alcohol frequency intake | -0.0490 | 0.0235 | -2.0806 | -0.0951 | -0.0028 | 1.0000 |
| **Ensemble model** | | | | | | |
| The measure | Coefficient | std err | T value | coefficient interval_S | coefficient interval_E | corrected_pvalue |
| Smoking status | 0.2488 | 0.0263 | 9.4661 | 0.1973 | 0.3004 | 0.0000 |
| Alcohol frequency intake | -0.1880 | 0.0267 | -7.0297 | -0.2404 | -0.1356 | 0.0000 |
| Ever smoked | 0.1769 | 0.0264 | 6.7097 | 0.1252 | 0.2286 | 0.0000 |
| Water intake | 0.1087 | 0.0265 | 4.1009 | 0.0567 | 0.1606 | 0.0016 |
| Tea intake | -0.1042 | 0.0263 | -3.9670 | -0.1556 | -0.0527 | 0.0028 |
| Time spent using computer | 0.1047 | 0.0265 | 3.9559 | 0.0528 | 0.1566 | 0.0029 |
| Lamb/mutton intake | 0.0929 | 0.0265 | 3.5040 | 0.0409 | 0.1449 | 0.0175 |
| Oily fish intake | 0.0906 | 0.0267 | 3.3968 | 0.0383 | 0.1428 | 0.0260 |
| Nap during day | 0.0890 | 0.0266 | 3.3439 | 0.0368 | 0.1412 | 0.0315 |
| duration of walk for pleasure | -0.0812 | 0.0264 | -3.0786 | -0.1329 | -0.0295 | 0.0792 |
| Coffee intake | 0.0782 | 0.0263 | 2.9724 | 0.0266 | 0.1298 | 0.1125 |
| Snoring | -0.0764 | 0.0263 | -2.9077 | -0.1279 | -0.0249 | 0.1386 |
| Never eat eggs, dairy, wheat, sugar | -0.0706 | 0.0263 | -2.6832 | -0.1222 | -0.0190 | 0.2774 |
| Former alcohol drinker | 0.0654 | 0.0263 | 2.4915 | 0.0140 | 0.1169 | 0.4838 |
| Sleeplessness / insomnia | -0.0645 | 0.0266 | -2.4263 | -0.1166 | -0.0124 | 0.5801 |
| Sleep duration | 0.0634 | 0.0264 | 2.4038 | 0.0117 | 0.1151 | 0.6170 |
| Duration of heavy DIY | 0.0368 | 0.0265 | 1.3904 | -0.0151 | 0.0886 | 1.0000 |
| Duration of light DIY | 0.0506 | 0.0264 | 1.9172 | -0.0011 | 0.1024 | 1.0000 |
| Duration of walk | -0.0059 | 0.0263 | -0.2247 | -0.0574 | 0.0456 | 1.0000 |
| Time spent driving | 0.0267 | 0.0267 | 1.0003 | -0.0256 | 0.0791 | 1.0000 |
| Time spent watching TV | -0.0190 | 0.0266 | -0.7134 | -0.0712 | 0.0332 | 1.0000 |
| Length of mobile phone use | -0.0154 | 0.0268 | -0.5767 | -0.0680 | 0.0371 | 1.0000 |
| Plays computer games | 0.0136 | 0.0263 | 0.5187 | -0.0379 | 0.0652 | 1.0000 |
| Getting up in morning | -0.0248 | 0.0270 | -0.9201 | -0.0778 | 0.0281 | 1.0000 |
| Alcohol drinker status | 0.0171 | 0.0263 | 0.6504 | -0.0344 | 0.0687 | 1.0000 |
| Time spend outdoors in summer | -0.0240 | 0.0268 | -0.8954 | -0.0766 | 0.0286 | 1.0000 |
| Time spent outdoors in winter | 0.0150 | 0.0267 | 0.5615 | -0.0373 | 0.0673 | 1.0000 |
| Cooked vegetable intake | 0.0163 | 0.0263 | 0.6175 | -0.0354 | 0.0679 | 1.0000 |
| Salad / raw vegetable intake | -0.0126 | 0.0264 | -0.4782 | -0.0643 | 0.0391 | 1.0000 |
| Fresh fruit intake | 0.0047 | 0.0264 | 0.1785 | -0.0471 | 0.0565 | 1.0000 |
| Dried fruit intake | -0.0454 | 0.0263 | -1.7237 | -0.0970 | 0.0062 | 1.0000 |
| Non-oily fish intake | 0.0111 | 0.0263 | 0.4205 | -0.0405 | 0.0627 | 1.0000 |
| Processed meat intake | 0.0017 | 0.0274 | 0.0626 | -0.0519 | 0.0553 | 1.0000 |
| Poultry intake | -0.0204 | 0.0263 | -0.7777 | -0.0720 | 0.0311 | 1.0000 |
| Beef intake | 0.0527 | 0.0263 | 2.0015 | 0.0011 | 0.1043 | 1.0000 |
| Pork intake | 0.0570 | 0.0264 | 2.1551 | 0.0052 | 0.1088 | 1.0000 |
| Cheese intake | 0.0149 | 0.0264 | 0.5647 | -0.0368 | 0.0666 | 1.0000 |
| Bread intake | -0.0368 | 0.0276 | -1.3340 | -0.0910 | 0.0173 | 1.0000 |